BIOMECHANICAL BEHAVIOR OF BIOPROSTHETIC HEART VALVE HETEROGRAFT TISSUES:

CHARACTERIZATION, SIMULATION, AND PERFORMANCE

Joao S. Soares[1], Kristen R. Feaver[1], Will Zhang[1], David Kamensky[1], Ankush Argarwal[1,2] and Michael S. Sacks[1]

[1] *Center for Cardiovascular Simulation*
Institute for Computational Engineering & Sciences
Department of Biomedical Engineering
The University of Texas at Austin, Austin, TX

[2] College of Engineering, Swansea University
Bay Campus, Fabian Way, Swansea, SA1 8EN

To be resubmitted to CVET

Current: July 11, 2016

For correspondence:
Michael S. Sacks, Ph.D.
W. A. Moncrief, Jr. Simulation-Based Engineering Science Chair I
Center for Cardiovascular Simulation
Institute for Computational Engineering and Sciences
Department of Biomedical Engineering
The University of Texas at Austin
201 East 24th Street, ACES 5.438
1 University Station, C0200
Austin TX 78712-0027 U.S.A.
email: msacks@ices.utexas.edu
Tel: 512-232-7773

Abstract:

The use of replacement heart valves continues to grow due to the increased prevalence of valvular heart disease resulting from an ageing population. Since bioprosthetic heart valves (BHVs) continue to be the preferred replacement valve, there continues to be a strong need to develop better and more reliable BHVs through and improved the general understanding of BHV failure mechanisms. The major technological hurdle for the lifespan of the BHV implant continues to be the durability of the constituent leaflet biomaterials, which if improved can lead to substantial clinical impact. In order to develop improved solutions for BHV biomaterials, it is critical to have a better understanding of the inherent biomechanical behaviors of the leaflet biomaterials, including chemical treatment technologies, the impact of repetitive mechanical loading, and the inherent failure modes. This review seeks to provide a comprehensive overview of these issues, with a focus on developing insight on the mechanisms of BHV function and failure. Additionally, this review provides a detailed summary of the computational biomechanical simulations that have been used to inform and develop a higher level of understanding of BHV tissues and their failure modes. Collectively, this information should serve as a tool not only to infer reliable and dependable prosthesis function, but also to instigate and facilitate the design of future bioprosthetic valves and clinically impact cardiology.

Keywords: bioprosthetic heart valve; heterograft;valve mechanics; constitutive modeling; mechanical testing; exogenous crosslinking; fluid structure interaction; modeling and simulation.

Table of Contents

Nomenclature

AHA	American Heart Association
AV	aortic valve
BHV	bioprosthetic heart valve
BP	bovine pericardium
ECM	extracellular matrix
FE	finite element
GAG	glycosaminoglycan
GLBP	glutaraldehyde bovine pericardium
GLUT	gluraraldehyde treatment
LEHI	linear elastic homogeneous incompressible
microCT	micro X-ray computed tomography
MRI	magnetic resonance images
MV	mitral valve
PAV	porcine aortic valve
PBS	phosphate buffered saline
PD	preferred direction
RVE	representative volume element
SALS	small angle light scattering
TEHV	tissue-engineered heart valve
UTS	ultimate tensile stregth
VEC	valvular endothelial cell
VIC	valvular interstitial cell
XD	cross-preferred direction

Symbols

ΔM	infinitesimal mass
ΔV	infinitesimal volume
ρ	mass density
ε	fiber uniaxial strain (in structural constitutive model)
θ	fiber orientation angle (in structural constitutive model)
c_f	volume fraction of fibers (in structural constitutive model)
$\mathbf{C}$	left Cauchy-Green stretch tensor
$D(\varepsilon)$	fiber recruitment statistical distribution (in structural constitutive model)
$\mathbf{E}$	Green-Lagrange strain tensor
E_{ij}	components of the Green-Lagrange strain tensor
$I(\theta)$	angular distribution of scattered light (in SALS analysis)
$R(\theta)$	fiber angular distribution (in structural constitutive model)
$\mathbf{S}$	second Piola-Kirchhoff stress tensor
S_{ij}	components of the second Piola-Kirchhoff stress tensor
$\mathbf{S}^f$	second Piola-Kirchhoff stress tensor in the fiber (in structural constitutive model)
S^f_{nn}	component of the Piola-Kirchhoff stress tensor in the fiber along fiber direction (in structural constitutive model)
W	stored energy function
$w(\varepsilon)$	stored energy function of fiber (in structural constitutive model)
W_f	stored energy function of the fiber ensemble (in structural constitutive model)
W_m	stored energy function of the matrix (in structural constitutive model)
I_1, I_2, I_3	principal invariants of the left Cauchy-Green stretch tensor

1 - Introduction

The valves of the heart are responsible for controlling the unidirectional flow of blood through the body. Annually each valve opens and close 30-40 million times, for a total of ~3 billion cycles in a lifetime [1]. Valvular heart disease is clinically typified by gradual narrowing of the valve due to calcification of the leaflets or regurgitation through the valve due to insufficient valve closure in one of four heart valves. Stenotic (too narrow and hardened to fully open) or incompetent (unable to close completely) valves cause blood flow in between the several heart chambers becomes pathological, imposing an increased mechanical load on the ventricle and leading to ventricular chamber enlargement, thickening, and progressive contractile failure. Valve repair or replacement are two available therapies to correct diseased valves, preserve cardiac function, and ultimately necessary to prevent congestive heart failure and death. According to the American Heart Association (AHA), the overall prevalence of any heart valve disease is 2.5%, and clinically diagnosed (moderate or greater) prevalence of 1.8% with an annual mortality of over 22,000 [2-5]. Valve replacement surgery, first performed in 1960, has significantly reduced the mortality rate of patients with valvular heart disease [6-8]. As reported by The Society of Thoracic Surgeons 59,555 Americans underwent valve replacement surgery in 2014 (48,060 AV replacement, 9,595 MV replacement, 1,900 both AV and MV replacement).. Of the various types of heart valves, the aortic valve (AV) has been studied most, followed next by the mitral valve (MV), whereas fewer studies have been performed on the valves of the pulmonary circulation, the pulmonary valve (PV) and the tricuspid valve. This is primarily due to the fact that the AV and MV are more commonly diseased than the PV, as indicated by AHA statistics, and more frequently warrant replacement surgery.. While important differences exist in valve geometries and function, the mechanics of the AV are primarily used as a baseline for the development of models of heart valve function. Valve repair is a feasible alternative for valve replacement and is an attractive approach in the treatment of severe mitral valve regurgitation. Ring annuloplasty allows robust and predictable mitral valve reconstructions and surgical corrections to restore leaflet mobility, large coaptation surface, and favorable remodeling of the annulus to offer optimal and stable orifice area [9]. However, meta-analyses indicate that mitral valve repair or mitral valve repair are indeed head-to-head in comparison: replacement was associated with a higher 30-day mortality (as the procedure is much more drastic and entails higher inherent risks), whereas repair is associated with higher rates of mitral regurgitation occurrence and the need for reoperation [10].

Current clinical implants used for surgical valve replacement utilize either mechanical valves (usually made of pyrolytic carbon or titanium) or valves constructed from biologically-derived soft tissues. Although mechanical prosthetic valves are very durable, they introduce a large degree of pathologic blood flow patterns, elicit a substantial thrombogenic response, and require lifelong post-

operative anticoagulation therapy with its inherent risks [8]. Bioprosthetic heart valves (BHVs), on the other hand, are comprised of decellularized bovine or porcine tissues (prosthesis constructed with either the native valve leaflets per se, or with connective tissues, most commonly the pericardium) and offer a higher degree of functionality including improved hemodynamics and a higher resistance to thrombosis. Although they are chemically fixed, these tissues are still prone to valve calcification, structural deterioration, and eventual failure [11, 12]. Durability is the major limitation of current BHV technology - the 15-year durability of heterograft BHVs in the aortic position is less than 50% for middle-aged patients and slightly better for older patients**,** however BHVs continue to be the preferred replacement valve [13]. Regardless of its shortcomings, heart valve replacement has had a substantial impact on cardiac surgery with a consistently increasing number of surgeries per year (Figure 1), and more recently on interventional cardiology with catheter based techniques. This may have saved the lives of millions of patients with valvular diseases, who before the advent of replacement therapies were faced with very limited clinical options and death by congestive heart failure as the likely result. The very first successful heart valve surgery was mitral commissurotomy performed in 1923 by Elliott Cutler [14]. The introduction of the heart-lung bypass machine in the 1950s allowed for entire valve replacement surgeries. In 1960, pioneer surgeons Nina S. Braunwald and Dwight E. Harken implanted the first artificial mitral and aortic valves respectively [7, 15]. BHVs have been a popular choice among surgeons since they were made commercially available in the 1960s (Figure 1). The Hancock porcine BHV, first implanted in 1970 and starting clinical trials in 1972, was the first commercially available glutaraldehyde-fixed BHV available for widespread use in humans in mid-to-late 70s [16]. Over the years, heart valve technology has improved slowly and steadily, providing significant increases in durability for both mechanical and bioprosthetic valves. However, the gold standard of current valve replacement technology utilizes essentially the same principles and concepts of the past. Progress within the field and development of novel technology has been limited by apprehension created by a few notable setbacks. While most mechanical valves tend to be very durable, the Bjork-Shiley mechanical prosthetic valve had a critical design flaw that caused the valve to fail in vivo, leading to numerous deaths [17] (and may explain the drop in mechanical valve surgeries in 1977, Figure 1). Setbacks have been observed in BHVs, usually as a result of attempts to increase the durability of BHVs through various fixation chemistries. A notable case is the Oxford Photofix stentless valve, a xenograft valve fixed with a dye-mediated photoxidiation process that failed numerous times in clinical studies due to cusp abrasion and perforation [18]. Regardless and despite of the many setbacks, significant developments have improved valve technology progressively over the years – examples of such are anti-calcification treatments such as α-amino oleic acid, Polysorbate 80, and ethanol

pretreatment, some of which have now been implemented in current technology present in commercial valves [19, 20].

The development of stentless valves provided an alternative delivery method for BHVs, however these did not really offer a superior alternative to stented valves as both have excellent clinical outcomes at short- and mid-term.[21, 22] However, stentless valves offer significant hemodynamic advantages, e.g. larger effective orifice area, better coronary flow, and lower trans-aortic pressure difference [23, 24], superior biomechanical properties by preserving increased distensability and lowering leaflet stress in comparison to stented valves, and may be advantageous in specific surgical cases such as AV endocarditis, aortic root pathologies, and may improve post-operative function in impaired ventricles [25]. The most recent development in BHV technology is the percutaneous (or transcatheter) valve replacement, which involves replacement of the aortic valve in a minimally invasive procedure with catheterization from a large blood vessel, most commonly the femoral artery. This procedure makes replacing failed BHVs less invasive and less risky (as several classes of patients may not be suited for open heart surgery), and initially posed substantial technological challenges on prosthesis design and required substantial refinement of the delivery technique. Currently, large randomized trials among high- and intermediate-risk patients with aortic stenosis have shown similar survival rates of transcatheter aortic valve replacement and surgical aortic valve replacement [26]. Currently, bovine pericardium (BP) and porcine AV tissues are still the only clinically approved xenograft biomaterial for BHVs and as such are the most frequently studied and employed sources of tissue (Figure 2). Other tissue sources have been pursued, but none has reached clinical widespread application.

BHVs have become the preferred replacement valve. The sustained growth of AV and MV replacement surgeries, the lack of substantial technological breakthroughs in the field over the last decades (Figure 3), and the continuous need to improve BHV durability, promotes a strong necessity to develop a higher understanding of the mechanisms involved in BHV function and failure. Critical BHV engineering aims to ensure valve functionality for its clinical performance with a combination of hemodynamic, biomechanical and biological aspects, e.g. sufficient effective orifice area, transvalvular pressure gradient, good leaflet coaptation without regurgitation, among others, and to predict and extend as much as possible valve durability. The major hurdle on the technology is simply the lifespan of the BHV implant, and substantial clinical impact can be achieved with its improvement, even if only slightly (e.g. increases of 3-5 years) [27].

This review seeks to establish the need for rational methodologies and quantitative approaches to optimize BHV design by providing a comprehensive overview of the different types of BHVs, chemical fixation treatments, the mechanical properties of various tissues used for BHVs, methods to

characterize them, and experimental results that provide insight on the mechanisms of BHV in vivo function and failure (Figure 4). Additionally, this review provides a detailed summary of the computational biomechanical simulations that have been used to aid in better understanding these tissues and their failure modes. The inclusion of high fidelity anatomical descriptions and better microstructural and macrostructural models of BHV material response into in silico environments for organ-level simulations under physiological and pathological conditions will certainly be of great importance towards the improvement of BHV technology in the future. The integration of modeling and simulation into technology development will not only guide and inform subsequent R&D steps with critical quantitative data and rational methods (instead of solely relying on trial-and-error), but also will allow different insights into the problems and better analysis and interpretation of empirical data.

2 - Primary tissue sources

2.1 - Bovine pericardium

The pericardial sac is a multi-layered connective tissue that surrounds and protects the heart: the visceral layer (also known as the epicardium) lies next to the cardiac muscle and is separated from the parietal layer by the pericardial cavity. Pericardium is primarily composed of collagen but also contains glycoproteins, glycosaminoglycans (GAGs) and cells. The collagen fiber distribution in pericardium is generally anisotropic and the overall collagen orientation and organization varies regionally. Structural variability and fiber alignment is high in pericardial tissue, which was characterized using small angle light scattering (SALS) [28, 29] (Figure 5). In SALS, laser light is passed through a tissue and the scattered light is quantified to determine the spatial distribution of structural orientation, i.e. identifying preferred-fiber direction (PD) and cross-preferred fiber direction (XD) and their degree of orientation, and thus allowing for the selection of structurally uniform specimens. Specimens pre-sorted by SALS were evaluated for biaxial mechanical properties and resulted in a much higher degree of uniformity and more consistent biomechanical data than results from previously reported non-sorted tissue tests [30]. In general, there are significant intra- and inter-sac variations in fibrous structure, which emphasizes the need for the careful selection of tissue for BHVs to achieve the highest degree of uniformity in the fiber orientation, uniform tissue thickness, and most importantly, reliable process reproducibility. Upon tissue selection aided by SALS, bovine pericardium (BP) can be chemically fixed, cut to size in the shape of a leaflet, and then affixed to a mechanical support to be sutured into the aortic wall (Figure 2A).

2.2 - Porcine aortic valve leaflet

The aortic valve (AV) has three leaflets, also known as cusps, which enable unidirectional flow from the left ventricle to the aorta and are comprised of three distinct layers: the fibrosa, spongiosa, and ventricularis [1, 31]. The fibrosa faces the aorta and is composed primarily of Type I collagen fibers, highly aligned in the circumferential direction (Figure **6**). The ventricularis faces the left ventricle and is composed of a mix of elastin and collagen. Valve leaflets contain a relatively low elastin content when compared with collagen (13% to 50% dry weight). During diastolic loading there is considerable realignment of collagen fibers extending passively as the cusps undergo beyond 50% strain. The elastin in the ventricularis exerts compressible forces to keep the fibrosa in its undulated confirmation in unloaded leaflets, and is responsible for ensuring the elastic recovery mechanisms [32]. The spongiosa is the middle layer between the fibrosa and the ventricularis and contains mostly water and glycosaminoglycans (GAGs), which have been shown to have no significant effects on static mechanical properties of biological tissues [33]. In addition to the valvular extracellular matrix (ECM)

components, the aortic valve is also rich in valvular interstitial cells (VICs) distributed throughout the valve, as well as valvular endothelial cells (VECs) at the blood-contacting surfaces. These cells help contribute to the maintenance of the valvular ECM and are linked with structural growth, remodeling, and repair. To prepare porcine AVs (PAVs) as BHVs, they must first be explanted, decellularized, and chemically fixed before being affixed to a mechanical support for implantation (Figure 2B). While the decellularization process is necessary to remove viable porcine cells and to decrease the risk of an immune response, it hampers other key features of heart valve function, in particular the biochemical processes occurring within the native valves. Liao et al. showed that decellularization causes a substantial loss in valve stiffness, but also significant microscopic ECM disruption [34]. The purpose of these cells, although much remains unknown, is to maintain the structure and to respond to environmental changes – if no longer present, the valve may indeed be more prone to failure and the natural mechanisms of ECM remodeling and repair are not present.

2.3 - Other tissue sources

Although bovine pericardium and porcine aortic tissues are the current standard materials for BHV construction, allograft and homograft biomaterials have also been used. Various other tissue sources have been evaluated as potential candidates for BHVs, including porcine pericardium, jugular vein valve [35], pulmonary valve, and intestinal mucosal membrane; however, these are less common alternatives, and additionally, the performance of the porcine pulmonary valve was shown to be far inferior to the porcine aortic BHV [36]. More exotic tissue sources including equine [37], canine [38, 39], even ostrich [40] and kangaroo [41] pericardium have been proposed for use in BHVs, but the relatively low availability of such materials and the risk of unexpected immune responses has raised concern and prevented these options from being evaluated further.

2.4 - Engineered tissue approaches.

Tissue-engineered heart valves (TEHVs) present a beneficial alternative as they have the potential to eliminate the immune response, offer native like characteristics of ECM remodeling and repair, and ideally, dismiss the need for subsequent valve replacement surgeries. The latter is particularly important in pediatric patients where a TEHV could accommodate somatic growth, especially when used to treat congenital heart valve diseases. The ultimate goal for TEHVs is to create a non-thrombogenic living tissue substitute that can grow, repair, and remodel and be fully integrated into the patient. The most common approach in creating TEHVs is to seed autologous cells onto a biodegradable scaffold and allow the cells to produce ECM. This process generates a living tissue-like valve construct for implantation into the body. There have been several promising studies that have successfully demonstrated in vivo functionality of TEHVs: (i) Hoerstrup et al. [42] implanted TEHVs in a

ovine model that demonstrated functionality without stenosis, thrombus, or aneurysm for up to 20 weeks and histological data and ECM quantification showed ECM content comparable to native tissues; (ii) Stock et al. [43] formed pulmonary artery tissue similar to native; (iii) Sutherland et al. successfully implanted TEHVs that demonstrated substantial in vivo remodeling and remained functional for at least four months [44]; and (iv) Rabkin et al. reported the development of multi-layered TEHVs, with variations in ECM components in each layer [45]. Much progress has been made in TEHVs, yet so far no patients have benefited from this nascent technology. While the results of these studies are indeed promising, TEHVs are still in early stages of development and have yet to become a truly viable heart valve replacement. As the body of knowledge surrounding TEHVs grows, it is important to fully understand the functional biomechanics of the engineered tissues and to compare their performance to their native counterparts to ensure a fully equivalent replacement tissue is generated. The current state of TEHVs and the engineering design and modeling principles that must be associated with future TEHV research has been extensively reviewed (cf. e.g. Sacks et al. [46]).

3 - Mechanical behavior of bioprosthetic heart valve tissues

Mechanical testing typically involves applying some type of stimulus and measuring a response, and is generally achieved through imposing deformations on material – displacements/strains are specified and controlled and then the forces/stresses needed for such are measured or computed. The reciprocal approach, i.e. subjecting the material to a known force and recording its response, is also valid, although the former is more common. A constitutive model (or *relation* since it relates stress to strain) describes the gross behavior of the material to the applied loads under certain conditions of interest [47]. Only the specific form of the constitutive model is assumed, whereas its parameters are either measured or computed. Moreover, without accurate constitutive models, one clearly cannot establish a valid relationship between forces and displacements with predictive capabilities, and perform even the most elementary modeling and analyses. Furthermore, it must be stressed that no constitutive model will describe well all ranges of stress and strain, strain rate, loading cycles, temperature, humidity, etc. Rather, a constitutive model describes a material's behavior under specific loading conditions that are of interest to a particular application. This rather intuitive statement is often overlooked – many discussions on the relative merits of different constitutive models often ignore that their intended uses are very different, and it is thus inappropriate to compare them. In general, in formulating a constitutive model for a material, one should delineate general characteristics of the material, establish an appropriate theoretical framework, identify a specific functional (i.e. mathematical) form of the model, calculate values of the material parameters, and finally, evaluate the predictive capability of the final relation [47]. It is first essential to stress the important distinction

between experiments for material behavior characterization and experiments for model parameter identification.

Central to the framework of continuum mechanics is the concept of a material continuum and its applicability. The discrete composition of matter is ignored in the classical concept of a continuum – matter is uniformly distributed within each of the infinitesimal particles. However, real materials, particularly biological tissues, are inhomogeneous and a tolerable error must be accepted. Notwithstanding, if the tissue of interest possesses a length scale that is large enough with respect to the local structural details such that it is composed by a large enough number of infinitesimal particles, the material can be treated as a continuum. Heterograft tissues, e.g. bovine pericardium or valve leaflets, are highly hierarchically organized materials that have several orders of structural organization across multiple length-scales, such as fibrous networks and other large-scale structures, so that determining an appropriate continuum scale can be very difficult. Generally, the proper continuum scale of each structure (tissue, collagen network, cell) must be accessed and even with the errors inherent in utilizing a finite lower bound and disregarding lower scale features, the inherent simplification in any analysis is enormous, but its practicality and applicability is crucial.

The framework of continuum mechanics is employed in the study of BHVs in two distinct but inter-related levels: (i) on one hand, valves function as a device, i.e. how in vivo loads affect valve leaflet deformation, is investigated at organ-level usually with the aid of finite element methods and is able to answer questions such as “what is the pressure differential that will cause valve prolapse?” or “how does the coaptation area changes with pressure?”; (ii) on the other hand, the framework or continuum mechanics is employed at tissue level, in association with systematic experiments such as uniaxial extension or biaxial extension, to determine the characteristic mechanical response of the valve material and to answer questions such as “what model should one employ to describe the response of the material?” or “how does the material moduli change with fixation treatments?”. In order to perform analyses of type (i) accurately, one needs to have sufficient confidence on models of type (ii) to be employed on them. However, additional modeling layers may be necessary to capture relevant biochemical and biological phenomena because these are complex and evolving tissues that interact with a living organism – these modeling layers could be included as coupled models at the cellular scale, or alternatively, incorporated ad hoc into the parameters of tissue-level models.

The formulation of constitutive frameworks to describe material behavior involves a two-pronged approach between theory and experiments. Initially, experiments are necessary to understand the response of the materials in question. The first step is to observe the many particular behaviors of interest, and then, by induction, delineate its general characteristics – this step is as critical as is difficult. The results of diverse exploratory experiments as well as pre-existing published results must

be distilled to depict the underlying mechanisms or general characteristics of importance. Once this is accomplished, one then attempts to formulate general hypotheses or theoretical frameworks, which must be followed by more experiments to test their validity. These validating experiments are different in concept from the initial experiments – not only may these necessitate the design and construction of new experimental systems, but also they are driven by the predictions of the theory. Designed experiments are required for the determination of values of the material parameters and allow the evaluation of the predictive capability of the theoretical framework. Based on the experimental data, one will often need to refine the theory and perform additional experiments and data analysis for validation purposes. This iterative procedure continues until the associated model has predictive capability. Only then can one begin to answer the applied questions of interest, often via parametric studies with numerical simulations and ultimately resulting in animal and clinical trials [47].

There have been many studies to evaluate and characterize the mechanical properties of BHV tissues, however most of the available published data provides uniaxial tensile data only. Uniaxial data is fairly straightforward to obtain and allows for basic assessments of tissue mechanics. The studies and data presented herein exemplify a small portion of all available data, but allow for the comparison of multiple fixation chemistries and provide baseline material characterization data. Certainly these studies are not directly related to each other and they were not done in any systematic or concerted fashion, but significant conclusions can be obtained from their meta-analysis. The biaxial and flexural studies, in particular, have laid the framework for most computational models.

3.1 - Uniaxial tensile mechanics

Uniaxial tensile testing is the most straightforward method used to evaluate very basic mechanical properties of biomaterials and cardiovascular tissues [48, 49]. Usually, samples are placed in ambient phosphate buffered saline (PBS) and preconditioned using up to ten cycles of loading and unloading at 30-50% of the estimated failure stress to obtain reproducible results. Preconditioning is used to obtain a pseudoelastic response, in which separate but repeatable loading and unloading behaviors are observed. Then controlled uniaxial tension is applied to a sample until it fails. Values directly obtained from such testing include ultimate tensile strength (UTS) and maximum elongation, but reported data usually includes the stress-strain relationship, failure stress, and failure strain. Uniaxial tensile behavior of heterograft tissues is generally nonlinear, with the exponential behavior commonly observed in biological tissues and attributed to collagen fiber undulation, de-crimping, and engagement upon extension [50, 51]. Simpler mechanical properties such as Young's elastic modulus are not able to fully characterize this inherently nonlinear response, and most importantly, are not suited because they entail the application of the linearized theory of isotropic elasticity (with the restriction to infinitesimal strains) to biomaterials of BHVs undergoing large deformations not only during testing (for

parameter determination) and but also during function (for subsequent mechanical analyses). However, it must be remarked that the Young's modulus of the material is the slope of the stress vs. strain curve at the origin and can be used directly to compare performance at infinitesimal strains.

On the other hand, uniaxial tensile testing by itself is useful in the sense that it can be used to obtain insights into material characteristics based on method of failure. The specimen can exhibit fracture via crack development and propagation, creep due to slow increase in deformation, buckling, or even plastic deformation. These results provide information about the brittleness and ductility of the samples, as well as the uniaxial strength. Furthermore, although failure modeling is usually somewhat unreliable due to the currently underdeveloped state-of-the-art of theoretical models of material failure or even the physical understanding of its specific mechanisms, it is possible to ascertain trends and general failure characteristics by critical and rational comparison of ultimate tensile strength experiments of several materials, e.g. "material A fails at a higher stress than material B, and if material B is acceptable, then material A is acceptable". Moreover, such characteristics can be correlated to other material characteristics, e.g. "if fatigue failure is assumed to be directly correlated with ultimate tensile strength, then material A will last higher number of cycles than material B" – however, caution must be taken when drawing conclusions from such inferences because one is implicitly assuming the direct correlation between both phenomena.

Multiple groups have evaluated the tensile strength of natural and chemically modified bovine pericardium [52, 53]. The preferred fiber direction can usually be assigned to samples of carefully harvested fibrous pericardium. This tissue orientation direction is usually employed as a testing axis and subsequently, its orthogonal direction is defined as the cross-preferred direction. Collagen fibers contribute significantly to the mechanical response of the tissue, and tension needed to achieve similar extensions is significantly higher in the preferred direction than in the cross-preferred direction, corroborating the expected anisotropic response of the material. Uniaxial testing does not provide a great deal of information about the tissue, but it is a tool to perform simple characterization for comparative studies. Sung et al. [54] (among many others) have conducted uniaxial extension experiments of both native and fixed BP (Table 1) Sung et al. [54] reported tangent modulus and have clearly observed the differences between the uniaxial characteristics for the PD and XD orientations, as well as the differences between multiple fixation chemistries including glutaraldehyde, epoxy and genipin, a naturally occurring crosslinking agent. Similar studies have been performed to characterize the uniaxial mechanical properties of porcine AV tissue [55-57]. Using a testing similar protocol, Sung et al. [58] reported uniaxial mechanical properties of fresh and fixed PAV (Table 1). On the other hand, published data on the human pulmonary valve mechanical and structural suitability as a long-term

substitute for aortic valve are limited – Stradins et al. [59] compared aortic and pulmonary valve properties (Table 1).

3.2 - Planar biaxial tensile mechanics

While uniaxial testing is useful for isotropic materials, biaxial tensile testing is necessary to properly characterize anisotropic materials. Biaxial loading testing allows one to obtain a tensorial relationship between stresses and strains. Most soft biological tissues exhibit significant anisotropy due to their fiber-oriented microstructure and thus their mechanical response is dependent on orientation. Biaxial tensile testing allows for a better understanding of the mechanical properties of the tissues under more complex loading conditions, more similar to those experienced in vivo. Additionally, the development and the employment of anisotropic constitutive models requires data obtained via biaxial testing. For biaxial mechanical tests, sutures are placed around the perimeter of rectangular shaped specimens and markers are placed in the center of the specimen. Similarly to uniaxial testing, specimens are placed in a bath of ambient PBS and undergo cyclic preconditioning up to 10 cycles. Then, controlled perpendicular biaxial tension is applied to the sample. The displacement of the markers is recorded and is subsequently used to calculate the in-plane strain tensor. Multiple test protocols are performed to fully characterize the sample under different loading states. Each protocol is stress- or strain-controlled and all protocols keep a constant ratio of stress or strain. Representative experimental data are a set of the stress vs. strain responses for multiple protocols (Figure 7). Data from all protocols serves as input into a constitutive model, and a single stress vs. strain response to one particular protocol is meaningless – only when the entire set of experimental data is reduced into the parameters of the model of choice by regression, the constitutive model is able to describe the response of the material in general, and then, a few illustrative responses of the model are usually reported (e.g. equibiaxial response). For the sake of comparison, the responses of various tissues to one protocol and the models describing such responses can be paired and are frequently reported as a result.

Sacks and Chuong performed a series of biaxial tests to characterize fresh and fixed bovine pericardium (Table 2) [30]. All chemically treated specimens were seen to exhibit mechanical anisotropy, with the pre-stretched tissues showing the most distinct anisotropic response, followed by the free-fixed and the control groups. The experimental data obtained in this study was then reduced to constants of a hyperelastic constitutive model. Christie and Barratt-Boyes performed the first porcine AV equibiaxial testing [60], however it was determined that in order to develop a constitutive model more complete multiprotocol data was required. Billiar and Sacks [61] were the first to compile comprehensive biaxial data for modeling the porcine aortic valve leaflet (Figure 7, Table 3). It was determined that the optimal tissue selection site was from the lower-belly region of the valve leaflet,

slightly off-center below the nodulus of Arantii. In light of the complex composition, curvature, and geometry of the aortic valve, this section of tissue has the most homogeneous strain field and fiber structure and the collagen alignment is primarily in the circumferential direction. Once again, data collected by Billiar and Sacks was reduced to constants of a structural constitutive model [62]. Christie and Barratt-Boyes [63] measured the biaxial properties of pulmonary and aortic leaflets in extension in the native and treated states (Table 4). Additionally, Martin and Sun [64] compared aortic valve tissues in humans and common animal models, namely porcine and ovine (Figure 8). Both ovine and porcine valvular tissues consistently show higher strain at 60 N/m membrane tension than human tissues, and this is an important consideration when developing preclinical models.

3.3 - Flexural tensile mechanics

Flexural mechanical testing is used to add further insight to tissue response, particularly when subjected to different modes of deformation that are not included in uniaxial and biaxial extension. In flexural analysis, different parts of the sample being tested are subjected to shear, tension, and compression. Flexure is vital for understanding the in-plane response of the material as this direction is not tested in uniaxial, strip-biaxial or multi-axis biaxial. Furthermore, flexural testing allows the determination of the effect of compressive forces on a tissue in a bent configuration, especially since this is considered to be a major deformation mode of the AV. Additionally, compressive stresses are believed to impact the degradation of bioprosthetic tissues [65, 66], and are thus critical to better understand in order to design improved BHVs. To test the flexural rigidity of a sample, an optical system is used to obtain curvature data and bending bar displacement, which are subsequently used to calculate the moment-curvature (M/I vs. $\Delta\kappa$) response (Figure 9). Data obtained from flexural testing can then be used to calculate the effective modulus of a tissue using the Euler-Bernoulli relationship (detailed testing methodology and experimental results for various flexural mechanical responses can be found in [67-69]).

Flexural mechanical testing has been used to effectively study cellular and structural effects on the flexural stiffness of both pericardial biomaterials and the aortic valve leaflet. Mirnajafi et al. [68] evaluated the effect of collagen fiber orientation on the flexural properties of pericardial heterograft tissues. When evaluated for flexural mechanics, native bovine pericardium produced a slightly non-linear moment-curvature response in both the visceral and epicardial directions of flexure (Figure 10). Due to the non-linearity of the results, instantaneous effective stiffness is reported (Table 5) [68]. This contrasts to porcine aortic valve tissue, which presented a very linear moment-curvature response. As expected, chemical fixation by glutaraldehyde increased the stiffness for BP and porcine AV. Upon fixation, non-linearity is maintained for BP just as linearity is maintained for porcine AV. The flexural mechanics of the belly region of the native porcine AV were measured in a study looking at the effects

of cellular contraction on stiffness by Merryman et al. [70] (Table 6). However, the complex geometry of the commissural region made it necessary to use a cantilever method to fully evaluate flexural mechanics of the porcine AV (Table 7) [71]. Additionally, while it has previously been unknown as to how the layers of the AV interact, recent transmural flexural data has shown that the fibrosa, spongiosa, and ventricularis act as one bonded unit, rather than sliding as has previously been thought to occur [72]. Flexural mechanical testing has also been used to evaluate the flexural stiffness of TEHV scaffolds and constructs [73, 69].

4 - Effect of exogenous cross-linking as a means for tissue preservation

Bioprosthetic heart valve tissue generated from heterograft tissues must be chemically fixed to preserve the tissue and to decrease potential in vivo structural degradation. The most commonly utilized crosslinking agent for bioprosthetic tissues is glutaraldehyde (GLUT). Glutaraldehyde fixation employs a Schiff-based aldehyde reaction to crosslink two amine groups, and is very effective at crosslinking collagen molecules. It is the current standard fixation method for bioprosthetic heterograft tissues, however glutaraldehyde significantly affects leaflet mechanics. Additionally, while tissues fixed by glutaraldehyde initially have no immune response, they are susceptible to eventual calcification, and using an aldehyde to fix implantable tissue has also raised concerns regarding cytotoxicity. Other fixation methods are being evaluated with the goal to reduce calcification potential, maintain mechanical properties similar to native valve tissues, and reduce cytotoxicity.

In a study on the effect of different fixation methods on bovine pericardium, polyglycidyl ether and glutaraldehyde caused substantial crosslinking, and changes in mechanical properties including a decreased stress relaxation and increased extensibility. Cyanimide (which crosslinks pure collagen) did not effectively crosslink tissue, heat-drying increased ultimate tensile strength and tissue modulus, and freeze-drying had no effect [74]. Genipin, a naturally occurring crosslinking agent, and carbodiimide were found to be effective crosslinking agents but produce distinct crosslinking structures, which may in turn affect other properties of the fixed tissue (Table 5) [75]. Mercuri et al. [76] looked into GAG-targeted fixation which allowed for higher retention of GAGs, but did not alter the calcification potential of the leaflets compared to conventional GLUT-treated tissue.

Zero-pressure GLUT-fixation has been shown to produce fixed tissue with minimal changes to functional biomechanics and produces a softer and more extensible tissue than one treated under even low pressure [77]. However, Wells and Sacks varied transvalvular fixation pressure and applied accelerated cyclic-loading tests and showed that zero pressure fixed porcine BHV demonstrated conformational changes under long-term cyclic loading and eventually decreased in extensibility to the level of the low-pressure fixed tissue [78].

Sung et al. [75] performed a study to investigate the effect of different fixation chemistries on porcine pericardium and found that genipin and carbodiimide are indeed effective crosslinking agents for tissue fixation. The authors have also incorporated the use of N-hydroxysuccinimide to increase the number of crosslinks introduced (Table 8).

5 - Constitutive models

Early attempts to describe valve tissue properties used the linear elastic model following the generalized Hooke's law [79]. Linear elastic models are appropriate when the stress-strain relationship is indeed linear, yet the linearized theory of elasticity is restricted to motions with relatively small displacement gradients. However, the stress-strain relationship of heterograft materials is grossly nonlinear, and valvular function typically involves finite large deformations. As a common computational mechanics alternative, Hamid et al. [80] and Li et al. [81] specified piece-wise linear tangent modulus to approximate non-linear material behavior, thus avoiding the numerical difficulties associated with full blown nonlinear material models. Nonetheless, the overwhelming disadvantage of the linearized elasticity framework lies in its inaccuracy dealing with finite deformations, thus prohibiting any realistic valve simulations. To overcome this challenge, hyperelastic models have been employed to describe biological tissue under finite deformations for simulation of the function of BHVs [82, 83]. The most common hyperelastic material model is the exponential model proposed by Fung [50], and has been utilized to date for characterizing the mechanical response of soft biological tissues, including skin [84], pericardium [85], epicardium [86], visceral pleura [87], and many others.

5.1 - Phenomenological Hyperelastic Models

Glutaraldehyde-treated pericardium tissue under biaxial stretch is properly described with an orthotropic, Fung type hyperelastic model. The second Piola-Kirchhoff stress **S** can be computed by

$$\mathbf{S} = \frac{\partial W}{\partial \mathbf{E}} \tag{0}$$

where **E** is the Green-Lagrange strain tensor, and W is the stored energy function of the BP heart valve material. Pericardial tissues and heart valve leaflets are thin membranes, therefore two-dimensional constitutive laws are often implicitly assumed. A Cartesian coordinate system ($\mathbf{e}_1$, $\mathbf{e}_2$, $\mathbf{e}_3$) is employed with the 1- and 2-directions commonly in the plane and aligned along preferred and cross-preferred fiber directions respectively, and the 3-direction as the transversal direction. The in-plane bending response is neglected, and although pericardium and heart valve leaflets are not homogeneous membranes (i.e. there are observable variations across the thickness), the state of plane stress is commonly assumed (by definition, $S_{13} = S_{23} = S_{33} = 0$ and consequently $E_{13} = E_{23} = 0$, but $E_{33} \neq 0$ and often overlooked experimentally). Notwithstanding, it is worth remarking that Sun et al. [88] have

observed high in-plane shear stresses in GLBP generated with substantially asymmetric protocols (e.g. 1:0.1) while covering a wide range of the strain-stress space. Asymmetric protocols showed not only large shear response, but also lesser extensibility for the normal components, suggesting a substantial change in mechanical behavior under extreme T_{11}:T_{22} ratios. In order to account for this difference, more general constitutive relations accounting for high in-plane shear response or bending stresses can be obtained simply by complementing the 2D-plane stress tensor with additive higher order terms (cf. [88]) – nevertheless, more general and capable constitutive models often imply additional constants to be determined, and mainly, multiprotocol experimental data to be made available. The generalized Fung-type elastic 2D-anisotropic model under the assumption of plane stress is

$$W = \frac{c}{2}\left(e^{Q} - 1\right) \tag{0}$$

with

$$Q = a_1 {E_{11}}^2 + a_2 {E_{22}}^2 + 2a_3 E_{11} E_{22} + a_4 {E_{12}}^2 + 2a_5 E_{11} E_{12} + 2a_6 E_{12} E_{22} \tag{0}$$

Constants *c* and a_i, $i = 1,2,..,6$ are material constants, characterize the mechanical response of the material, and must be determined from experimental data reduction. Li and Sun performed biaxial mechanical testing on 25 mm x 25 mm squares of native and treated bovine and porcine pericardium [89], have observed the usual anisotropy of these tissues, and identified the X_1 direction as the stiffer orientation of the material and X_2 direction along the less stiffer direction determined by the equibiaxial testing protocol. Conducting a systematic set of stress-controlled test protocols with different stress ratios on 10 samples of each type of tissue, the authors have determined a set of constants using the Marquardt-Levenberg non-linear least squares method with a simultaneous fit of all the collected experimental data with a different testing protocols to reduce the effect of multiple collinearities (Table 9 and Figure 11).

Sacks and Chuong [90] have employed a different orthotropic stored energy function of the form (adopted from Choi and Vito [91] proposed for canine pericardium):

$$W = b_0\left[\exp\left(\tfrac{1}{2} b_1 {E_{PD}}^2\right) + \exp\left(\tfrac{1}{2} b_1 {E_{XD}}^2\right) + \exp\left(b_3 E_{PD} E_{XD}\right) - 3\right] \tag{0}$$

where PD and XD are tissue directions aligned with preferred fiber direction and perpendicular to preferred fiber direction determined by SALS. Choi and Vito [91] and Sacks and Chuong [90] have both obtained good fits of experimental data obtained with biaxial testing for canine and bovine pericardium respectively (not shown), and the latter have conducted a study on the effects of different chemical treatments on the mechanical properties of the tissue (Table 10).

Although the Fung model has been in the literature for many years, and systematic experiments to obtain its constants describing chemically treated multi-species pericardium have been conducted and published, its actual implementation into finite element formulations has been very limited – a major reason for this is the inherent numerical instability/convergence of the Fung model in numerical schemes due to its conditional convexity/elipticity [92] and exponential behavior (making small changes in strain result in large changes of stress). One often overlooked aspect of the employment of phenomenlogically-based hyperelastic models (not only Fung's model, but other models as well, e.g. such as Mooney-Rivlin's $W = \mu_1(I_1 - 3) + \mu_2(I_2 - 3)$ where I_1 and I_2 are the principal invariants of the left Cauchy-Green stretch tensor **C** and μ_1 and μ_2 are material parameters) to fit experimental data is associated with the restrictions necessary to be enforced in the parameter space such that the second law of thermodynamics is not violated. The stored energy function must remain positive-definite, and best fit values of the material parameters must yield physically realistic results for all deformations within the range of interest – two ways of ensuring this are either (i) to restrict a priori the allowable ranges of parameters that the regression can choose, or (ii) to check a posteriori that one does in fact obtain reasonable predictions with the best-fit parameters. The former has been subject of extensive research: particularly related with biological materials, Humphrey et al. [93, 94] performed biaxial testing on excised myocardium and has identified inequalities necessary to be satisfied by the best fit parameters, and Sun and Sacks [82] have restricted the parameter space of Equations (0) and (0) with the following inequalities

$$\begin{aligned} &c > 0, \\ &a_1 > |a_3|, \\ &a_2 > |a_3|, \\ &a_1 a_2 a_4 + 2a_3 a_5 a_6 - a_2 a_5^2 - a_1 a_6^2 - a_4 a_3^2 > 0 \end{aligned} \tag{0}$$

and demonstrated that these numeric constraints need to be imposed in order to achieve computational stability and have presented the first valve simulation using the Fung elastic model [82].

Not much novelty in regard to material models has been employed in BHV simulations besides standard hyperelasticity, where the application of phenomenologically-reasoned exponential forms (as originally proposed by Fung) has dominated over the polynomial and the logarithmic forms in the accurate description of cardiovascular tissue in general. However, these models do not account for fiber orientation directly (but here, it must be stressed that anisotropic hyperelastic material models are in fact naturally able to account for tissue anisotropy originating due to fiber orientation), and fiber orientation and material inhomogeneity is a key aspect not only of native heart valves, but also of bovine pericardium (Figure 12 and Table 10). The impact of material inhomogeneity in BHVs is twofold: (i) Sacks and Chuong [30] used small angle light scattering (SALS) to quantify the collagen fiber

architecture of the bovine pericardium sac and have observed large animal-to-animal variability in fiber architecture, precluding the use of an anatomic location as a simple guideline for selecting structurally consistent specimens, not only for material characterization but also for BP heart valve fabrication; and (ii) tissue structure and collagen fiber architecture are major factors of the anisotropic response of the tissue, therefore in order to minimize difficulties with its intrinsic structural and mechanical variability, structurally uniform specimens must be selected from the BP sac for material characterization [29, 28]. Only by conducting a two-step pre-sorting procedure with bovine pericardium examined with SALS, Sacks and Chuong [30] were able to collect biaxial test samples with a high degree of structural uniformity from regions of good structural consistency. The consistency of the samples was then reflected in the consistency of the mechanical properties and the small standard errors in the material constants for all specimens (Figure 13, Table 10), and in the ability to combine all experimental data into a single data set and reduce it to group material constants representing the data reasonably well and showing predictive capability.

Another important aspect is the inherent inability of phenomenologically-based hyperelastic models with parameters determined by fitting experimental data to obtain reliable predictions outside of the range of conditions tested. Although the determined parameters are reliable descriptors of the material behavior within the tested conditions (i.e. when one in interpolating material behavior from the experimental data), they fail considerably in ranges beyond the conditions tested. Phenomenologically-based hyperelastic models should not be used for extrapolating material behavior. Faced with such scenario, new datasets of material response under these new conditions of interest must be obtained, and new parameters must be fitted such that the hyperelastic model is once again able to interpolate material behavior. Overall, phenomenologically-based models are always hampered by the amount of experimental data that is or is not collected, and most importantly, the inherent need of multiprotocol data to capture effects that may not be observable within a certain experimental regime – indeed, only an infinite number of experiments is able to fully characterize an hyperelastic material. Finally, it is also generally perceived that these models encompass further disadvantages: they (i) require a large number of parameters to obtain accurate data fits, (ii) originate parameters without direct physically meaning, and (iii) possess a natural difficulty to account for regional differences in material behavior. These drawbacks have been responsible to drive the general preference to structurally-informed models where spatial dependent fiber orientation is explicitly incorporated in the constitutive model [95, 96, 51, 97].

5.2 - Structurally-informed Hyperelastic Models

The ability to go beyond the tested conditions with at least some degree of confidence and robustness is the main reason why structurally-informed models, derived from critical reasoning of

material structure and response, might be considered advantageous over their phenomenological counterparts. Over the last decade Sacks and co-workers have been developing and refining structural based constitutive models of planar soft tissues [98, 62, 51, 97], an approach based on the theoretical framework of Lanir [95, 99]. Structural models rely on experimental data characterizing the tissue microstructure and a representative volume element (RVE), which is large enough to represent the processes associated with the microstructure of the material in some average sense (particularly, the collagen fiber architecture), but yet small compared to the characteristic length scale of the bulk tissue (i.e. the tissue thickness). The RVE is treated as a fiber-reinforced three-dimensional continuum and it is assumed that the stress in the material can be obtained from the stored energy function of a hyperelastic solid following Equation (0).

Within the RVE, the following assumptions are made:

(i) Pericardium can be idealized as a planar network of collagen fibers embedded in a compliant ground substance, i.e. the matrix. Since pericardium contains only a small amount of elastin [100], its contribution is usually ignored. Further, the hydrostatic forces generated by the matrix are considered negligible compared to the fibers forces and are usually ignored (recently, Fata et al. [101] have proposed a 3 component structural model for pulmonary artery remodeling on which the effect of muscle and elastin were included because not only the mass fractions of each component were determined with biochemical assays, but also the effect of passive muscle and the elastin micro-structure was available using novel-biaxial mechanical-multiphoton microscopy).

(ii) Collagen fibers are undulated, and their undulation gradually disappears with stretch. The load required to straighten the collagen is negligible compared to the load transmitted by the stretched fibers. Hence, each collagen fiber transmits load only if stretched beyond the point when all its undulation has disappeared, and is assumed to be linear elastic.

(iii) The degree of fiber undulation can vary considerably. At the tissue level, the gradual straightening of the linear elastic collagen fibers with variable undulations produces the classical non-linear stress-strain relationship of soft tissues.

(iv) Fiber strain can be computed from the tensorial transformation of the global strain tensor referenced to the fiber coordinate system (i.e. the affine transformation assumption).

(v) The strain energy function of the tissue is the sum of the individual fiber strain energies.

Affine transformation from the bulk tissue to the collagen microstructure allows the determination of the uniaxial strain ε along each fiber from the global tissue strain state **E**

$$\varepsilon = \mathbf{n} \cdot \mathbf{E}\mathbf{n} \tag{0}$$

where **n** is a unit vector aligned with the fiber orientation ($\mathbf{n} = \cos\theta \mathbf{e_1} + \sin\theta \mathbf{e_2}$, thus θ is the angle of the fiber with the tissue $\mathbf{e_1}$ direction). The 2nd Piola-Kirchhoff stress in the fiber is given as a function of the fiber strain, and because the fiber is only able to carry stress along its direction, results in

$$\mathbf{S^f} = \mathbf{S^f}(\varepsilon) = S^f_{nn}(\varepsilon)\mathbf{n} \otimes \mathbf{n} \tag{0}$$

One component of the structural model is the fiber uniaxial stress-uniaxial strain law $S^f_{nn}(\varepsilon)$, which can simply be given by

$$S^f_{nn}(\varepsilon) = A\left[\exp(B\varepsilon) - 1\right] \tag{0}$$

with A and B positive constants.

The other component of the structural model is the tissue stress-strain relationship. The stored energy function of the fiber ensemble is the summation of the stored energies functions $w(\varepsilon)$ of each individual fiber of the ensemble and is achieved with the integration along all fiber directions

$$W_f = c_f \int_{-\pi/2}^{\pi/2} R(\theta) w(\varepsilon)\, d\theta \tag{0}$$

where c_f is the fiber volume fraction. Fiber angular distribution function $R(\theta)$ is a key component of the structural model. Unlike in many man-made composites, the angular orientation of collagen fibers in tissues is not known a priori. This feature is measured experimentally with small angle light scattering (SALS). SALS principle relies on the fact that angular distribution of scattered light $I(\theta)$ is directly proportional to the angular distribution of fibers [102].

The tissue stored energy function, assuming an isotropic strain energy contribution due to the matrix and a volume fraction of fibers given by c_f, results in

$$W = c_f W_f + (1 - c_f) W_m \tag{0}$$

with

$$W_m = \frac{c_0}{2} \exp\left[c_1 \left({E_{11}}^2 + {E_{22}}^2 + 2E_{11}E_{22} \right) \right] \tag{0}$$

where c_0 and c_1 are constants characterizing the isotropic mechanical response of the matrix. Finally, the stress-strain relationship,

$$\mathbf{S} = \frac{\partial W}{\partial \mathbf{E}} = c_f \int_{-\pi/2}^{\pi/2} R(\theta) S^f_{nn}(\varepsilon) \mathbf{n} \otimes \mathbf{n}\, d\theta + (1 - c_f) \frac{\partial W_m}{\partial \mathbf{E}} \tag{0}$$

or, in component form along the tissue directions, is given by

$$
\begin{aligned}
S_{11} &= c_f \int_{-\pi/2}^{\pi/2} R(\theta) S_{nn}^f(\varepsilon) \cos^2\theta \; d\theta \\
&\quad + (1-c_f) c_0 c_1 (E_{11}+E_{22}) \left[c_1 \left({E_{11}}^2 + {E_{22}}^2 + 2E_{11}E_{22} \right) \right] \\
S_{12} &= c_f \int_{-\pi/2}^{\pi/2} R(\theta) S_{nn}^f(\varepsilon) \cos\theta \sin\theta \; d\theta \\
S_{22} &= c_f \int_{-\pi/2}^{\pi/2} R(\theta) S_{nn}^f(\varepsilon) \sin^2\theta \; d\theta \\
&\quad + (1-c_f) c_0 c_1 (E_{11}+E_{22}) \left[c_1 \left({E_{11}}^2 + {E_{22}}^2 + 2E_{11}E_{22} \right) \right]
\end{aligned}
\tag{0}
$$

Sacks [51] employed the structural model described above and obtained good agreement with experimental data and small variations on constants A, B, c_0 and c_1 in Equations (0) and (0) (Table 11). Fiber angular distribution $R(\theta)$ is experimentally determined by SALS, thus values of constants A and B can be determined by fitting the results obtained with the equibiaxial strain test protocol ($E_{11} = E_{22} = E$) on which the contribution of the isotropic matrix can be removed by considering the stress difference $S_{11} - S_{22}$. Once A and B are determined, constants c_0 and c_1 could be found, while fiber volume fraction c_f was not known and was set at $c_f = 0.5$.

Alternatively, more complex structural models can be sought, particularly models incorporating a higher level of information of the microstructure, if available, and naturally able to describe the mechanisms of fiber recruitment and alignment upon deformation. This can be done in a structural sense starting from the mechanical response of individual fibers. However, as the number of fibers in a RVE can be one hundred or more, modeling individual fibers fully is not feasible. Therefore a stochastic approach is needed to derive a new ensemble stress-strain response using the mean fiber stress-strain response.

The structure of a collagen fiber network is composed of individually crimped fibers interwoven together. The crimping can be either sinusoidal in flat membrane like tissues [103] or helical in tendons [104]. Once straightened, these fibers appear to behave linearly in force vs. displacement [105-108] and this relation appears to hold valid for strains less than 0.35 [109]. The straightening behavior of the crimped phase, also unknown as the elastica effect, has been modeled by Freed et al. [110] and Garikipati et al. [111]. However, the simulation using a finite element model and Garikipati et al. model shows no significant or impactful effect at the fiber ensemble scale (Figure 14).

Within the tissue composite, small angle X-ray scattering and second harmonic imaging results demonstrate that these fibers also appear to follow affine deformation in valvular tissue [112].

Therefore, the local fiber stretches can be determined from the stretch of the fiber ensemble and the fiber strain ε required to straight the fibers. The gradual recruitment of fibers can be emulated using a statistical distribution $D(\varepsilon)$ [113, 114]. Physically, $D(\varepsilon)$ represent the fraction of fibers fully straightened between ξ and $\varepsilon+\Delta\varepsilon$, and can be represented by e.g. a Beta distribution

$$D(\varepsilon)=\frac{\Gamma(\alpha+\beta)}{\Gamma(\alpha)\Gamma(\beta)}\frac{x^{\alpha-1}(1-x)^{\beta-1}}{UB-LB};\qquad x=\frac{\varepsilon-LB}{UB-LB} \tag{0}$$

with α and β positive constants. Beta distributions are attractive in that the bounds of the distribution can be set, preventing unrealistic or even negative crimp values, and the parameters α and β can be expressed in terms of the mean and variance.

$$\alpha=-\mu\frac{(\sigma^2+\mu^2-\mu)}{\sigma^2},\qquad \beta=(\mu-1)\frac{(\sigma^2+\mu^2-\mu)}{\sigma^2} \tag{0}$$

Thus, an alternative to Equations (0) and (0) and assuming a mean elastic modulus *K* for the collagen fibers can be established. In previous literature, the stress strain relation that is linear in 2nd Piola Kirchhoff stress-Green Lagrange strain common [95, 114, 113], with the fiber stress-strain relationship

$$S_{nn}^{f}(\varepsilon)=K\int_0^{\varepsilon}D(x)\frac{\varepsilon-x}{(2x+1)^2}dx \tag{0}$$

However, based on a linear force displacement relation, a stress-strain relation that is linear in 1st Piola Kirchhoff stress-stretch can also be used:

$$S_{nn}^{f}(\varepsilon)=K\int_0^{\varepsilon}D(x)\frac{1}{2x+1}\left(1-\frac{\sqrt{2x+1}}{\sqrt{2\varepsilon+1}}\right)dx \tag{0}$$

For parameter estimation purposed, the two models behave with no observable difference. Due to the relatively small variations in crimped length of collagen fibers common is valvular and pericardial tissue, the collagen fibers extend by no more that 4-5% under physiological loading. Thus the two models, when integrated into an ensemble, are effectively the same; albeit the modulus estimated will be different.

In order to assess the improvements obtained with this better description of the microstructure and its inherent microstructural deformation mechanisms, Sacks [97] employed and compared both models, the fiber recruitment model with the two parameter model, but without considering the effect of the matrix to describe biaxial testing experimental data of untreated bovine pericardium (Table 12). Although both models attempt to describe the same microstructural behavior (fiber reinforcement, recruitment and lengthening), the former shows certain advantages when compared to the later. One key difference resides in the different models of fiber response (Equations (0) and (0)) and results in an

important characteristic that can be denominated terminal stiffness. Due to the simple exponential term present in Equation (0), it can be easily observed that the stress on the fiber increases exponentially with strain, therefore fiber stiffness (slope of the stress vs. strain curve) increases as strain increases; on the other hand, Equation (0) results in a linear increase of stress and a maximum fiber stiffness beyond a certain strain value, i.e. the terminal stiffness, which is observed experimentally. Overall, the advantage of the fiber recruitment structural model is its ability to provide insight into tissue function. In particular, the structural model allows for an explicit relationship between fiber straightening and recruitment and bulk tissue strain, and most importantly, allows for the formulation of hypothesis regarding tissue function at the microstructural level and their evaluation with parametric studies and sensitivity analyses, such as e.g. the influence of different degrees of collagen crimping on overall tissue response [97].

An important feature of the current structural approach is that summing the two expressions for the normal stresses under equibiaxial strain conditions ($E_{11} = E_{22}, E_{12} = 0$, thus $S_{12} = 0$), the fiber stress-strain law can be obtained directly from the experimental data using $S_{nn}^{f} = S_{11} + S_{22}$. Thus, the material parameters for S_{nn}^{f} (A and B on Equation (0) or K, α, and β in Equations (0)-(0)) are experimentally determined directly from the equibiaxial test data using the Marquardt-Levenberg nonlinear least squares method, which together with experimentally obtained fiber angular distribution $R(\theta)$ compose the entire set of material parameters of the fiber ensemble in the structural model. Once found, the matrix properties can then be determined with any of the non-equilibrated protocols. Other mechanical properties of other components of the stored energy function that could be accounted for, such as in plane bending stiffness, are determined afterwards with other experimental protocols.

Sacks et al. [115] recently developed the first rigorous full structural model (i.e. incorporating various features of the collagen fiber architecture) for exogenously cross-linked soft tissues. This was made possible, in-part, with the use of native-cross-linked matched experimental dataset and an extension to the collagenous structural constitutive model so that the uncross-linked collagen fiber responses could be mapped to the cross-linked configuration. This separated the effects of cross-linking from kinematic changes induced in the cross-linking process, which in turn allowed the non-fibrous tissue matrix component and the interaction effects to be identified. Native and cross-linked valvular tissues exhibit minimal time dependent effects [116-119]. Exogenous-cross-links induce fiber-fiber and fiber-matrix interactions that are mechanically significant. Sacks et al. [120] considered pericardial tissues to be composed only of collagen fivers and a matrix constituent that represents non-cross-linked and cross-linked components, and water. The contributions from elastin or other tissue components are ignored since they have either negligible mass or stiffness. In all previous structural

models of soft tissues, interactions between components have been ignored and Sacks et al. utilized the following hyperelastic general form

$$\Psi(\mathbf{C}) = \phi_c\left[\Psi_c(\mathbf{C}) + \Psi_{int}(\mathbf{C})\right] + (1-\phi_c)\Psi_m(\mathbf{C}) + p(J-1) \qquad (0)$$

where ϕ_c is the mass fraction of the collagen fibers, Ψ_c, Ψ_m, Ψ_{int} are the strain energy density functions of the collagen, matrix, and interaction terms, respectively, J=det(**F**), and p is the Lagrange multiplier to enforce incompressibility. The following *final form* of the constitutive model was used

$$\begin{aligned}
&\mathbf{S} = \mathbf{S}_c + \mathbf{S}_{int} + \mathbf{S}_m = \\
&\frac{\phi_c\eta_c}{{}_1^t\lambda}\int_{\theta_1}\Gamma_1\left[\mu_\Gamma,\sigma_\Gamma,\theta_1\right]\left\{\int_1^{{}_1^t\lambda}\frac{D_1(\mu_0,\sigma_0,{}_0\lambda_{lb}\,{}_0\lambda_{ub},{}_0^1\lambda\left[\theta_0(\theta_1)\right],x)}{x}\left(\frac{{}_1^t\lambda}{x}-1\right)dx\right\}(\mathbf{n}_0\otimes\mathbf{n}_0)\,d\theta_1 + \\
&\phi_c\int_\alpha\int_\beta\Gamma(\alpha)\Gamma(\beta)\left[d_0 d_1\left(\lambda_\alpha\lambda_\beta-1\right)e^{d_1\left(\lambda_\alpha\lambda_\beta-1\right)^2}\left[\frac{\lambda_\beta}{\lambda_\alpha}(\mathbf{n}_0\otimes\mathbf{n}_0)+\frac{\lambda_\alpha}{\lambda_\beta}(\mathbf{m}_0\otimes\mathbf{m}_0)\right]\right]d\alpha\,d\beta + \\
&(1-\phi_c)\left(\mu_a\left(I_1-3\right)^{a-1}+\mu_b\left(I_1-3\right)^{b-1}\right)\left(\mathbf{I}-C_{33}\mathbf{C}^{-1}\right)
\end{aligned} \qquad (0)$$

It is understood that $\mathbf{n}_0$ and $\mathbf{m}_0$ are referred to β_1 and that we merged the Lagrange multiplier with the matrix by assuming a planar tissue to simplify the formulation. This final model parameters has eleven independent fitted parameters $\left(\eta_c,\mu_\Gamma,\sigma_\Gamma,\mu_0,\sigma_0,a,b,\mu_a,\mu_b,d_0,d_1\right)$ and three directly determined parameters $\left(\phi_c,{}_0\lambda_{lb},{}_0\lambda_{ub}\right)$, all with a physical meaning.

While at first glance this appears to be a major non-linear optimization undertaking with all the usual pitfalls, a sequence to make actual parameter estimation quite tractable was employed:

1. From the native tissue mechanical data, we can predict the collagen phase parameters $\left(\eta_c,\mu_\Gamma,\sigma_\Gamma,\mu_0,\sigma_0\right)$ using standard procedures [121, 122].
2. From the pre-transition collagen recruitment portion of all of the EXL tissue mechanical data, determine the matrix parameters $\left(a,b,\mu_a,\mu_b\right)$.
3. Using the ${}_1^t\mathbf{S}_c\left(\eta_c,\mu_\Gamma,\sigma_\Gamma,\mu_0,\sigma_0\right)$ and $\mathbf{S}_m\left(a,b,\mu_a,\mu_b\right)$responses, determine the interaction stress responses for *all test protocols* using $\mathbf{S}_{int} = \mathbf{S} - \frac{1}{\varphi_c}\left(\varphi_c\,{}_1^t\mathbf{S}_c + (1-\varphi_c)\mathbf{S}_m\right)$.
4. Using the results of step 3, determine the final two parameters $\left(d_0,d_1\right)$ by fitting Eqn. (0) but only allowing them to vary while keeping the other terms to their above fitted values.

This basic sequence ensured a robust parameter set to be obtained, since the entire model is never fit at once. Moreover, this approach allowed the separation of the contributions to the stress of each of these mechanisms. The most novel findings were that (Figure **15**): 1) the effective collagen fiber modulus was unaffected by cross-linking, and 2) fiber-ensemble interactions played a large role in stress development, often dominating the total tissue response (depending on the stress component and loading path considered). An important utility of the present model is its ability to separate the effects of exogenous cross-linking on the fibers from changes due to the matrix. Applications of this approach include utilization in the design of novel chemical treatments that produce specific mechanical responses and the study of fatigue damage in BHV biomaterials.

5.3 - BHV critical engineering: modeling-driven experimentation and experimentally-based modeling

Critical BHV engineering aims to ensure valve functionality for its clinical performance with a combination of hemodynamic, biomechanical and biological aspects, e.g. sufficient effective orifice area, transvalvular pressure gradient, good leaflet coaptation without regurgitation, among others, and to predict and extend as much as possible valve durability. Rational methodologies and a quantitative approach must be pursued to optimize the device at all stages of its design process. However, experimental testing for material characterization alone cannot provide a reasonable assurance for comparing different candidate heterograft materials, as it is inconsequential to compare two different BHVs solely based on values of the material properties of its leaflets. Rather, it is essential to integrate multiple tests to increase the knowledge about the tissue and to generate a predictive model of its behavior, and only then, try to analyze biomechanical function, and possibly predict durability and provide assistance against the failure of the valve. While leaflet tears are the main failure mode of porcine valves [123], these can be caused by many factors including mechanical stresses, calcification, or crosslink deterioration. The mechanisms of fatigue and valve deterioration are very complex and are currently not completely understood, and ultimately the durability of a tissue is most frequently estimated experimentally via the use of an accelerated wear tester, which attempts to mimic the valve in vivo function.

Material property data can easily be obtained from basic experimental tests, such uniaxial, biaxial, or flexural mechanical testing. However, all heterograft tissues are composite materials, are highly inhomogeneous, clearly show anisotropic behavior, and undergo large deformations. Experiments for material behavior characterization must be performed with the objective of motivating the choice of proper models., and once the suitable model is defined, subsequent experiments must be performed not only to infer the validity of the model chosen, but also to determine the constants that describe the behavior of the material accurately. Unfortunately, systematic experimental data of bovine

pericardium, particularly, when subjected to biaxial test protocols, do not exist. To date, no material model is able to account in full for such complex observed microstructure and biological behavior, and the inclusion of such detailed information would certainly prove useful in extending the ability to better model and simulate the response of BHVs.

Nonetheless, (i) theoretical developments resulting in new and better models to describe the behavior of BHV tissues, and (ii) experimental advancements with novel techniques collecting data to understand and quantify such behavior, must proceed simultaneously and closely tied. With the objective of providing reliable experimental data for BHV simulation, Mirnajafi et al. conducted a systematic set of flexural experiments on native and glutaraldehyde-treated bovine pericardium and to date these seem to be the most employed set of material parameters describing these materials [68] upon flexure. With the goal of improving the understanding of the micromechanical changes chemical modification induces in native tissues utilized in BHV, the authors have investigated the relation between collagen fiber preferred direction and the resulting flexural properties, and have concluded that the flexural properties are indeed dominated by inter-fiber cross-links as opposed to the stiffness of the collagen fibers themselves. Subsequently, Mirnajafi et al. conducted tests following similar experimental techniques on porcine BHV heterograft materials with the objective of characterizing the fatigue failure behavior occurring in these materials upon cyclic flexure [115].

Once a suitable initial model has been established, the choice of experiments to support the model must be carefully considered. The three main considerations are the (i) determination of the constitutive model form, (ii) determination of the material parameters, and (iii) constitutive model validation. All three tasks are interrelated. Perhaps the best and earliest example of using data to guide the form of the material model is by Humphrey et al. [93, 94]. Here, the invariants suitable for the material were established initially. The mechanical testing was controlled so that only a single invariant was allowed to vary at a time, thus deducing the dependency of the model on each. For more complex models, such as structurally informed models, this may not always be possible. However, certain kinematical state, i.e. equibiaxial strain, can be used to independently determine the contribution of the fiber ensemble response by summing the principal components [124, 113]. Additional, the fiber and matrix contributions can be separated by subtraction [124, 113].

Alternative testing methods can also be used as a way to valid the form of the model. For example, although uniaxial testing provide an incomplete description of the tissue mechanical behavior, when the fibers are highly aligned, uniaxial stretch along the preferred direction can be used as another way to estimate the ensemble behavior. In elastin rich tissues, low stress biaxial testing and flexural studies can be used to determine behavior of matrix and elastin separately from the behavior of the collagen fiber ensemble [124]. Imaging methods, such as small angle X-ray scattering, have been used

in combination with mechanical testing to examine the form and modulus of the stress-strain relation of collagen fibrils [105-108]. Obviously, structural parameters are best measured directly rather than obtained through optimization. Given sufficient a priori information, the number of parameters in structural models that needed to be optimized can be drastically reduced. The remaining parameters should be optimized against a sufficient range of data relative to those needed for ultimately simulation purposes and then validated against different datasets. In cases where data such as the above cannot be acquired on a specimen to specimen basis, they may be measured separately and used as validation. Through the process, it is common to find the need to alter/refine the model assumptions based on unexpected/unpredictable experimental results. At this point, additional experiments for hypothesis formulation and subsequent parameter determination should be done – model development is an iterative process between experimentation, theoretical formulation, and validation of predictive capabilities.

The employment a proper constitutive model – not only the choice of its specific form, but also the correct determination of its parameters – gains relevance when the next step is to perform FE simulations of the entire BHV to compute leaflet strains and stresses. In reality, leaflet tissues will deform by the same amount in response to the same force independently of the choice of constitutive model one uses in the attempt to describe such behavior. The forces and displacements measured in the laboratory, and consequently, the strains and stresses experimentally determined, will not change if a different constitutive model is chosen to describe its response. However, the descriptive/predictive capabilities of any analysis conducted with a computational model and the underlying constitutive formulation necessary will depend dramatically on all modeling assumptions made. Crucial questions are “what is the impact of picking different constitutive models in the organ-level simulation of a BHV?”, “what difference do phenomenological or structurally-based constitutive models make?”, and “what difference does different experimental protocols to obtain material parameters have?”

The answers to these questions are not straightforward. First, one must understand that biological tissues have complex morphology and response; therefore a certain degree of approximation is always associated with the choice of a constitutive model. The choice of a constitutive model is not an easy task to undertake as it is highly subjective and dependent on the desired degree of complexity/effort/accuracy. Certainly some models are better than others, but on the other hand, there are certain kinds of behavior that can be disregarded outright for the sake of simplicity, and sufficiently accurate simulation can still be achieved. Simulations and sensitivity analyses have been conducted with different extents of simplifying assumptions, such as e.g. different choices between phenomenological or structurally-based models (e.g., de Hart et al. [125] and Driessen et al. [126]), and on constitutive assumptions such as material homogeneity or non-homogeneity, isotropy or anisotropy,

and elasticity or viscoelasticity. Experimental evidence and computational simulations by Burriesci et al. [127] and Li et al. [81] have shown the impact of different choices of constitutive models to simulate valve function and have observed that the stress and strain distribution in the leaflets was severely impacted by the homogeneous/inhomogeneous and isotropic/anisotropic modeling choice. Sun et al. [128] have compared the effect of spatial inhomogeneity in the material parameters of the valves and have determined material properties of each leaflet individually and have observed significant differences between two simulations of the entire valve apparatus: (i) one simulation was conducted with material properties corresponding to each leaflet, whereas (ii) the second simulation employed properties of one leaflet in all three. The authors have observed substantial differences in the leaflet stress and strain distributions Experimental evidence by Stella et al. [118] showed strain rate indifference upon deformation of valvular tissues across several orders of magnitude of strain rates has demonstrated that the dissipative mechanisms for creep and stress relaxation are functionally independent and may indicate that the viscoelastic component is indeed negligible in valve physiology and in organ level simulations of valve function.

Notwithstanding, the simplifying assumptions described above were still employed successfully (to some extent) not only to critically aid BHV design, but also to improve the existing knowledge of the mechanisms of valve failure. Without pursuing the goal of complete comprehensiveness, typical state-of-the-art computational simulation of BHVs is reviewed below.

6 - Computational Simulations

6.1 - Overview

The analysis of native and prosthetic valve mechanics has been extensively conduced in silico through computational simulations with the aid of the finite element method [129, 130]. Although most studies have initially been conducted with simplified geometries and basic material models, and sometimes, with idealized physical settings, finite element modeling studies have been able to guide design and manufacturing techniques with relative success [131-138]. Simply by changing leaflet shapes and frame mounting methods, the stress distribution pattern acting on the leaflets is altered – as illustrative examples, Hamid et al. have predicted an increase of stresses on the closed leaflets as stent height is reduced [136], and Cacciola et al. demonstrated that a stentless design could reduce stress peaks by up to 80% for a sinusoidal fiber reinforcement layout with respect to a stented valve with the same reinforcement [137, 138]. Through observations made from computational simulations and experimental data, Salgo et al. proposed a teleologic argument of the characteristic saddle shape of mammalian mitral valve leaflet as a configuration that confers a mechanical advantage by adding curvature and reducing stress [139]. Each of these small pieces of knowledge, if seen individually,

certainly may have had just slight impact on the modus operandi associated with the overall design process of BHV. On the other hand, if taken as a whole and over the course of the 30 years since the inception of BHV, one is able to perceive and quantify the huge impact on success rates of clinical interventions and on the feasibility of the technology achieved with dramatic improvement on the durability of BHVs and better chemical treatments for heterograft materials. Nonetheless, the field has reached a point of current stagnation and general lack of progress – durability issues continue to hamper BHVs and the range of 10-15 years has remained unchanged over the last decade. The continued lack of rigorous mechanistic knowledge of in vivo durability and means to simulate effectively xenograft biomaterial responses in new designs (besides heart valve replacement in large animal studies with their associated difficulties, cost, and experimental variability) has hampered the research and development of novel and better BHVs.

Continued progress requires a much more sophisticated level of understanding. Computational simulations, in conjunction with bench-top and large animal experimental studies, can help to define how evolving biomaterial biomechanical properties drive valve function and performance. Computational studies are certainly limited on their range of applicability, in particular when applied to complex mechanical problems such as in BHVs, but have had the ability to shed light into the clarification of possible mechanisms of valve failure and to quantify BHV design improvements, at least, indirectly. Regions of high stress concentration determined computationally, particularly high tensile and bending stresses, have so far been correlated successfully with regions of tearing in BHV observed in vivo [140, 141] – the adverse mechanical environment occurring within the leaflet can either directly accelerate tissue structural fatigue damage, or initiate calcification by causing structural disintegration and enabling multiple calcification pathways that lead to valve failure [11, 142]. Although details of the process are unclear, it is widely and pragmatically accepted that valve designs that reduce leaflet stress are more likely to result in improved performance in long-term applications. Computational studies can be employed in a very cost effective and reliable manner to optimize such design process.

Even from a purely mechanical standpoint, computational simulations of functioning heart valves are not at all trivial [143]. The realistic geometry of a heart valve is quite complex, and in particular, leaflets are very thin (on the order a few hundred μm). The unpressurized geometry of a BHV can be carefully characterized at the bench, however upon implantation is deformed into place. Most importantly, substantial host-implant interactions and adaptations occur acutely, evolve over time, and the resultant in vivo geometry of a BHV is rather difficult to predict reliably. Segmentation of medical images is difficult to conduct for such thin and complex structures and there are always crude approximations whenever realistic geometries are attempted from stacks of microCT, ultrasound or MRI data. Moreover, not only the realistic geometry is taxing, but also can pose certain problems in regard

to meshing due to its thinness. The heterograft material is highly inhomogeneous, being composed of collagen bundles aligned along preferred directions with multiple dispersions, and both parameters are highly dependent on spatial location within the leaflet. Leaflets are adjoined at the commissures, and a general lack of detail of the particularities of these junctions, e.g. local microstructural environment, still exists. Sliding contact with friction in between leaflets occurs in the co-aptation area upon closing, and inertial effects may be important due to the rapid dynamic motion of valve function. Heart valves function on a highly dynamic fluid environment and realistic boundary conditions are either difficult to specify (for example, assuming hydrostatic differential pressure, but disregarding shear tractions occurring due to blood flow), or difficult to compute with fluid-structure interaction techniques (a severely difficult meshing problem as the fluid domain changes topology with valve closing). All of the above challenges are related with mechanical aspects and modeling assumptions are usually made to either simplify the problem or tackle the difficulties – on top of those, the biological aspect must be somehow included, and here, the lack of fundamental understanding is even more pronounced. The purist desire to model rigorously and accurately every detail and phenomena involved in BHV function is clearly ill-posed and will not be certainly possible within the near-future – on the other hand, the approach should be pragmatic instead. Modeling efforts should focus on clinically-driven critical engineering with the sole objective of better informing design methods to achieve clinical improvements, mitigate valve dysfunction, and improve valve durability.

Numerous challenges are encountered in numerical simulations of native and BHV, including: (i) proper determination of a geometry, either idealized [131, 136, 132] or morphologically realistic obtained from ultrasound, computed tomography, or magnetic resonance imaging [130]; (ii) challenges of rigorous fluid-structure interaction analyses [144-146, 130] and the role of mechanical forces in leaftlet coaptation [147, 148] and valve dysfunction; (iii) inhomogeneous, nonlinear, and anisotropic leaflet mechanical properties [149, 90, 98, 150]; and lastly and quite often overlooked, (iv) the experimental validation of in silico simulations [133, 134, 151] or the lack of thereof.

The importance of experimental validation, in addition to accurate material models and simulation methodologies, cannot be overstated. However, experimental measurements of leaflet strain for validation are difficult to preform owing to practical limitations in obtaining measurements very close to the leaflets and valve housing. Thus, previous finite element studies offered no experimental validation (e.g. [132, 133, 152, 136, 149]), or simple validations that only demonstrate comparisons of gross leaflet geometric configurations with pulse duplicator images [134, 151]. Gorman et al. developed a sonomicrometry technique to track the three-dimensional geometry of native heart valves in vivo. The technique relies on the determination of the path of an array of sonocrystals placed in the leaflet and allows the calculation of the local strain field and the validation of computational simulations [153].

Gorman et al. imaged the ovine mitral valve [153], and Sacks et al. employed the technique to determine the dynamic in vivo strain field of a functioning mitral valve anterior leaflet, which indicated large anisotropic strains and very high strain rates [154] (Figure 15). Sonomicrometry has been extensively used up to 16-weeks in vivo in native heart valves in the ovine model and has provided critical information to improve clinical interventions such as ring annuloplasty and mitral valve repair [155, 156]. Nevertheless, it must be remarked that sonomicrometry is a limited technique and yet unproven in BHVs – although it has been shown that markers do not interfere with the biaxial mechanical properties of the tissues tested in vitro and the shape and motion of instrumented valves in vivo obtained with echocardiographic imaging, the limited size of markers arrays usually result in a poor resolution of the strain field. Moreover, the technique is not trivial and there are several difficulties associated with marker tracking, marker detachment, and data post-processing. Validation techniques should rely on the resolution of the motion during valve function, either in vivo or in vitro – several techniques have been developed, mostly relying in the tracing of implanted markers [157-159]. An alternative possible validation methodology employs the methodology of Iyengar et al. [160] of resolving leaflet motion using structural light projection. Their system features a structured laser-light projection technique, eliminates the need of markers, and allows imaging of the complete valve leaflet surface dynamically with high temporal and spatial resolutions.

6.2 - Representative biomechanical modeling results

Computational simulations have been used mainly with the purpose of determining the stress distribution on the leaflets, correlate regions of stress concentration with regions of leaflet calcification and/or leaflet tear in implanted valves, and guide the design process with such information. Rousseau et al. incorporated fiber reinforcement and the viscoelastic properties of a porcine bioprosthetic valve leaflet in their FE analysis with time-varying pressure load on the leaflets and have found that regions of high fiber stress, located near the aortic ring, correlated with some common regions of valve failure [161]. Grande-Allen et al. have employed realistic geometries obtained with MR images of human valve specimens with higher order shell elements that incorporated anisotropic material behavior coinciding with the collagen fiber alignment. The authors were able to analyze the variations of stress across the valve and root, attributed such differences to inherent morphologic asymmetry and stress sharing, and claimed that bioprosthetic valves should be assembled using leaflets from three different porcine valves or from bovine pericardium with the objective of better replication the normal human valve asymmetry and human leaflet size arrangement [162]. Subsequently, Grande-Allen et al. extended their computational analysis to study the effects of aging [163], aortic root dilation [164], valvular incompetence due to Marfan syndrome [165], and clinical procedures associated with valve sparing [166, 167]. Overall, the geometries of the AV and of the aortic root play a substantial role in AV

biomechanical function. Most importantly, the characteristics of the aortic root are very patient-specific, and are pivotal to optimize surgical procedures and could possibly inform bioprosthetic valve design. Through computational simulations with morphologically realistic aortic root obtained from MRI data, Conti et al. [168] has shown that anatomical differences between leaflet-sinus causes substantial differences in stress and strain patterns, specifically due to leaflet asymmetry. Labrosse et al. [169] employed a comparable methodology from transesophageal echocardiography to obtain patient-specific geometric models of the AV and aortic sinus. The computational simulations demonstrated agreement in leaflet coaptation area with the medical images, and the authors were able to associate in a comparative sense regions with higher values of mechanical stress to regions of higher risk of tearing and/or development of calcification.

Sun et al. [83] presented a study of prosthetic valve deformation under quasi-static loading. In this study, quasi-static leaflet deformations under 40, 80, and 120 mmHg transvalvular pressures were simulated in a pericardial BHV (Figure 17). A Fung-elastic material model utilizing material parameters derived from actual leaflet biaxial tests and measured leaflet collagen fiber structure axes obtained from physical leaflets were used (Figure 18) [82, 170]. Rigorous experimental validation of the predicted leaflet strain field was used to validate the computational results of the simulations. An overall discrepancy of 2.36% strain between the FE model results and the experimental measurements was obtained, indicating excellent agreement between computed and measured principal strains. Results generally indicate that the peak stress always occurred in the vicinity of the commissures, with the lowest stress occurring near the free edges (Figure 17). High stresses were also observed in the belly region in all three leaflets in similar locations on the aortic side. The free edge experienced the less amount of stress on the ventricular side surface, consistent with the stress levels determined at the free edge on the aortic side. This is most likely to be due to the contact of the leaflets that lead to compressive stress at the free edge. Sun et al. extended the analysis to infer the effects of tissue anisotropy by conducting parametric studies utilizing the material parameter set from one leaflet for all three leaflets and noticed that a substantial variation in leaflet stress and strain distributions, and concluded the importance of using actual leaflet material properties and the profound impact of the degree of material anisotropy for accurate BHV FE simulations [83]. Subsequently, Li and Sun extended the computational simulations to investigate the effects of pericardial tissue thickness and pericardial material orientation and have observed a general decrease of peak stresses with decreasing leaflet thickness and when the stiffer direction of the material is aligned with the circumferential direction of the leaflet [89]. This type of material orientation is indeed observed in native aortic leaflets, where the collagen bundles are predominantly aligned along the circumferential direction [98].

Sun et al. also conducted simulations to investigate the correlations between calculated stress distribution and common regions of failure in tissue valves [83]. The failure phenomena of leaflets in valve prostheses basically may be divided into the following three types: (i) leaflet calcification, tearing and laceration [171]; (ii) tears in the leaflets in the vicinity of the commissure [172]; and (iii) leaflet tears associated with suture attachments [172, 173]. Sun et al. simulation results indicate that the highest tensile stresses occurred in the vicinity of the commissure region and in the belly region. It is possible that the tears and perforations that were observed in these regions are due to these high tensile stresses. Valves in the closed state also experience bending stress, especially at the co-aptation area. Negative values of the minimum principal stress are found in the co-aptation area and edges where the leaflets are attached to the stent. These compressive stresses, despite their minimal magnitude, may cause fiber wrinkling and lead to the flexure damage of collagen fibers and, consequently, damage leaflets [174].

Kim et al. proposed a new modeling approach for heart valve leaflets using the stress resultant shell theory [175, 176] – the point of departure is the employment of separately characterized constitute models for the in-plane and flexure response of the leaflet tissue, the former characterized with biaxial in-plane material tests [82], and the latter with three-point bending [69]. Kim et al. implemented the anisotropic models into the stress resultant, geometrically exact shell element developed by Simo et al. [177, 178]. Kim et al. performed dynamic analyses of a pericardial BHV during the opening and closing phases of a human complete cardiac cycle under physiological conditions and obtained results that compare favorably with in vitro dynamic simulation in a pulse duplicator. Wavy wrinkles were observed along the free edges during closing as the leaflet moved quickly inward due to the high pressure load on the aortic side, but disappeared when the free edge region reached the contact position (Figure 18). Co-aptation area was approximately 35% (clinical studies considered ideal co-aptation when 30-50% of cusp area is involved [179]), hence Kim et al. result indicates that the dynamic simulation well-represented a healthy pericardial BHV at the fully closed position. Relatively high stresses first occurred near the belly and free edge region and then spread over both sides of the commissural attachment area during the opening phase. The highest stress were then observed primarily in the vicinity of both sides of the cuspal commissure at the fully closed position, correlating properly with photographs and radiographs of calcified areas in the BHV reported in previous studies [140] and supporting the hypothesis that in-plane stress concentration within the leaflets induces calcification. Bending moment distribution demonstrated slight different patterns from the in-plane stress distribution, particularly during the closing phase. Relative high bending moments were observed near the center region of the co-aptation edge line where high curvature is induced, and this finding shows good agreement with the areas of mechanically damaged collagen fibers within BHV leaflets [180]. Similarly, regions of

compressive stresses during the closing phase correlated with regions structural damage [11]. These results favor the hypothesis that collagen fiber structures are more vulnerable to in-plane compression rather than in-plane tension (the latter usually associated with calcification), and that dramatic curvature changes and even curvature reversal occurring during valve operation induces high flexural strain and damage by severe inter-laminar shearing, and consequently, out-of-plane bending stresses might be more hazardous for structural damage than in plane stresses after all.

6.3 - Challenges in the computational simulation BHV function – fluid structure interaction.

BHVs operate in the vasculature: their mechanical environment includes the surrounding blood flow. The influence of blood flow on a closed valve may be modeled as a (quasi-) static pressure load, but insight into the dynamic opening and closing processes requires a more sophisticated modeling approach. These considerations motivate ongoing research on fluid—structure interaction (FSI) simulations of heart valves, which couple numerical methods for structural mechanics of valves to those for computational fluid dynamics (CFD) of the surrounding blood flow. FSI studies of BHVs are still nascent – as FSI techniques generally improve and the effects of blood flow are accounted in BHV simulations, their accuracy and relevance will certainly improve.

Native and prosthetic valves present a number of unique challenges for FSI analysis. Foremost among these is the fact that the heart valve leaflets contact one another, changing the topology of the fluid subdomain. Standard arbitrary Lagrangian-Eulerian (ALE) [181-183] or deforming-spatial-domain/space-time (DSD/ST) [184, 185] numerical schemes, which continuously deform a mesh of fluid elements that is fitted to the moving fluid-structure interface, are no longer directly applicable. To salvage such methods, one must augment them with special techniques to handle extreme deformations like topology changes. One solution is re-meshing, i.e. generating a new mesh for the fluid sub domain whenever its deformation becomes too extreme [186-189]. This allows computations to proceed, but introduces additional computational cost and numerical errors associated with the projection of fluid solutions from old to new meshes. Recent work by Takizawa et al. [190] introduced the space-time with topology change (ST-TC) method, which extended the DSD/ST framework to allow topology changes without re-meshing. The ST-TC method was employed to resolve the fluid dynamics problem of a heart valve with prescribed leaflet motion,[191] but the application of ST-TC to complex FSI with sliding and/or unpredictable structural self-contact remains an open problem. Makhijani et al. [192] reported a boundary-fitted BHV FSI simulation, but replaced true contact with inverse-square repulsive forces between leaflets and a symmetry plane. While the results were promising, no further analysis using this method was pursued.

In light of the difficulties encountered in boundary-fitted FSI analysis of heart valves, the overwhelming majority of work to-date on native and BHV FSI analysis has followed in the tradition of

Peskin's immersed boundary method [193]. While it is not a universal convention, thi review follows references [194, 195] in applying the term "immersed boundary method" liberally, to any numerical method in which the fluid and structure meshes are not required to match at the fluid-structure interface.. Highly variable interpretations of the term "immersed boundary methods" do exist, and explicit clarification of its meaning is highly recommended. Immersed boundary methods greatly simplify the treatment of large structural deformations and structural self-contact, but add some disadvantages (relative to ALE and DSD/ST), specifically in capturing boundary layers near the FSI.[196]. Takizawa et al. [197] found that the resolution of such layers is essential to obtaining accurate interface shear stresses in hemodynamic analysis. A comprehensive overview of various immersed boundary methods, their properties, and diverse applications can be found in several review articles (cf. references [194, 195]). An even more radical departure from boundary-fitted FSI is to discretize the fluid using a mesh-free approach, such as smoothed-particle hydrodynamics (SPH) [198]. SPH is not widely used in CFD or FSI areas of research, but has been applied to evaluate mechanical,, bioprosthetic, and native mitral valve function [199].

Peskin originally introduced the immersed boundary concept in 1972 with a crude representation of the heart valve as a collection of markers connected by elastic fibers,[193] specifically to meet the demands of heart valve FSI analysis. In the early 2000s, de Hart et al. [200-202] and van Loon et al. [203-205] used the immersed boundary method re-introduced by Baaijens [206] to couple finite element discretizations of heart valves and with computational fluid dynamics analyses of blood flow. This allowed for investigation of various constitutive models, but numerical instabilities prevented analysis at realistic Reynolds numbers and transvalvular pressure levels. Increasing availability of parallel computing resources in the last decade has led to higher resolution simulations of heart valves in recent years. Griffith [207] adapted Peskin's original immersed boundary approach to modern distributed-memory architectures and included adaptive mesh refinement for the fluid sub problem to compute FSI of a native aortic valve throughout a full cardiac cycle, with physiological flow velocities and pressure differences. The highest resolution heart valve FSI simulation is due to Borazjani [208], who applied the curvilinear immersed boundary (CURVIB) method [209, 210] to simulate systolic ejection through a bioprosthetic aortic valve. The valve leaflet models of Griffith and Borazjani suffered from deficiencies; Griffith applied Peskin's original connected markers; while Borazjani omitted bending stiffness. The CURVIB method was recently extended to include fluid-shell structure interaction by Gilmanov et al. [211, 212], but the efficacy of the approach has not yet been demonstrated for the portion of the cardiac cycle in which the leaflets are coapted and must support large transvalvular pressure differentials. Kamensky et al. [213-216] have modeled the valve leaflets as Kirchhoff—Love thin shell structures using isogeometric analysis (IGA) [217] (cf. Kiendl et al. [218, 219] for methodology

details and Figure 19 for representative results). Recent work by Kiendl et al. [220] and Buganza-Tepole et al. [221] has shown that IGA of Kirchhoff—Love shell structures can easily incorporate a wide variety of 3D constitutive models specifically suited for thin biological membranes with complex anistropic behavior. Morganti et al. [222] found that IGA greatly improved the representation of leaflet co-aptation in structural simulations of native aortic valves, with traditional finite element analysis requiring approximately 200 times as many nodes as IGA to compute a qualitatively-correct co-aptation region.

Current state-of-the-art immersed boundary FSI approaches have relied on academic research codes. However, the commercial software LS-DYNA [223] have been used for FSI simulations of bioprosthetic and native aortic valves [224-227] since the late 1990s with immersed boundary methods. The time-explicit procedures used by LS-DYNA result in severe Courant—Friedrichs—Lewy conditions that limit the maximum stable time step size in hemodynamic computations, because blood is nearly incompressible, rendering the problem effectively parabolic.[228, 229] Sturla et al. [226] circumvented this difficulty in an aortic valve simulation by artificially reducing the speed of sound in blood by a factor of 10, reporting that the fluid density variations introduced by this deliberate modeling error were negligible. The use of other commercial off-the-shelf analysis software for heart valve FSI analysis may be possible using so-called “black box” coupling algorithms [230] to connect independent finite element analysis and CFD programs without access to their internal details. Specialized methods are required for stable and efficient black box coupling of fluids to thin, light structures such as heart valve leaflets [231, 232]. Astorino et al. [233] applied a novel black box coupling algorithm to FSI analysis of an idealized aortic valve.

Current immersed boundary FSI techniques are able to incorporate both the physiological flow conditions and realistic solid constitutive models needed to produce estimates of bending and tensile stresses in heart valve leaflets. However, their weakness in resolving boundary layers prevents accurate predictions of shear stresses at the interfaces and phenomena associated with them such as hemolysis, thrombosis, or cavitation. The further development of boundary-fitted FSI analysis techniques therefore remains important to computational simulation of heart valves. Determining the range of applicability of any FSI model will depend ultimately on rigorous experimental validation, comparing computed leaflet deformations to quantitative in vitro measurements. Such measurements may be collected through techniques such as stereo photogrammetry [159, 234] or structured light projection [235, 236]. However, no such validation has ever been carried out.

6.4 - Challenges in the computational simulation BHV function –geometry and properties.

Valve leaflets are thin-walled structures that have sometimes been modeled as membranes [79, 152, 161] or shells [133, 132], the key difference being the modeler’s choice to exclude (i.e. neglect) or

include bending stiffness respectively. Even though each formulation has its own limitations, these are the most appropriate and realistic types to represent the characteristics of thin-walled leaflet structures. Modeling leaflets as tension-only membrane structures essentially eliminates bending effects. However, previous studies using shell elements did show that leaflets were subjected to bending, bending stresses are substantial in BHVs during the cardiac cycle due to the large deflections leaflets undergo [132, 160], and bending damage is one of the main causes of valve mechanical damage [174]. Another alternative is the use of three-dimensional elements [134], however it was noticed that there are severe problems of modeling thin structures with brick elements [237]. Moreover, three-dimensional FE formulations will necessitate a three-dimensional constitutive model, which requires the determination of tissue properties in the out-of-plane direction, or else, the addition of underlying assumptions or the expansion of two-dimensional experimental data into a three-dimensional constitutive law [238, 150, 170]. Enforcing material incompressibility is another aspect whose difficulty is rather simplified with a two-dimensional approach, realized by kinematic constraints for the plane stress [82], whereas the three dimensional approach requires a generalized penalty method.

The effects of using different material models has also been investigated by Patterson et al., who compared the effects of using linear and nonlinear isotropic elastic models of leaflets [239]. The authors found that the nonlinear model was more responsive to time-varying pressure waves, and induced a lower compressive, but higher tensile stresses in leaflets. Burriesci et al. [151] studied the effects of mechanical orthotropy of a pericardial heart valve and found that even a small amount of orthotropy can significantly affect the mechanical behavior of the simulated valve. Li et al. [149] modeled porcine heart valves as transversely isotropic material with fiber-reinforced composite based on uniaxial extension experiments and have observed significant changes in the stress patterns and in the location of the peak stress due to the nonlinear anisotropic behavior of the material model composing the leaflets. Moreover, even though native [98] and bioprosthetic leaflet mechanical properties [90, 150] have been demonstrated to be mechanically anisotropic, no studies yet have utilized leaflet mechanical properties, geometry, and fibrous structural information of actual BHV to assess the effect of inter-leaflet variability in the resulting leaflet stress.

The unpressurized geometry of a BHV can be carefully characterized at the bench, however upon implantation is deformed into place. Most importantly, substantial host-implant interactions and adaptations occur acutely, evolve over time, and the resultant in vivo geometry of a BHV is rather difficult to predict reliably.

The geometric characterization of a BHV and the translation of mechanical properties measured at the bench into in silico simulations is of crucial importance for accurate and rigorous BHV simulations. The unpressurized geometry of a BHV can be carefully determined at the bench before

implantation; however, this configuration may not be free of residual/internal stresses originating from fixation/manufacturing processes. Subsequently, BHVs are implanted, interact and adapt acutely with the host tissue, and over time, long term evolution occurs in an unavoidable process that will eventually terminate in failure at the end-life of the implant. Evolution of the implant entails not only a progressive shift in the initially-considered "reference" configuration, but also on a substantial change in measurable mechanical properties. The most commonly used technique for determining the mechanical properties of heart valve leaflets is direct ex-vivo experimentation; however, such techniques require explanation, preventing their usability in a clinical setting. Also, changes in tissue structure and shape as it is explanted (e.g. valve's reference configuration [156]), leads to challenges in relating ex-vivo measurements to its in vivo behavior. With the objective of avoiding the need for excision, inverse modeling approaches have been employed to determine accurately and reliably the mechanical properties of valve leafletsRecent advancements in 3D ultrasound technology provide the opportunity to obtain patient specific valve images in vivo [240], specifically the shape of the leaflets as they are loaded during the closing phase without the need to include physical markers that severely hamper the clinical applicability of the inverse-modeling approach – these methods are certainly the only resort to characterize native leaflets non-invasively in vivo, but their direct translation to monitor the performance of BHVs over their service life could yield important data to improve insight on failure mechanisms and possibly aid the design of more durable heterograft tissues and better BHVs.

BHV leaflets are highly non-homogeneous materials, composed by collagenous bundles inside extracellular matrix composed of elastin, GAGs, and other traditional connective tissue components. Collagenous bundles have a preferred direction of alignment and some degree of dispersion, and most importantly, these parameters are spatially dependent within the leaflet and confer local anisotropy to the tissue. Material models accounting for such spatial distribution, which can nowadays be accurately resolved experimentally with e.g. small angle light scattering [102], are of the utmost importance for accurate computational simulations of the function of BHV. Material microstructure and their multiple length scales are usually dealt with two distinct strategies – on one hand, micromechanics and multiscale methods attempt to segment and describe the detailed microstructural topology of the material and the interaction in between constituents and their response, and with such, structurally informed models are built; on the other hand, homogenization techniques attempt to employ such information in a representative volume element to obtain homogenized constitutive models; nevertheless, the pivotal point is that both strategies should yield models able to describe the experimental data collected on the mechanical behavior of the material at the bulk level and be employed accurately in properly validated BHV simulations. Regardless, it is not presently possible to determine the fiber structure of native heart valve of BHV leaflets on per-patient basis without

explanting them. While this is less of a problem in BHVs at implantation stage (where the materials employed to construct them are well defined and characterized), the determination of possible evolutions of fiber orientation after implantation requires either explantation followed by ex vivo material analysis and characterization, or alternatively, inverse modeling approaches with population averages to yield such measurements [156, 240].

Current state-of-the-art in incorporating biological material inhomogeneity into computational models employs techniques based on population averages, structure templates, and three-dimensional mapping. Aggarwal et al. [241] have developed a spline fitting techniques to connect surface deformation with structure. More generally, determining the biomechanical behavior of heart valve leaflet tissues in a non-invasive manner remains an important clinical goal. While advances in 3D imaging modalities have made in-vivo valve geometric data available, optimal methods to exploit such information in order to obtain functional information remain to be established. Aggarwal et al. [242] developed a novel leaflet shape-based framework to estimate the biomechanical behavior of heart valves from surface deformations by exploiting tissue structure. The authors determined accuracy levels using an "ideal" in-vitro dataset,[82, 83] in which the leaflet geometry, strains, mechanical behavior, and fibrous structure were known to a high level of precision. By utilizing a simplified structural model for the leaflet mechanical behavior (cf. Equation (0)), the number of parameters to be determined per leaflet were reduced to only two. This approach allowed dramatically reduced computational time and easily visualize the cost function to guide the minimization process. It was determined that the image resolution and the number of available imaging frames were important components in the accuracy of the framework. Furthermore, their results suggest that it is possible to detect differences in fiber structure, thus allowing an opportunity to diagnose asymptomatic valve diseases and begin treatment at their early stages. Lastly, good agreement of the final resulting stress-strain response was observed when an averaged fiber architecture was used. This suggests that population-averaged fiber structural data may be sufficient for the application to in-vivo studies, although clearly much work remains to extend the present approach to in-vivo problems.

6.5 - Challenges in the computational simulation BHV function – modeling material evolution.

Material models should indeed advance in the path of more complexity to improve their descriptive capability and accuracy, always with the aid of observations from systematic and carefully designed experiments. It is well know that biological tissues show a significant amount of viscoelastic effects, but to date only a few computational simulations have employed viscoelastic models, and at the same time, only a few experimental studies have attempted to fully characterize the viscoelastic behavior of BHV leaflets. Pre-existing stress is another key aspect for accurate biomechanical simulations [243], and the same argument can be made in regard to it – not only it is usually neglected

computationally, but also is often overlooked experimentally. Better and more critical experimental techniques are methodologies are certainly in need, not only to fully characterize the present state of the leaflet tissue, but also its evolution.

In fact, the highly dynamic motion of BHVs and its lifetime presents yet another challenge: BHV function occurs in cycles of approximately 1 Hz, with the valve undergoing a full cycle of opening and closing, but on the other hand, BHV dysfunction occurs in a much longer timescale, with its endpoint occurring at approximately 10-15 years after hundreds of millions of cycles. Bridging this huge temporal scale gap is certainly a challenge – it is ill-posed to conduct a complex and detailed simulation of one valve cycle for such high number of cycles, and simulation strategies must be developed to deal with this class of multi-timescale problems.

The ultimate goal of modeling and computational simulation of BHVs is the prediction of the progression of damage and their durability in response to dynamic in vivo biomechanical and biological environment. So far, most attention has been focused on the former, the mechanics, but the importance of the latter, the biology, is properly recognized yet much more difficult to tackle. BHVs function occurs in vivo; therefore its evolving biochemistry must be taken into account. Yet, most BHV biochemical research has focused almost exclusively on mitigation of calcification, which is puzzling as calcification affects less than half of failed BHV while tears due to structural degradation is the predominant mode of failure. Little attention has been paid to understanding the basic biological mechanisms of BHV tissue degeneration to improve long-term durability. Glutaraldehyde treatment forms stable crosslinks within and between extracellular matrix molecules providing resistance to enzymatic and chemical degradation. However, glutaraldehyde crosslinking does not stabilize elastin and GAGs originally present in valve tissue [244, 245]. The alteration in the behavior of collagen fibers during valve function as well as the inability of the BHV tissue to remodel can result in abnormal leaflet motion. Damage accumulation has been shown to occur in the collagen microstructure, likely making it more prone to failure [244]. Reduction in GAG content is also thought to be involved in this process, possibly resulting in tissue buckling and the reduction of the valve's ability to sustain high compressive loads [246]. The loss of GAGs might also be responsible for the presence of interlaminar shearing, resulting in delamination and loss of collagen fibers from the functioning valve.

Long-term loss of these components may ultimately accelerate valve failure, so that development of models to describe and predict the evolution of these components could guide design better methods to preserve them and enhance BHV durability. Observed changes in BHV tissue shape and mechanical behavior can be a result of gross fiber structural changes (e.g. changes in fiber alignment and architecture), or the effective stiffness of the fibers themselves, or the loss of other tissue components such as elastic or GAGs [247, 180]. Purely mechanical experiments alone are insufficient

to characterize the evolution of the constituents of the valve leaflet tissue and its mechanical response, and the progression of damage over service life. A shift towards a biochemically driven modeling approach is clearly necessary to account for observable evolving quantities such as constituent mass fractions, GAG depletion, collagen fiber intrinsic stiffness, orientation, recruitment, and fiber-fiber interactions. Carefully designed critical experiments will then be needed to provide further insight into the mechanisms of BHV damage progression. Only with the aid of reliable models backed by observed experimental data, hypothesis formulation to guide BHV design and improve chemical treatment methods can subsequently be developed and tested. Ultimately, the ability to predict biomaterial durability will certainly result in a crucial simulation tool for bioprosthetic heterograft tissue and valve design.

7 – Future perspectives

Replacement of diseased natural heart valves with prosthetic replacements has been a lifesaving procedure for millions of patients over the last 50 years and will certainly continue with ever increasing number of deployments, success, and safety. Since BHV do not require anticoagulant therapy, and exhibit good medium- to long-term durability, the heterograft alterative is currently the most favored heart valve substitute biomaterials. For at least the next 20-30 years, BHV fabricated from heterograft tissues will continue to be extensively used and will probably remain as the dominant valve design. Moreover, as developing countries continue to improve their medical delivery infrastructure, worldwide heart valve replacement will continue to rise. BHVs should not be dismissed as the “been there, done that” technology of the last decade – heterograft tissues for BHVs will continue to be extensively used, improved and refined. Rational and scientifically-based approaches to BHV biomaterial development and design can lead to significantly improved BHV over the coming decades, which will impact millions of patients worldwide with heart valve disease.

Durability of BHVs still is the major limitation of the current technology for most patients. Modest improvements in valve durability (e.g., an increase in average durability by 3-5 years) can have dramatic clinical impact. The improvement of the experimental and processing techniques, the accuracy of the assessment of material properties, and the advancement of methods for simulation of heart valve function reviewed here offer rational approaches to further improve the design and durability of BHVs.

Novel approaches to valve implantation, such as percutaneous valve technologies, offer new hope to patients in need of heart valve replacement who are unable to undergo valve replacement surgery. These heart valve designs require novel biomaterials that are substantially thinner than current heterograft tissues and can withstand collapse within a delivery catheter without suffering damage

during valve deployment. In the long term, novel tissue sources or new approaches to manufacturing, such as genetically manipulated pigs or engineered tissue heart valves offer great promise for better heart valve prosthesis. Genetic manipulations of animal donors for xenotransplantation may prove to be extremely beneficial to hamper immune response and prevent calcification and structural deterioration. Tissue engineering approaches are particularly attractive for the pediatric population were accounting for somatic growth is paramount. Non-invasive techniques for BHV functional assessment, especially the degree of calcification and the evolution of leaflet mechanical properties (changing due to material fatigue, the major failure mechanism of the biomaterial), will be of considerable clinical use in determining when and where a prosthetic heart valve may be reaching the end of its functional life. Most importantly, the improvement of minimally-invasive assessment technologies will be crucial to provide critical experimental data for model development and computational simulation, which in turn may confer a higher degrees of rationality to the majorly empirical modus operandi of BHV research and development.

Over the last 20 years, the mechanical function of BHVs has been well defined and the mechanical requirements for functional performance carefully characterized. Similarly, methods and protocols for tissue fixation, processing, and BHV manufacturing have been extensively attempeed, tested, and developed, and may have been refined to optimal state. However, accelerated wear testing still is the one and only pass/fail test regarding durability and these neglect all the biochemical and biological aspects of BHV function. A push towards better understanding of the biological and biochemical events associated with valve function is definitely necessary. This knowledge, when framed into novel methods and frameworks rendering mechanical theories of valve function with critical biological aspects, will certainly lead to substantial advancements in BHV durability. Overall, rigorous modeling and simulation with the objective of complementing exploratory experimentation and technological invention will be crucial to BHV design and fabrication, in vivo biochemical and biological interactions post implantation, and the long-term fate of BHVs.

Acknowledgements

National Institute of Health, Award Number R01 HL119297 and R01 HL63954 to MSS.

National Institute of Health, Award T32 to KRF.

American Heart Association, Post Doctoral Fellowship 14POST18720037 to AA.

List of Figures

Figure 12: Overview of two-tiered BP tissue sorting procedure with vector plots showing distribution of regional fiber preferred directions (from Sacks and Chuong (1998) [30]). (a) A course small angle light scattering (SALS) scan of an anterior section of the BP sac showing where a 50 mm x 75mm rectangular cutout regions were extracted, (b) a rescan of the cutout showing where the 25 mm x 25 mm biaxial testing specimen was selected, and (c) high spatial resolution scan of the biaxial test specimen overlaid on a gray scale OI values demonstrating high uniformity of both fiber preferred directions and OI, along with definition of the preferred and cross direction axes.

Figure 13: Biaxial mechanical behavior of glutaraldehyde treated bovine pericardium for five strain protocols (indicated beside each curve) for the (a) preferred direction (PD, 11 in the above nomenclature) and the (b) cross direction (CD, 22 in the current nomenclature). Also shown is the fit of the structural constitutive orthotropic model (cf. Equation (0)), which demonstrated a very good fit to the data for all protocols (adapted from [51]).

Figure 14: (A) The Elastic response of a single collagen fiber: comparing the standard model with no elastica effect, the analytical model based on Garikipati et al. **[111]**, and a FE simulation of 3D Neo Hookean fiber using the FEniCs project. (B) The simulated ensemble response of the Elastica model and the standard model shoes minimal difference.

Figure 15: Complete EXL structural model results or the S_{11} and S_{22} stress components for three protocols. The interactions produced the largest contribution to S_{11} followed by matrix and collagen fibers; however, the contributions towards S_{22} are dependent on loading path, with collagen dominating when $\lambda_1 > \lambda_2$ and matrix dominating when $\lambda_2 > \lambda_1$. The contribution of the matrix was much less loading path sensitive, owing to its near-linear, isotropic behavior (from Sacks et al. [120]).

Figure 16: (A) A schematic of the nine sonocrystals placement on the mitral valve arterial leaflet surface, showing crystal positions in relation to valvular geometry. (B) Two three-dimensional reconstructed views of the nine sonocrystals in the unloaded reference state (t=0 ms) and the fully coapted state (t =500 ms). The evaluation of valve deformation is extremely difficult and, being crucial for simulation validation, still remains a significant challenge (from Sacks et al. [154]).

Figure 17: Maximum in-plane principal strain magnitude plotted using the same color fringe scale for pressure levels of 40, 80 and 120 mm Hg. It is interesting to note that the free edge of one leaflet was slightly higher than that of the other two leaflets at 120 mm Hg and this feature was captured by the FE model (from Sun et al. [83]).

Figure 18: Representative SALS data for three leaflets of an pericardial BHV. The vectors represent the local preferred fiber orientations, the color indicates the degree of collagen fiber orientation. Most leaflets have a ±45° preferred orientation and a fairly uniform degree of orientation throughout the leaflet (from Sun et al. [83]).

Figure 19: Sequence of displacement of the BHV resultant shell model during the complete cardiac cycle (from Kim et al. [176]).

Figure 19. Volume rendering of the velocity field at several points during a cardiac cycle. The immersogeometric fluid structure interaction methodology applied to BHV modeling and simulation grants higher levels of automation, robustness, and realism than its standalone structural dynamics counterpart (from Hsu et al. [216]).

Figure 20: (a) Quadrilateral mesh used, (b) fiber structure of three leaflets measured experimentally with SALS and then mapped onto valve geometry using spline technique, and (c) another view of the final valve mesh with fiber structure (from Aggarwal and Sacks [242])

List of Tables

Table 12 Fiber stress-strain model parameters for grouped specimens data for both fiber models (cf. [97] and Equations (0)-(0) and Equations (0)-(0) respectively).

Compliance with Ethical Standards

1. No human studies were carried out by the authors for this article.
2. No animal studies were carried out by the authors for this article.
3. None of the authors have any conflicts of interest to report.

References

1. Thubrikar M. The Aortic Valve. Boca Raton: CRC; 1990.

2. Roger VL, Go AS, Lloyd-Jones DM, Benjamin EJ, Berry JD, Borden WB et al. Heart disease and stroke statistics--2012 update: a report from the American Heart Association. Circulation. 2012;125(1):e2-e220. doi:10.1161/CIR.0b013e31823ac046.

3. Go A, Mozaffarian D, Roger V, Benjamin E, Berry J, Borden W et al. Heart disease and stroke statistics--2013 update: a report from the American Heart Association. Circulation. 2013;127(1):e6-e245.

4. Go AS, Mozaffarian D, Roger VL, Benjamin EJ, Berry JD, Blaha MJ et al. Heart disease and stroke statistics--2014 update: a report from the American Heart Association. Circulation. 2014;129(3):e28-e292. doi:10.1161/01.cir.0000441139.02102.80.

5. Mozaffarian D, Benjamin EJ, Go AS, Arnett DK, Blaha MJ, Cushman M et al. Heart disease and stroke statistics--2015 update: a report from the American Heart Association. Circulation. 2015;131(4):e29-322. doi:10.1161/CIR.0000000000000152.

6. Ross DN. Replacement of aortic and mitral valves with a pulmonary autograft. Lancet. 1967;2(7523):956-8.

7. Braunwald NS, Cooper T, Morrow AG. Complete replacement of the mitral valve. Successful clinical application of a flexible polyurethane prosthesis. J Thorac Cardiovasc Surg. 1960;40:1-11.

8. Pibarot P, Dumesnil JG. Valvular Heart Disease: Changing Concepts in Disease Management. Circulation. 2009;119:1034-48.

9. Jouan J. Mitral valve repair over five decades. Ann Cardiothorac Surg. 2015;4(4):322-34. doi:10.3978/j.issn.2225-319X.2015.01.07.

10. Salmasi MY, Acharya M, Humayun N, Baskaran D, Hubbard S, Vohra H. Is valve repair preferable to valve replacement in ischaemic mitral regurgitation? A systematic review and meta-analysis. European journal of cardio-thoracic surgery : official journal of the European Association for Cardio-thoracic Surgery. 2016. doi:10.1093/ejcts/ezw053.

11. Sacks MS, Schoen FJ. Collagen fiber disruption occurs independent of calcification in clinically explanted bioprosthetic heart valves. J Biomed Mater Res. 2002;62(3):359-71.

12. Vyavahare N, Ogle M, Schoen FJ, Zand R, GLoeckner DC, Sacks MS et al. Mechanisms of bioprosthetic heart valve failure: Fatigue causes collagen denaturation and glycosaminoglycan loss. Journal of Biomedical Materials Research. 1999;46:44-50.

13. Siddiqui RF, Abraham JR, Butany J. Bioprosthetic heart valves: modes of failure. Histopathology. 2009;55(2):135-44.

14. Cohn LH. Cutler,Elliot,Carr mitral-valve surgery at Peter-Bent-Brigham-Hospital 1923. J Card Surg. 1994;9:137-8.

15. Harken DE, Soroff HS, Taylor WJ, Lefemine AA, Gupta SK, Lunzer S. Partial and complete prostheses in aortic insufficiency. The Journal of thoracic and cardiovascular surgery. 1960;40:744-62.

16. Cohn LH, Collins JJ, Jr., Disesa VJ, Couper GS, Peigh PS, Kowalker W et al. Fifteen-Year Experience with 1678 Hancock Porcine Bioprosthetic Heart Vavle Replacements. Ann Surg. 1989;210(4):435-42.

17. Blackstone EH. Could it happen again? The Bjork-Shiley convexo-concave heart valve story. Circulation. 2005;111(21):2717-9.

18. Schoen FJ. Pathologic findings in explanted clinical bioprosthetic valves fabricated from photooxidized bovine pericardium. J Heart Valve Dis. 1998;7(2):174-9.

19. Girardot MN, Torrianni M, Girardot JM. Effect of AOA on glutaraldehyde-fixed bioprosthetic heart vavlve cusps and walls: binding and calcification studies. Int J Artif Organs. 1994;17:76-82.

20. Jones M, Eidbo EE, Hilbert SL, Ferrans VJ, Clark RE. Anticalcification treatments of bioprosthetic heart valves: in vivo studies in sheep. J Card Surg. 1989;4(1):69-73.

21. Ali A, Halstead JC, Cafferty F, Sharples L, Rose F, Coulden R et al. Are stentless valves superior to modern stented valves? A prospective randomized trial. Circulation. 2006;114(1 Suppl):I535-40. doi:10.1161/CIRCULATIONAHA.105.000950.

22. Ennker J, Albert A, Ennker IC. Stentless aortic valves. Current aspects. HSR proceedings in intensive care & cardiovascular anesthesia. 2012;4(2):77-82.

23. Perez de Arenaza D, Lees B, Flather M, Nugara F, Husebye T, Jasinski M et al. Randomized comparison of stentless versus stented valves for aortic stenosis: effects on left ventricular mass. Circulation. 2005;112(17):2696-702. doi:10.1161/CIRCULATIONAHA.104.521161.

24. Payne DM, Koka HP, Karanicolas PJ, Chu MW, Nagpal AD, Briel M et al. Hemodynamic performance of stentless versus stented valves: a systematic review and meta-analysis. J Card Surg. 2008;23(5):556-64. doi:10.1111/j.1540-8191.2008.00705.x.

25. Funder JA. Current status on stentless aortic bioprosthesis: a clinical and experimental perspective. European journal of cardio-thoracic surgery : official journal of the European Association for Cardio-thoracic Surgery. 2012;41(4):790-9. doi:10.1093/ejcts/ezr141.

26. Leon MB, Smith CR, Mack MJ, Makkar RR, Svensson LG, Kodali SK et al. Transcatheter or Surgical Aortic-Valve Replacement in Intermediate-Risk Patients. The New England journal of medicine. 2016. doi:10.1056/NEJMoa1514616.

27. Jamieson WR LH, Burr LH, Fradet GJ, Miyagishima RT, Janusz MT, Lichtenstein SV. Carpentier-Edwards supraannular porcine bioprosthesis evaluation over 15 years. Ann Thorac Surg. 1998;66(6 Suppl):S49-52.

28. Hiester ED, Sacks MS. Optimal bovine pericardial tissue selection sites. I. Fiber architecture and tissue thickness measurements. J Biomed Mater Res. 1998;39(2):207-14.

29. Hiester ED, Sacks MS. Optimal bovine pericardial tissue selection sites. II. Cartographic analysis. J Biomed Mater Res. 1998;39(2):215-21.

30. Sacks MS, Chuong CJ. Orthotropic mechanical properties of chemically treated bovine pericardium. Ann Biomed Eng. 1998;26(5):892-902.

31. Schoen F. Aortic valve structure-function correlations: Role of elastic fibers no longer a stretch of the imagination. Journal of Heart Valve Disease. 1997;6:1-6.

32. Vesely I. The role of elastin in aortic valve mechanics. Journal of Biomechanics. 1998;31(2):115-23.

33. Kronick PL, Sacks MS. Matrix Macromolecules That Affect the Viscoelasticity of Calfskin. J Biomech Eng-T Asme. 1994;116(2):140-5. doi:Doi 10.1115/1.2895712.

34. Liao J, Joyce EM, Sacks MS. Effects of decellularization on the mechanical and structural properties of the porcine aortic valve leaflet. Biomaterials. 2008;29(8):1065-74. doi:S0142-9612(07)00896-4 [pii]

10.1016/j.biomaterials.2007.11.007.

35. Quinonez LG, Breitbart R, Tworetsky W, Lock JE, Marshall AC, Emani SM. Stented bovine jugular vein graft (Melody valve) for surgical mitral valve replacement in infants and children. The Journal of thoracic and cardiovascular surgery. 2014;148(4):1443-9. doi:10.1016/j.jtcvs.2013.10.059.

36. Jennings LM, Butterfield M, Booth C, Watterson KG, Fisher J. The pulmonary bioprosthetic heart valve: its unsuitability for use as an aortic valve replacement. J Heart Valve Dis. 2002;11(5):668-78.

37. Harada Y, Kawada M, Ishihara K, Higashidate M, Kurosawa H, Imai Y. A new valved conduit with commissures using a glutaraldehyde preserved equine pericardium. Kyobu Geka. 1989;42(6):457-9.

38. Lee JM, Boughner DR. Tissue Mechanics of Canine Pericardium in Different Test Environments. Circulation Research. 1981;49:533-44.

39. Wiegner AW, Bing OH, Borg TK, Caulfield JB. Mechanical and structural correlates of canine pericardium. Circ Res. 1981;49(3):807-14.

40. Maestro MM, Turnay J, Olmo N, Fernández P, Suárez D, García Páez JM et al. Biochemical and mechanical behavior of ostrich pericardium as a new biomaterial. Acta biomaterialia. 2006;2(2):213-9.

41. Neethling WM, Cooper S, Van Den Heever JJ, Hough J, Hodge AJ. Evaluation of kangaroo pericardium as an alternative substitute for reconstructive cardiac surgery. J Cardiovasc Surg (Torino). 2002;43(3):301-6.

42. Ye Q, Zund G, Jockenhoevel S, Hoerstrup SP, Schoeberlein A, Grunenfelder J et al. Tissue engineering in cardiovascular surgery: new approach to develop completely human autologous tissue. Eur J Cardiothorac Surg. 2000;17(4):449-54.

43. Stock UA, Sakamoto T, Hatsuoka S, Martin DP, Nagashima M, Moran AM et al. Patch augmentation of the pulmonary artery with bioabsorbable polymers and autologous cell seeding. J Thorac Cardiovasc Surg. 2000;120(6):1158-67; discussion 68.

44. Sutherland FW, Perry TE, Yu Y, Sherwood MC, Rabkin E, Masuda Y et al. From stem cells to viable autologous semilunar heart valve. Circulation. 2005;111(21):2783-91.

45. Rabkin E, Hoerstrup SP, Aikawa M, Mayer JE, Jr., Schoen FJ. Evolution of cell phenotype and extracellular matrix in tissue-engineered heart valves during in-vitro maturation and in-vivo remodeling. Journal of Heart Valve Disease. 2002;11(3):308-14; discussion 14.

46. Sacks MS, Schoen FJ, Mayer JE. Bioengineering challenges for heart valve tissue engineering. Annu Rev Biomed Eng. 2009;11:289-313. doi:10.1146/annurev-bioeng-061008-124903.

47. Humphrey JD. Cardiovascular Solid Mechanics: Cells, Tissues, and Organs. Lightning Source, UKltd.; 2002.

48. Lee JM, Boughner DR, Courtman DW. The glutaraldehyde-stabilized porcine aortic valve xenograft. II. Effect of fixation with or without pressure on the tensile viscoelastic properties of the leaflet material. Journal of Biomedical Materials Research. 1984;18:79-98.

49. Vesely I, Noseworthy R. Micromechanics of the fibrosa and the ventricularis in aortic valve leaflets. Journal of Biomechanics. 1992;25(1):101-13.

50. Chuong CJ, Fung YC. Three-dimensional stress distribution in arteries. Journal of biomechanical engineering. 1983;105(3):268-74.

51. Sacks MS. A structural constitutive model for chemically treated planar tissues under biaxial loading. Comput Mech. 2000;26(3):243-9. doi:Doi 10.1007/S004660000175.

52. Crofts CE, Trowbridge EA. The tensile strength of natural and chemically modified bovine pericardium. Journal of Biomedical Materials Research. 1988;22:89-98.

53. Lee JM, Haberer SA, Boughner DR. The bovine pericardial xenograft: I. Effect of fixation in aldehydes without constraint on the tensile properties of bovine pericardium. Journal of Biomedical Materials Research. 1989;23:457-75.

54. Sung HW, Chang Y, Chiu CT, Chen CN, Liang HC. Crosslinking characteristics and mechanical properties of a bovine pericardium fixed with a naturally occurring crosslinking agent. J Biomed Mater Res. 1999;47(2):116-26.

55. Leeson-Dietrich J, Boughner D, Vesely I. Porcine Pulmonary and Aortic Valves: A Comparison of Their Tensile Viscoelastic Properties at Physiological Strain Rates. The Journal of Heart Valve Disease. 1995;4:88-94.

56. Sauren AA, van Hout MC, van Steenhoven AA, Veldpaus FE, Janssen JD. The mechanical properties of porcine aortic valve tissues. J Biomech. 1983;16(5):327-37.

57. Carew EO, Garg A, Barber JE, Vesely I. Stress relaxation preconditioning of porcine aortic valves. Ann Biomed Eng. 2004;32(4):563-72.

58. Sung HW, Chang Y, Chiu CT, Chen CN, Liang HC. Mechanical properties of a porcine aortic valve fixed with a naturally occurring crosslinking agent. Biomaterials. 1999;20(19):1759-72.

59. Stradins P, Lacis R, Ozolanta I, Purina B, Ose V, Feldmane L et al. Comparison of biomechanical and structural properties between human aortic and pulmonary valve. Eur J Cardiothorac Surg. 2004;26(3):634-9.

60. Christie G, Barratt-Boyes B, editors. Time-dependent changes to the leaflet elasticity of the Medtronic Intact valve in-vivo. World Symposium on Heart Valve Disease; 1999; London,UK.

61. Billiar KL, Sacks MS. Biaxial mechanical properties of the natural and glutaraldehyde treated aortic valve cusp--Part I: Experimental results. Journal of biomechanical engineering. 2000;122(1):23-30.

62. Billiar KL, Sacks MS. Biaxial mechanical properties of the native and glutaraldehyde-treated aortic valve cusp: Part II--A structural constitutive model. Journal of biomechanical engineering. 2000;122(4):327-35.

63. Grant CW, Barrat-Boyes, B.G. Mechanical Properties of Porcine Pulmonary Valve Leaflets: How Do They Differ From Aortic Leaflets? Annals of Thoracis Surgery. 1995;60(Supplement 2):S195-S9.

64. Martin C, Sun W. Biomechanical characterization of aortic valve tissue in humans and common animal models. J Biomed Mater Res A. 2012;100(6):1591-9.

65. Thubrikar MJ, Skinner JR, Eppink RT, Nolan SP. Stress analysis of porcine bioprosthetic heart valves in vivo. Journal of biomedical materials research. 1982;16(6):811-26. doi:10.1002/jbm.820160607.

66. Vesely I, Boughner D. Analysis of the bending behaviour of porcine xenograft leaflets and of neutral aortic valve material: bending stiffness, neutral axis and shear measurements. J Biomech. 1989;22(6-7):655-71.

67. Gloeckner DC, Billiar KL, Sacks MS. Effects of mechanical fatigue on the bending properties of the porcine bioprosthetic heart valve. Asaio J. 1999;45(1):59-63.

68. Mirnajafi A, Raymer J, Scott MJ, Sacks MS. The effects of collagen fiber orientation on the flexural properties of pericardial heterograft biomaterials. Biomaterials. 2005;26(7):795-804. doi:10.1016/j.biomaterials.2004.03.004.

69. Engelmayr GC, Jr., Hildebrand DK, Sutherland FW, Mayer JE, Jr., Sacks MS. A novel bioreactor for the dynamic flexural stimulation of tissue engineered heart valve biomaterials. Biomaterials. 2003;24(14):2523-32.

70. Merryman WD, Huang HY, Schoen FJ, Sacks MS. The effects of cellular contraction on aortic valve leaflet flexural stiffness. J Biomech. 2006;39(1):88-96.

71. Mirnajafi A, Raymer JM, McClure LR, Sacks MS. The flexural rigidity of the aortic valve leaflet in the commissural region. Journal of biomechanics. 2006;39(16):2966-73. doi:10.1016/j.jbiomech.2005.10.026.

72. Buchanan RM, Sacks MS. Interlayer micromechanics of the aortic heart valve leaflet. Biomech Model Mechanobiol. 2013. doi:10.1007/s10237-013-0536-6.

73. Engelmayr GC, Sacks MS. A structural model for the flexural mechanics of nonwoven tissue engineering scaffolds. J Biomech Eng. 2006;128:610-22.

74. Pereira CA, Lee JM, Haberer SA. Effect of alternative crosslinking methods on the low strain rate viscoelastic properties of bovine pericardial bioprosthetic material. Journal of Biomedical Materials Research. 1990;24:345-61.

75. Sung HW, Chang WH, Ma CY, Lee MH. Crosslinking of biological tissues using genipin and/or carbodiimide. J Biomed Mater Res. 2003;63(3):427-38.

76. Mercuri JJ, Lovekamp JJ, Simionescu DT, Vyavahare NR. Glycosaminoglycan-targeted fixation for improved bioprosthetic heart valve stabilization. Biomaterials. 2007;28(3):496-503. doi:S0142-9612(06)00794-0 [pii]

10.1016/j.biomaterials.2006.09.005.

77. Christie GW. Anatomy of aortic heart valve leaflets: the influence of glutaraldehyde fixation on function. European Journal of Cardio-Thoracic Surgery. 1992;6:S25-S33.

78. Wells SM, Sacks MS. Effects of fixation pressure on the biaxial mechanical behavior of porcine bioprosthetic heart valves with long-term cyclic loading. Biomaterials. 2002;23(11):2389-99.

79. Cataloglu A, Clark RE, Gould PL. Stress Analysis of Aortic-Valve Leaflets with Smoothed Geometrical Data. J Biomech. 1977;10(3):153-8. doi:Doi 10.1016/0021-9290(77)90053-7.

80. Hamid MS, Sabbah HN, Stein PD. Influence of Stent Height upon Stresses on the Cusps of Closed Bioprosthetic Valves. Journal of Biomechanics. 1986;19:759-69.

81. Li J, Luo XY, Kuang ZB. A nonlinear anisotropic model for porcine aortic heart valves. J Biomech. 2001;34(10):1279-89.

82. Sun W, Sacks MS. Finite element implementation of a generalized Fung-elastic constitutive model for planar soft tissues. Biomech Model Mechan. 2005;4(2-3):190-9. doi:Doi 10.1007/S10237-005-0075-X.

83. Sun W, Abad A, Sacks MS. Simulated bioprosthetic heart valve deformation under quasi-static loading. Journal of biomechanical engineering. 2005;127(6):905-14.

84. Tong P, Fung YC. The stress-strain relationship for the skin. Journal of biomechanics. 1976;9(10):649-57.

85. Chew PH, Yin FC, Zeger SL. Biaxial stress-strain properties of canine pericardium. Journal of molecular and cellular cardiology. 1986;18(6):567-78.

86. Humphrey JD, Strumpf RK, Yin FC. A constitutive theory for biomembranes: application to epicardial mechanics. Journal of biomechanical engineering. 1992;114(4):461-6.

87. Humphrey JD, Vawter DL, Vito RP. Mechanical behavior of excised canine visceral pleura. Ann Biomed Eng. 1986;14(5):451-66.

88. Sun W, Sacks MS, Sellaro TL, Slaughter WS, Scott MJ. Biaxial mechanical response of bioprosthetic heart valve biomaterials to high in-plane shear. Journal Biomechanical Engineering. 2003;125:372-80.

89. Li K, Sun W. Simulated thin pericardial bioprosthetic valve leaflet deformation under static pressure-only loading conditions: implications for percutaneous valves. Ann Biomed Eng. 2010;38(8):2690-701. doi:10.1007/s10439-010-0009-3.

90. Sacks MS, Chuong CJ. Orthotropic mechanical properties of chemically treated bovine pericardium. Ann Biomed Eng. 1998;26(5):892-902. doi:Doi 10.1114/1.135.

91. Choi HS, Vito RP. Two-dimensional stress-strain relationship for canine pericardium. Journal of biomechanical engineering. 1990;112(2):153-9.

92. Wilber JP, Walton JR. The convexity properties of a class of constitutive models for biological soft issues. Math Mech Solids. 2002;7(3):217-35. doi:Doi 10.1177/108128602027726.

93. Humphrey JD, Strumpf RK, Yin FC. Determination of a constitutive relation for passive myocardium: I. A new functional form. J Biomech Eng. 1990;112(3):333-9.

94. Humphrey JD, Strumpf RK, Yin FC. Determination of a constitutive relation for passive myocardium: II. Parameter estimation. J Biomech Eng. 1990;112(3):340-6.

95. Lanir Y. A structural theory for the homogeneous biaxial stress-strain relationships in flat collagenous tissues. Journal of biomechanics. 1979;12(6):423-36.

96. Holzapfel GA, Gasser TC, Ogden RW. A new constitutive framework for arterial wall mechanics and a comparative study of material models. J Elasticity. 2000;61(1-3):1-48. doi:Doi 10.1023/A:1010835316564.

97. Sacks MS. Incorporation of experimentally-derived fiber orientation into a structural constitutive model for planar-collagenous tissues. J Biomech Eng-T Asme. 2003;125(2):280-7. doi:Doi 10.1115/1.1544508.

98. Billiar KL, Sacks MS. Biaxial mechanical properties of the natural and glutaraldehyde treated aortic valve cusp - Part I: Experimental results. J Biomech Eng-T Asme. 2000;122(1):23-30. doi:Doi 10.1115/1.429624.

99. Lanir Y. Plausibility of structural constitutive equations for swelling tissues--implications of the C-N and S-E conditions. Journal of biomechanical engineering. 1996;118(1):10-6.

100. Trowbridge EA, Lawford PV, Crofts CE. Pericardial heterografts: a comparative study of suture pull-out and tissue strength. J Biomed Eng. 1989;11(4):311-4.

101. Fata B, Carruthers CA, Gibson G, Watkins S, Gottlieb D, Mayer Jr JE et al. Regional structural and biomechanical alterations of the ovine main pulmonary artery during postnatal growth. Journal Biomechanical Engineering. 2013;135(2).

102. Sacks MS, Smith DB, Hiester ED. A small angle light scattering device for planar connective tissue microstructural analysis. Ann Biomed Eng. 1997;25(4):678-89.

103. Parry DA. The molecular and fibrillar structure of collagen and its relationship to the mechanical properties of connective tissue. Biophys Chem. 1988;29(1-2):195-209.

104. Yahia LH, Drouin G. Microscopical investigation of canine anterior cruciate ligament and patellar tendon: collagen fascicle morphology and architecture. J Orthop Res. 1989;7(2):243-51. doi:10.1002/jor.1100070212.

105. Sasaki N, Odajima S. Elongation mechanism of collagen fibrils and force-strain relations of tendon at each level of structural hierarchy. J Biomech. 1996;29(9):1131-6.

106. Sasaki N, Odajima S. Stress-strain curve and Young's modulus of a collagen molecule as determined by the X-ray diffraction technique. J Biomech. 1996;29:655-8.

107. Liao J, Yang L, Grashow J, Sacks MS, editors. Collagen fibril kinematics in mitral valve leaflet under biaxial elongation, creep, and stress relaxation. Society for Heart Valve Disease Third Biennial Meeting; 2005; Vancouver: SHVD.

108. Liao J, Yang L, Grashow J, Sacks MS. The relation between collagen fibril kinematics and mechanical properties in the mitral valve anterior leaflet. Journal of biomechanical engineering. 2007;129(1):78-87. doi:10.1115/1.2401186.

109. Buehler MJ. Atomistic and continuum modeling of mechanical properties of collagen: Elasticity, fracture, and self-assembly. Journal of Materials Research. 2006;21(08):1947-61. doi:doi:10.1557/jmr.2006.0236.

110. Freed AD, Doehring TC. Elastic model for crimped collagen fibrils. J Biomech Eng. 2005;127(4):587-93.

111. Garikipati K, Göktepe S, Miehe C. Elastica-based strain energy functions for soft biological tissue. J Mech Phys Solids. 2008;56(4):1693-713. doi:http://dx.doi.org/10.1016/j.jmps.2007.07.005.

112. Lee C-H, Zhang W, Liao J, Carruthers Christopher A, Sacks Jacob I, Sacks Michael S. On the Presence of Affine Fibril and Fiber Kinematics in the Mitral Valve Anterior Leaflet. Biophysical Journal. 2015;108(8):2074-87. doi:http://dx.doi.org/10.1016/j.bpj.2015.03.019.

113. Sacks MS. Incorporation of experimentally-derived fiber orientation into a structural constitutive model for planar collagenous tissues. J Biomech Eng. 2003;125(2):280-7.

114. Fan R, Sacks MS. Simulation of planar soft tissues using a structural constitutive model: finite element implementation and validation. J Biomech. 2014;47:2043-54.

115. Mirnajafi A, Zubiate B, Sacks MS. Effects of cyclic flexural fatigue on porcine bioprosthetic heart valve heterograft biomaterials. J Biomed Mater Res A. 2010;94(1):205-13. doi:10.1002/jbm.a.32659.

116. Grashow JS, Sacks MS, Liao J, Yoganathan AP. Planar biaxial creep and stress relaxation of the mitral valve anterior leaflet. Ann Biomed Eng. 2006;34(10):1509-18.

117. Grashow JS, Yoganathan AP, Sacks MS. Biaixal stress-stretch behavior of the mitral valve anterior leaflet at physiologic strain rates. Ann Biomed Eng. 2006;34(2):315-25. doi:10.1007/s10439-005-9027-y.

118. Stella JA, Liao J, Sacks MS. Time-dependent biaxial mechanical behavior of the aortic heart valve leaflet. J Biomech. 2007;40(14):3169-77. doi:S0021-9290(07)00151-0 [pii]

10.1016/j.jbiomech.2007.04.001.

119. Eckert CE, Fan R, Mikulis B, Barron M, Carruthers CA, Friebe VM et al. On the biomechanical role of glycosaminoglycans in the aortic heart valve leaflet. Acta biomaterialia. 2013;9(1):4653-60. doi:10.1016/j.actbio.2012.09.031.

120. Sacks MS, Zhang W, Wognum S. A novel fibre-ensemble level constitutive model for exogenous cross-linked collagenous tissues. Interface Focus. 2016;6(1):20150090. doi:10.1098/rsfs.2015.0090.

121. Fata B, Zhang W, Amini R, Sacks M. Insights into Regional Adaptations in the Growing Pulmonary Artery Using a Meso-Scale Structural Model: Effects of Ascending Aorta Impingement. J Biomech Eng. 2014. doi:10.1115/1.4026457.

122. Zhang W, Ayoub S, Liao J, Sacks MS. On the mechanical role of collagen and elastin fibers in the layers of the mitral heart valve leaflet. J Mech Behav Biomed Mater. in press.

123. Vesely I, Barber JE, Ratliff NB. Tissue damage and calcification may be independent mechanisms of bioprosthetic heart valve failure. J Heart Valve Dis. 2001;10(4):471-7.

124. Fata B, Zhang W, Amini R, Sacks MS. Insights into regional adaptations in the growing pulmonary artery using a meso-scale structural model: effects of ascending aorta impingement. J Biomech Eng. 2014;136(2):021009. doi:10.1115/1.4026457.

125. De Hart J, Baaijens FP, Peters GW, Schreurs PJ. A computational fluid-structure interaction analysis of a fiber-reinforced stentless aortic valve. Journal of biomechanics. 2003;36(5):699-712.

126. Driessen NJ, Bouten CV, Baaijens FP. A structural constitutive model for collagenous cardiovascular tissues incorporating the angular fiber distribution. Journal of biomechanical engineering. 2005;127(3):494-503.

127. Burriesci G, Howard IC, Patterson EA. Influence of anisotropy on the mechanical behaviour of bioprosthetic heart valves. J Med Eng Technol. 1999;23(6):203-15.

128. Sun W, Abad A, Sacks MS. Simulated bioprosthetic heart valve deformation under quasi-static loading. Journal of Biomechanial Engineering. 2005;127(6):905-14.

129. Sacks MS, Mirnajafi A, Sun W, Schmidt P. Bioprosthetic heart valve heterograft biomaterials: structure, mechanical behavior and computational simulation. Expert review of medical devices. 2006;3(6):817-34.

130. Chandran KB. Role of Computational Simulations in Heart Valve Dynamics and Design of Valvular Prostheses. Cardiovascular engineering and technology. 2010;1(1):18-38. doi:10.1007/s13239-010-0002-x.

131. Gould PL, Cataloglu A, Dhatt G, Chattopadhyay A, Clark RE. Stress analysis of the human aortic valve. Computers & Structures. 1973;3(2):377-84.

132. Huang X, Black MM, Howard IC, Patterson EA. A two-dimensional finite element analysis of a bioprosthetic heart valve. Journal of biomechanics. 1990;23(8):753-62.

133. Black MM, Howard IC, Huang X, Patterson EA. A three-dimensional analysis of a bioprosthetic heart valve. Journal of biomechanics. 1991;24(9):793-801.

134. Krucinski S, Vesely I, Dokainish MA, Campbell G. Numerical simulation of leaflet flexure in bioprosthetic valves mounted on rigid and expansile stents. Journal of biomechanics. 1993;26(8):929-43.

135. Leat ME, Fisher J. Comparative-Study of the Function of the Abiomed Polyurethane Heart-Valve for Use in Left-Ventricular Assist Devices. J Biomed Eng. 1993;15(6):516-20. doi:Doi 10.1016/0141-5425(93)90068-A.

136. Hamid MS, Sabbah HN, Stein PD. Influence of Stent Height Upon Stresses on the Cusps of Closed Bioprosthetic Valves. J Biomech. 1986;19(9):759-69. doi:Doi 10.1016/0021-9290(86)90199-5.

137. Cacciola G, Peters GW, Baaijens FP. A synthetic fiber-reinforced stentless heart valve. Journal of biomechanics. 2000;33(6):653-8.

138. Cacciola G, Peters GW, Schreurs PJ. A three-dimensional mechanical analysis of a stentless fibre-reinforced aortic valve prosthesis. Journal of biomechanics. 2000;33(5):521-30.

139. Salgo IS, Gorman JH, Gorman RC, Jackson BM, Bowen FW, Plappert T et al. Effect of annular shape on leaflet curvature in reducing mitral leaflet stress. Circulation. 2002;106(6):711-7. doi:Doi 10.1161/01.Cir.0000025426.39426.83.

140. Schoen FJ, Fernandez J, Gonzalezlavin L, Cernaianu A. Causes of Failure and Pathological Findings in Surgically Removed Ionescu-Shiley Standard Bovine Pericardial Heart-Valve Bioprostheses - Emphasis on Progressive Structural Deterioration. Circulation. 1987;76(3):618-27.

141. Hilbert SL, Ferrans VJ, Swanson WM. Optical methods for the nondestructive evaluation of collagen morphology in bioprosthetic heart valves. Journal of biomedical materials research. 1986;20(9):1411-21. doi:10.1002/jbm.820200914.

142. Thubrikar MJ, Deck JD, Aouad J, Nolan SP. Role of mechanical stress in calcification of aortic bioprosthetic valves. J Thorac Cardiovasc Surg. 1983;86(1):115-25.

143. Sacks MS, Mirnajafi A, Sun W, Schmidt P. Bioprosthetic heart valve heterograft biomaterials: structure, mechanical behavior and computational simulation. Expert Rev Med Devic. 2006;3(6):817-34. doi:Doi 10.1586/17434440.3.6.817.

144. Makhijani VB, Yang HQ, Dionne PJ, Thubrikar MJ. Three-dimensional coupled fluid-structure simulation of pericardial bioprosthetic aortic valve function. Asaio J. 1997;43(5):M387-92.

145. Kunzelman KS, Einstein DR, Cochran RP. Fluid-structure interaction models of the mitral valve: function in normal and pathological states. Philosophical transactions of the Royal Society of London Series B, Biological sciences. 2007;362(1484):1393-406. doi:10.1098/rstb.2007.2123.

146. Sotiropoulos F, Borazjani I. A review of state-of-the-art numerical methods for simulating flow through mechanical heart valves. Medical & biological engineering & computing. 2009;47(3):245-56. doi:10.1007/s11517-009-0438-z.

147. Gnyaneshwar R, Kumar RK, Balakrishnan KR. Dynamic analysis of the aortic valve using a finite element model. The Annals of thoracic surgery. 2002;73(4):1122-9.

148. Sripathi VC, Kumar RK, Balakrishnan KR. Further insights into normal aortic valve function: Role of a compliant aortic root on leaflet opening and valve orifice area. Ann Thorac Surg. 2004;77(3):844-51. doi:Doi 10.1016/S0003-4975(03)01518-2.

149. Li J, Luo XY, Kuang ZB. A nonlinear anisotropic model for porcine aortic heart valves. J Biomech. 2001;34(10):1279-89. doi:Doi 10.1016/S0021-9290(01)00092-6.

150. Sun W, Sacks MS, Sellaro TL, Slaughter WS, Scott MJ. Biaxial mechanical response of bioprosthetic heart valve biomaterials to high in-plane shear. J Biomech Eng-T Asme. 2003;125(3):372-80. doi:Doi 10.1115/1.1572518.

151. Burriesci G, Howard IC, Patterson EA. Influence of anisotropy on the mechanical behaviour of bioprosthetic heart valves. J Med Eng Technol. 1999;23(6):203-15.

152. Hamid MS, Sabbah HN, Stein PD. Comparison of Finite-Element Stress-Analysis of Aortic-Valve Leaflet Using Either Membrane Elements or Solid Elements. Computers & Structures. 1985;20(6):955-61. doi:Doi 10.1016/0045-7949(85)90015-X.

153. Gorman JH, 3rd, Gupta KB, Streicher JT, Gorman RC, Jackson BM, Ratcliffe MB et al. Dynamic three-dimensional imaging of the mitral valve and left ventricle by rapid sonomicrometry array localization. The Journal of thoracic and cardiovascular surgery. 1996;112(3):712-26.

154. Sacks MS, Enomoto Y, Graybill JR, Merryman WD, Zeeshan A, Yoganathan AP et al. In-vivo dynamic deformation of the mitral valve anterior leaflet. The Annals of thoracic surgery. 2006;82(4):1369-77. doi:10.1016/j.athoracsur.2006.03.117.

155. Gorman JH, 3rd, Gorman RC, Jackson BM, Enomoto Y, St John-Sutton MG, Edmunds LH, Jr. Annuloplasty ring selection for chronic ischemic mitral regurgitation: lessons from the ovine model. The Annals of thoracic surgery. 2003;76(5):1556-63.

156. Amini R, Eckert CE, Koomalsingh K, McGarvey J, Minakawa M, Gorman JH et al. On the in vivo deformation of the mitral valve anterior leaflet: effects of annular geometry and referential configuration. Ann Biomed Eng. 2012;40(7):1455-67. doi:10.1007/s10439-012-0524-5.

157. Thubrikar MJ, Heckman JL, Nolan SP. High speed cine-radiographic study of aortic valve leaflet motion. The Journal of heart valve disease. 1993;2(6):653-61.

158. Lo D, Vesely I. Biaxial strain analysis of the porcine aortic valve. The Annals of thoracic surgery. 1995;60(2 Suppl):S374-8.

159. Gao ZB, Pandya S, Hosein N, Sacks MS, Hwang NHC. Bioprosthetic heart valve leaflet motion monitored by dual camera stereo photogrammetry. J Biomech. 2000;33(2):199-207. doi:Doi 10.1016/S0021-9290(99)00165-7.

160. Iyengar AKS, Sugimoto H, Smith DB, Sacks MS. Dynamic in vitro quantification of bioprosthetic heart valve leaflet motion using structured light projection. Ann Biomed Eng. 2001;29(11):963-73.

161. Rousseau EPM, Vansteenhoven AA, Janssen JD, Huysmans HA. A Mechanical Analysis of the Closed Hancock Heart-Valve Prosthesis. J Biomech. 1988;21(7):545-62. doi:Doi 10.1016/0021-9290(88)90218-7.

162. Grande KJ, Cochran RP, Reinhall PG, Kunzelman KS. Stress variations in the human aortic root and valve: The role of anatomic asymmetry. Ann Biomed Eng. 1998;26(4):534-45. doi:Doi 10.1114/1.122.

163. Grande KJ, Cochran RP, Reinhall PG, Kunzelman KS. Mechanisms of aortic valve incompetence in aging: a finite element model. The Journal of heart valve disease. 1999;8(2):149-56.

164. Grande KJ, Cochran RP, Reinhall PG, Kunzelman KS. Mechanisms of aortic valve incompetence: finite element modeling of aortic root dilatation. The Annals of thoracic surgery. 2000;69(6):1851-7.

165. Grande-Allen KJ, Cochran RP, Reinhall PG, Kunzelman KS. Mechanisms of aortic valve incompetence: finite-element modeling of Marfan syndrome. The Journal of thoracic and cardiovascular surgery. 2001;122(5):946-54. doi:10.1067/mtc.2001.116314.

166. Grande-Allen KJ, Cochran RP, Reinhall PG, Kunzelman KS. Re-creation of sinuses is important for sparing the aortic valve: a finite element study. The Journal of thoracic and cardiovascular surgery. 2000;119(4 Pt 1):753-63.

167. Grande-Allen KJ, Cochran RP, Reinhall PG, Kunzelman KS. Finite-element analysis of aortic valve-sparing: influence of graft shape and stiffness. IEEE transactions on bio-medical engineering. 2001;48(6):647-59. doi:10.1109/10.923783.

168. Conti CA, Votta E, Della Corte A, Del Viscovo L, Bancone C, Cotrufo M et al. Dynamic finite element analysis of the aortic root from MRI-derived parameters. Med Eng Phys. 2010;32(2):212-21. doi:10.1016/j.medengphy.2009.12.003.

169. Labrosse MR, Beller CJ, Boodhwani M, Hudson C, Sohmer B. Subject-specific finite-element modeling of normal aortic valve biomechanics from 3D+t TEE images. Med Image Anal. 2015;20(1):162-72. doi:10.1016/j.media.2014.11.003.

170. Sun W, Sacks MS, Scott MJ. Effects of boundry conditions on the estimation of the planar biaxial mechanical properties of soft tissues. J Biomech Eng-T Asme. 2005;127(4):709-15. doi:Doi 10.1115/1.1933931.

171. Gabbay S, Bortolotti U, Wasserman F, Tindel N, Factor SM, Frater RW. Long-term follow-up of the Ionescu-Shiley mitral pericardial xenograft. The Journal of thoracic and cardiovascular surgery. 1984;88(5 Pt 1):758-63.

172. Trowbridge EA, Crofts CE. Pericardial heterograft valves: an assessment of leaflet stresses and their implications for heart valve design. J Biomed Eng. 1987;9(4):345-55.

173. Moore MA, Phillips RE, Jr., McIlroy BK, Walley VM, Hendry PJ. Evaluation of porcine valves prepared by dye-mediated photooxidation. The Annals of thoracic surgery. 1998;66(6 Suppl):S245-8.

174. Gloeckner DC, Billiar KL, Sacks MS. Effects of mechanical fatigue on the bending properties of the porcine bioprosthetic heart valve. Asaio J. 1999;45(1):59-63. doi:Doi 10.1097/00002480-199901000-00014.

175. Kim H, Chandran KB, Sacks MS, Lu J. An experimentally derived stress resultant shell model for heart valve dynamic simulations. Ann Biomed Eng. 2007;35(1):30-44. doi:10.1007/s10439-006-9203-8.

176. Kim H, Lu J, Sacks MS, Chandran KB. Dynamic simulation of bioprosthetic heart valves using a stress resultant shell model. Ann Biomed Eng. 2008;36(2):262-75. doi:10.1007/s10439-007-9409-4.

177. Simo JC, Fox DD. On a Stress Resultant Geometrically Exact Shell-Model .1. Formulation and Optimal Parametrization. Comput Method Appl M. 1989;72(3):267-304. doi:Doi 10.1016/0045-7825(89)90002-9.

178. Simo JC, Fox DD, Rifai MS. On a Stress Resultant Geometrically Exact Shell-Model .3. Computational Aspects of the Nonlinear-Theory. Comput Method Appl M. 1990;79(1):21-70. doi:Doi 10.1016/0045-7825(90)90094-3.

179. Howard IC, Patterson EA, Yoxall A. On the opening mechanism of the aortic valve: some observations from simulations. J Med Eng Technol. 2003;27(6):259-66. doi:10.1080/0309190031000096621.

180. Smith DB, Sacks MS, Pattany PM, Schroeder R. Fatigue-induced changes in bioprosthetic heart valve three-dimensional geometry and the relation to tissue damage. J Heart Valve Dis. 1999;8(1):25-33.

181. Hughes TJR, Liu WK, Zimmermann TK. Lagrangian-Eulerian finite element formulation for incompressible viscous flows. Comput Method Appl M. 1981;29:329-49.

182. Donea J, Giuliani S, Halleux JP. An arbitrary Lagrangian-Eulerian finite element method for transient dynamic fluid-structure interactions. Computer Methods in Applied Mechanics and Engineering. 1982;33:689-723.

183. Donea J, Huerta A, Ponthot J-P, Rodriguez-Ferran A. Arbitrary Lagrangian-Eulerian Methods. Encyclopedia of Computational Mechanics. 2004.

184. Tezduyar TE, Behr M, Liou J. A new strategy for finite element computations involving moving boundaries and interfaces - the deforming-spatial-domain/space-time procedure: I1 The concept and the preliminary numerical tests. Comput Method Appl M. 1992;94(3):339-51.

185. Tezduyar TE, Behr M, Mittal S, Liou J. A new strategy for finite element computations involving moving boundaries and interfaces - the deforming-spatial-domain/space-time procedure: II1 Computation of free-surface flows, two-liquid flows, and flows with drifting cylinders. Comput Method Appl M. 1992;94(3):353-71.

186. Johnson AA, Tezduyar TE. Parallel Computation of Incompressible Flows with Complex Geometries. Int J Numer Meth Fl. 1997;24:1321-40.

187. Tezduyar T, Aliabadi S, Behr M, Johnson A, Mittal S. Massively Parallel Finite Element Computation of 3D Flows - Mesh Update Strategies in Computation of Moving Boundaries and Interfaces. Parallel Computational Fluid Dynamics - New Trends and Advances. 1995; p. 21-30.

188. Johnson AA, Tezduyar TE. 3D Simulation of Fluid-Particle Interactions with the Number of Particles Reaching 100. Comput Method Appl M. 1997;145:301-21.

189. Johnson AA, Tezduyar TE. Advanced Mesh Generation and Update Methods for 3D Flow Simulations. Computational Mechanics. 1999;23:130-43.

190. Takizawa K, Tezduyar TE, Buscher A, Asada S. Space-time interface-tracking with topology change (ST-TC). Computational Mechanics. 2013.

191. Takizawa K, Tezduyar T, Buscher A, Asada S. Spaceâ€“time fluid mechanics computation of heart valve models. Computational Mechanics. 2014:1-14.

192. Makhijani VB, Yang HQ, Dionne PJ, Thubrikar MJ. Three-Dimensional Coupled Fluid-Structure Simulation of Pericardial Bioprosthetic Aortic Valve Function. ASAIO Journal. 1997;43:M387-M92.

193. Peskin CS. Flow patterns around heart valves: A numerical method Journal of Computational Physics 1972;10(2):252-71.

194. Mittal R, Iaccarino G. Immersed boundary methods. Annual Review of Fluid Mechanics. 2005;37:239-61.

195. Sotiropoulos F, Yang X. Immersed boundary methods for simulating fluid-structure interaction. Prog Aerosp Sci. 2014;65:1-21.

196. Tezduyar TE. Computation of Moving Boundaries and Interfaces and Stabilization Parameters. Int J Numer Meth Fl. 2003;43:555-75.

197. Takizawa K, Moorman C, Wright S, Christopher J, Tezduyar TE. Wall Shear Stress Calculations in Space-Time Finite Element Computation of Arterial Fluid-Structure Interactions. Computational Mechanics. 2010;46:31-41.

198. Gingold RA, Monaghan JJ. Smoothed particle hydrodynamics: theory and application to non-spherical stars. Monthly Notices of the Royal Astronomical Society. 1977;181(3):375-89. doi:10.1093/mnras/181.3.375.

199. Toma M, Jensen MO, Einstein DR, Yoganathan AP, Cochran RP, Kunzelman KS. Fluid-Structure Interaction Analysis of Papillary Muscle Forces Using a Comprehensive Mitral Valve Model with 3D Chordal Structure. Ann Biomed Eng. 2015. doi:10.1007/s10439-015-1385-5.

200. de Hart J. Fluid-Structure Interaction in the Aortic Heart Valve: a three-dimensional computational analysis [Ph.D. Thesis]. Eindhoven, Netherlands: Technische Universiteit Eindhoven; 2002.

201. De Hart J, Peters GWM, Schreurs PJG, Baaijens FPT. A three-dimensional computational analysis of fluid-structure interaction in the aortic valve Journal of Biomechanics 2003;36:103-12.

202. De Hart J, Baaijens FPT, Peters GWM, Schreurs PJG. A computational fluid-structure interaction analysis of a fiber-reinforced stentless aortic valve. Journal of Biomechanics 2003;36:699-712.

203. van Loon R. A 3D method for modelling the fluid-structure interaction of heart valves [Ph.D. Thesis]. Eindhoven, Netherlands: Technische Universiteit Eindhoven; 2005.

204. van Loon R, Anderson PD, van de Vosse FN. A fluid-structure interaction method with solid-rigid contact for heart valve dynamics. Journal of Computational Physics. 2006;217:806-23.

205. van Loon R. Towards computational modelling of aortic stenosis. International journal for numerical methods in biomedical engineering. 2010;26:405-20.

206. Baaijens FPT. A fictitious domain/mortar element method for fluid-structure interaction. Int J Numer Meth Fl. 2001;35(7):743-61.

207. Griffith BE. Immersed boundary model of aortic heart valve dynamics with physiological driving and loading conditions. International journal for numerical methods in biomedical engineering. 2012;28(3):317-45.

208. Borazjani I. Fluid-structure interaction, immersed boundary-finite element method simulations of bio-prosthetic heart valves. Comput Method Appl M. 2013;257:103-16.

209. Ge L, Sotiropoulos F. A numerical method for solving the 3D unsteady incompressible Navier-Stokes equations in curvilinear domains with complex immersed boundaries Journal of Computational Physics 2007;225(2):1782-809.

210. Borazjani I, Ge L, Sotiropoulos F. Curvilinear immersed boundary method for simulating fluid structure interaction with complex 3D rigid bodies Journal of Computational Physics 2008;227(16):7587-620.

211. Gilmanov A, Le TB, Sotiropoulos F. A numerical approach for simulating fluid structure interaction of flexible thin shells undergoing arbitrarily large deformations in complex domains. Journal of Computational Physics. 2015;300:814-43. doi:http://dx.doi.org/10.1016/j.jcp.2015.08.008.

212. Gilmanov A, Sotiropoulos F. Comparative hemodynamics in an aorta with bicuspid and trileaflet valves. Theoretical and Computational Fluid Dynamics. 2015;30(1):67-85. doi:10.1007/s00162-015-0364-7.

213. Kamensky D, Hsu M-C, Schillinger D, Evans JA, Aggarwal A, Bazilevs Y et al. An immersogeometric variational framework for fluid-structure interaction: Application to bioprosthetic heart valves Comput Method Appl M. 2015;284:1005-53.

214. Hsu M-C, Kamensky D, Bazilevs Y, Sacks MS, Hughes TJR. Fluid-structure interaction analysis of bioprosthetic heart valves: significance of arterial wall deformation. Computational Mechanics. 2014;54:1055-71.

215. Hsu M-C, Kamensky D, Xu F, Kiendl J, Wang C, Wu MCH et al. Dynamic and fluid-structure interaction simulations of bioprosthetic heart valves using parametric design with T-splines and Fung-type material models. Computational Mechanics. 2015:1-15.

216. Hsu M-C, Kamensky D, Xu F, Kiendl J, Wang C, Wu MH et al. Dynamic and fluid–structure interaction simulations of bioprosthetic heart valves using parametric design with T-splines and Fung-type material models. Comput Mech. 2015;55(6):1211-25. doi:10.1007/s00466-015-1166-x.

217. Hughes TJR, Cottrell JA, Bazilevs Y. Isogeometric analysis: CAD, finite elements, NURBS, exact geometry, and mesh refinement. Computer Methods in Applied Mechanics and Engineering. 2005;194:4135-95.

218. Kiendl J, Bletzinger K-U, Linhard J, W\"uchner R. Isogeometric shell analysis with Kirchhoff-Love elements. Comput Method Appl M. 2009;198:3902-14.

219. Kiendl J. Isogeometric Analysis and Shape Optimal Design of Shell Structures: Lehrstuhl f\"ur Statik, Technische Universit\"at M\"unchen; 2011.

220. Kiendl J, Hsu M-C, Wu MCH, Reali A. Isogeometric Kirchhoff-Love shell formulations for general hyperelastic materials Comput Method Appl M. 2015;291(0):280-303.

221. Tepole AaB, Kabaria H, Bletzinger K-U, Kuhl E. Isogeometric Kirchhoff-Love shell formulations for biological membranes Comput Method Appl M. 2015(0): -

222. Morganti S, Auricchio F, Benson DJ, Gambarin FI, Hartmann S, Hughes TJR et al. Patient-specific isogeometric structural analysis of aortic valve closure. Comput Method Appl M. 2015;284:508-20.

223. Corp. L-DFESLST. http://www.lstc.com/products/ls-dyna.

224. Chew GG, Howard IC, Patterson EA. Simulation of damage in a porcine prosthetic heart valve. J Med Eng Technol. 1999;23(5):178-89.

225. Carmody CJ, Burriesci G, Howard IC, Patterson EA. An approach to the simulation of fluid-structure interaction in the aortic valve. Journal of Biomechanics. 2006;39:158-69.

226. Sturla F, Votta E, Stevanella M, Conti CA, Redaelli A. Impact of modeling fluid-structure interaction in the computational analysis of aortic root biomechanics. MedEngPhys. 2013;35:1721-30.

227. Wu W, Pott D, Mazza B, Sironi T, Dordoni E, Chiastra C et al. Fluid-Structure Interaction Model of a Percutaneous Aortic Valve: Comparison with an In Vitro Test and Feasibility Study in a Patient-Specific Case. Ann Biomed Eng. 2016;44(2):590-603. doi:10.1007/s10439-015-1429-x.

228. Courant R, Friedrichs K, Lewy H. On the partial difference equations of mathematical physics. IBM J Res Develop. 1967;11:215-34.

229. Courant R, Friedrichs K, Lewy H. \"Uber die partiellen Differenzengleichungen der mathematischen Physik. Mathematische Annalen. 1928;100(1):32-74.

230. Bogaers AEJ, Kok S, Reddy BD, Franz T. Quasi-Newton methods for implicit black-box FSI coupling. Comput Method Appl M. 2014;279(0):113-32.

231. van Brummelen EH. Added mass effects of compressible and incompressible flows in fluid-structure interaction. Journal of Applied Mechanics. 2009;76:021206.

232. Michler C, van Brummelen H, de Borst R. An investigation of Interface-GMRES(R) for fluid-structure interaction problems with flutter and divergence. Computational Mechanics. 2011;47(1):17-29.

233. Astorino M, Gerbeau J-F, Pantz O, Traor\'e K-F. Fluid-structure interaction and multi-body contact: Application to aortic valves. Comput Method Appl M. 2009;198:3603-12.

234. Gao BZ, Pandya S, Arana C, Hwang NHC. Bioprosthetic Heart Valve Leaflet Deformation Monitored by Double-Pulse Stereo Photogrammetry. Annals of Biomedical Engineering. 2002;30(1):11-8.

235. Iyengar AKS, Sugimoto H, Smith DB, Sacks MS. Dynamic In Vitro Quantification of Bioprosthetic Heart Valve Leaflet Motion Using Structured Light Projection. Annals of Biomedical Engineering. 2001;29(11):963-73.

236. Sugimoto H, Sacks MS. Effects of Leaflet Stiffness on In Vitro Dynamic Bioprosthetic Heart Valve Leaflet Shape. Cardiovascular engineering and technology. 2013;4(1):2-15.

237. Thornton MA, Howard LC, Patterson EA. Three-dimensional stress analysis of polypropylene leaflets for prosthetic heart valves. Med Eng Phys. 1997;19(6):588-97. doi:Doi 10.1016/S1350-4533(96)00042-2.

238. Sacks MS, Sun W. Multiaxial mechanical behavior of biological materials. Annu Rev Biomed Eng. 2003;5:251-84. doi:Doi 10.1146/Annurev.Bioeng.5.011303.120714.

239. Patterson EA, Howard IC, Thornton MA. A comparative study of linear and nonlinear simulations of the leaflets in a bioprosthetic heart valve during the cardiac cycle. J Med Eng Technol. 1996;20(3):95-108. doi:Doi 10.3109/03091909609008387.

240. Pouch A, Tian S, Takabe M, Wang H, Yuan J, Cheung A et al. Segmentation of the Aortic Valve Apparatus in 3D Echocardiographic Images: Deformable Modeling of a Branching Medial Structure. In: Camara O, Mansi T, Pop M, Rhode K, Sermesant M, Young A, editors. Statistical Atlases and Computational Models of the Heart - Imaging and Modelling Challenges. Lecture Notes in Computer Science: Springer International Publishing; 2015. p. 196-203.

241. Aggarwal A, Ferrari G, Joyce E, Daniels MJ, Sainger R, Gorman JH, 3rd et al. Architectural trends in the human normal and bicuspid aortic valve leaflet and its relevance to valve disease. Ann Biomed Eng. 2014;42(5):986-98. doi:10.1007/s10439-014-0973-0.

242. Aggarwal A, Sacks M. A Framework for Determination of Heart Valves' Mechanical Properties Using Inverse-Modeling Approach. In: van Assen H, Bovendeerd P, Delhaas T, editors. Functional Imaging and Modeling of the Heart. Lecture Notes in Computer Science: Springer International Publishing; 2015. p. 285-94.

243. Chuong CJ, Fung YC. On residual stresses in arteries. Journal of biomechanical engineering. 1986;108(2):189-92.

244. Vyavahare N, Ogle M, Schoen FJ, Zand R, Gloeckner DC, Sacks M et al. Mechanisms of bioprosthetic heart valve failure: fatigue causes collagen denaturation and glycosaminoglycan loss. J Biomed Mater Res. 1999;46(1):44-50.

245. Lovekamp JJ, Simionescu DT, Mercuri JJ, Zubiate B, Sacks MS, Vyavahare NR. Stability and function of glycosaminoglycans in porcine bioprosthetic heart valves. Biomaterials. 2006;27(8):1507-18. doi:10.1016/j.biomaterials.2005.08.003.

246. Mako WJ, Vesely I. In vivo and in vitro models of calcification in porcine aortic valve cusps. The Journal of heart valve disease. 1997;6(3):316-23.

247. Smith DB, Sacks MS, Pattany PM, Schroeder R. High-resolution magnetic resonance imaging to characterize the geometry of fatigued porcine bioprosthetic heart valves. J Heart Valve Dis. 1997;6(4):424-32.

248. Starr A. The artificial heart valve. Nat Med. 2007;13:1160-4.

249. Huang HY, Liao J, Sacks MS. In-situ deformation of the aortic valve interstitial cell nucleus under diastolic loading. J Biomech Eng. 2007;129(6):880-89. doi:10.1115/1.2801670.

Table 1

		Fix	Thickness (mm)	UTS (MPa)	Strain at Fracture (%)	Tissue Modulus (MPa)	Toughness (MPa)	Shrinkage (%)
Bovine Pericardium	PD		n=10	n=5	n=5	n=5	n=5	n=5
		Fresh	0.252 ± 0.027	25.6 ± 4.5	82.7 ± 4.7	69.6 ± 9.6	6.3 ± 0.7	N/A
		GLUT	0.448 ± 0.06	17.7 ± 3	120.6 ± 7.1	43.9 ± 10.6	5.7 ± 1	17.2 ± 0.5
		Epoxy	0.376 ± 0.059	16.4 ± 3.4	114.7 ± 12.4	40.5 ± 4.7	6.5 ± 1.5	14.9 ± 2.7
		Genipin	0.059 ± 0.08	21.3 ± 5.4	120.2 ± 10.9	42.5 ± 8.3	6.8 ± 2.4	17.1 ± 2
	XD		n=10	n=5	n=5	n=5	n=5	n=5
		Fresh	0.252 ± 0.027	12.7 ± 1.9	55.3 ± 4.6	48.8 ± 7.3	2.8 ± 0.7	N/A
		GLUT	0.448 ± 0.06	12.2 ± 3.5	103.6 ± 15.4	31.4 ± 8.1	3.8 ± 0.9	23.7 ± 3.5
		Epoxy	0.376 ± 0.059	11.6 ± 1.9	103.9 ± 16.8	24.8 ± 1.8	4.3 ± 1.5	23.9 ± 4
		Genipin	0.059 ± 0.08	21.7 ± 2.3	102.2 ± 9.8	41 ± 9.9	6.3 ± 1.6	23.2 ± 1.5
Porcine Aortic Valve	PD		n=12	n=6	n=6	n=6	n=6	n=6
		Fresh	0.261 ± 0.026	8.3 ± 0.9	48.7 ± 7.3	44.7 ± 5.3	1.8 ± 0.3	N/A
		GLUT	0.334 ± 0.043	8.3 ± 1.3	59.2 ± 7.6	32.1 ± 6.6	2 ± 0.1	6.7 ± 4.3
		Genipin	0.397 ± 0.051	7.6 ± 0.7	69.8 ± 5.1	25.6 ± 4.8	2.3 ± 0.1	12.5 ± 4.3
	XD		n=12	n=6	n=6	n=6	n=6	n=6
		Fresh	0.261 ± 0.026	1.4 ± 0.2	134.8 ± 27.7	6.4 ± 0.9	0.8 ± 0.1	N/A
		GLUT	0.334 ± 0.043	1.2 ± 0.2	164.6 ± 17	5.3 ± 0.5	0.9 ± 0	11.3 ± 2.2
		Genipin	0.397 ± 0.051	1.2 ± 0.3	177.3 ± 19.8	4.9 ± 0.5	1 ± 0.1	15.3 ± 6.4
Human Valves			n=11	n=11	n=11	n=11		
	Pulmonary (circ)		0.397 ± 0.114	2.78 ± 1.05	19.4 ± 3.91	16.05 ± 2.02		
	Aortic (circ)		0.605 ± 0.196	1.74 ± 0.29	18.35 ± 7.61	15.34 ± 3.84		
	Pulmonary (rad)		0.397 ± 0.114	0.29 ± 0.06	29.67 ± 4.41	1.32 ± 0.93		
	Aortic (rad)		0.605 ± 0.196	0.32 ± 0.04	23.92 ± 3.94	1.98 ± 0.15		

Table 2

Group	Strain at Fixation	Max. Strain	Thickness (μm)	Peak stress (kPa)		Max. Tangent Modulus (MPa)	
				PD	XD	PD	XD
Control	N/A	0.16	343 ± 10	323.18 ± 22.56	107.12 ± 6.75	14.96 ± 2.77	2.8 ± 0.35
GLFF	Free	0.16	781 ± 114	168.73 ± 9.74	96.66 ± 8.09	3.27 ± 0.25	1.31 ± 0.18
GLPS	0.22	0.06	430 ± 81	429.47 ± 49.28	122.46 ± 5.00	39.89 ± 11.14	1.28 ± 0.2
POFF	Free	0.16	719 ± 77	66.17 ± 2.31	37.53 ± 5.16	1.22 ± 0.06	0.46 ± 0.1
POPS	0.22	0.16	512 ± 91	125.34 ± 11.29	43.57 ± 2.98	2.43 ± 0.31	0.42 ± 0.05

Table 3

		Width (mm)	Thickness (mm)	Green's Strain at 1 N/m	Green's Strain at 9 N/m	Green's Strain at 60 N/m	Index of Isotropy	Shear Angle α (deg)
Radial	Fresh	13.68 ± 0.46	0.466 ± 0.02	0.646 ± 0.035	0.913 ± 0.061	1.109 ± 0.075	0.247 ± 0.023	5.88 ± 1.326
	Fixed	11.32 ± 0.27	0.457 ± 0.02	0.292 ± 0.028	0.619 ± 0.047	0.958 ± 0.07	0.022 ± 0.012	13.02 ± 1.58
Circunferential	Fresh	14.23 ± 0.42	0.466 ± 0.02	0.194 ± 0.012	0.244 ± 0.016	0.264 ± 0.017	0.247 ± 0.023	5.88 ± 1.326
	Fixed	13 ± 0.19	0.457 ± 0.02	0.001 ± 0.006	0.01 ± 0.008	0.024 ± 0.012	0.022 ± 0.012	13.02 ± 1.58

Table 4

Stretch at 60 N/m (percent)		
	Radial	Circumferential
Aortic, natural	74.5 ± 7.8	12.4 ± 1.8
Pulmonary, natural	90.3 ± 5.7	10 ± 1.9
Aortic, GLUT	64.3 ± 5.8	9.5 ± 1.8
Pulmonary, GLUT	88.8 ± 2.6	13.5 ± 1.0

Table 5

	Thickness (mm)	Width (mm)	I (mm^4)	Max M VIS (mn-mm)	Max M EPI (mn-mm)	Max Δκ VIS (mm^{-1})	Max Δκ EPI (mm^{-1})	$\bar{E}$ at Δκ= 0.02 mm^{-1}
PD Native	0.35 ± 0.02	3.3 ± 0.1	0.0125 ± 0.0025	0.9049 ± 0.3753	0.6033 ± 0.1666	0.169 ± 0.0171	0.1853 ± 0.0412	0.128 ± 0.062
XD Native	0.35 ± 0.02	3.9 ± 0.2	0.0147 ± 0.0024	0.7363 ± 0.1431	0.6182 ± 0.093	0.1245 ± 0.0119	0.1102 ± 0.0157	0.391 ± 0.064
PD GLPB	0.67 ± 0.02	2.8 ± 0.31	0.0716 ± 0.0082	0.3691 ± 0.0828	0.4739 ± 0.1044	0.281 ± 0.0168	0.2369 ± 0.0162	0.7201 ± 0.1549
XD GLPB	0.65 ± 0.95	2.55 ± 0.02	0.0624 ± 0.0479	0.5033 ± 0.0066	0.5409 ± 0.0395	0.2535 ± 0.0687	0.2307 ± 0.017	1.2097 ± 0.1156

Table 6

	Thickness (mm)	I (mm^4)	Max M (mN-mm)	Max Δκ (mm^{-1})	E_{eff} (kPa)
AC	0.38 ± 0.03	1.00E-02 ± 2.18E-03	1.529 ± 0.204	0.268 ± 0.025	703.05 ± 132.58
WC	0.43 ± 0.02	2.75E-02 ± 3.65E-03	1.701 ± 0.203	0.153 ± 0.018	491.69 ± 135.17

Table 7

	Forward direction	Reverse direction
Effective modulus, E, at flexure angle of 30° (kPa)	42.73 ± 4.44	75.01 ± 14.53
dE/dϕ (kPa/°)	-2.24 ± 0.6	-1.9 ± 0.3

Table 8

Fixation Chemistry	Thickness (mm) n=10, ±SD	Tensile Strength (MPa) n=5, ±SD	Strain at Fracture (%) n=5, ±SD
Fresh	0.095 ± 0.008	18.1 ± 1.6	55.6 ± 13.5
Genipin	0.167 ± 0.006	16 ± 1.2	81.9 ± 5.9
Carbodiimide	0.114 ± 0.004	13.1 ± 1	60 ± 10.9
Carbodiimide + NHS	0.119 ± 0.008	13.4 ± 0.6	60.5 ± 9.1
Genipin then Carbodiimide + NHS	0.154 ± 0.014	15.9 ± 1.4	84.1 ± 13.4
Carbodiimide + NHS then Genipin	0.168 ± 0.008	15.7 ± 0.9	85.3 ± 13.3

Table 9

	c (kPa)	a_1	a_2	a_3	a_4	a_5	a_6	r^2
Bovine Pericardium	16.24	66.73	34.52	1.29	24.09	0.77	0.53	0.99
Porcine Pericardium	20.23	59.33	26.1	-2.68	24.04	-1.35	1.51	0.99

Table 10

Click here to download Table Table 15.png

Group	n	b_0 (kPa)		b_1 (kPa)		b_2 (kPa)		b_3 (kPa)		r^2	
		Specimen	Group	Specimen	Group	Specimen	Group	Specimen	Group	Specimen	Group
Control	7	0.243 ± 0.117	0.217	288.96 ± 45.88	256.3	154.01 ± 25.66	144.13	131.67 ± 24.74	113.01	0.933 ± 0.038	0.842
GLIFF	12	1.873 ± 0.153	1.738	106.93 ± 2.79	111.23	71.39 ± 6.04	74.16	45.52 ± 2.60	46.83	0.970 ± 0.003	0.723
POFF	11	0.838 ± 0.088	0.834	101.5 ± 4.00	100.80	63.29 ± 5.48	64.28	43.19 ± 0.79	42.09	0.990 ± 0.002	0.947
GLPS	9	3.677 ± 0.470	4.93	601.8 ± 57.78	517.47	107.29 ± 25.24	88.56	124.1 ± 7.30	88.55	0.982 ± 0.003	0.924
POPS	10	2.151 ± 0.439	1.55	99.36 ± 8.526	104.99	43.99 ± 5.57	44.98	33.64 ± 5.08	38.32	0.991 ± 0.002	0.881

Table 11

Click here to download Table Table 16.png

	A (kPa)	B	c_0	c_1	r^2
Bovine Pericardium, GLBP	10.9299	16.1559	2.3432	26.9825	0.9616

Table 12

	Two Parameter Model			*Fiber Recruitment model*			
	A (kPa)	*B*	r^2	*K (kPa)*	α	β	r^2
Bovine Pericardium, untreated	0.336	44.921	0.913	58.73	5.6470	0.0428	0.899

Figure 1

Click here to download Figure Figure 1.png

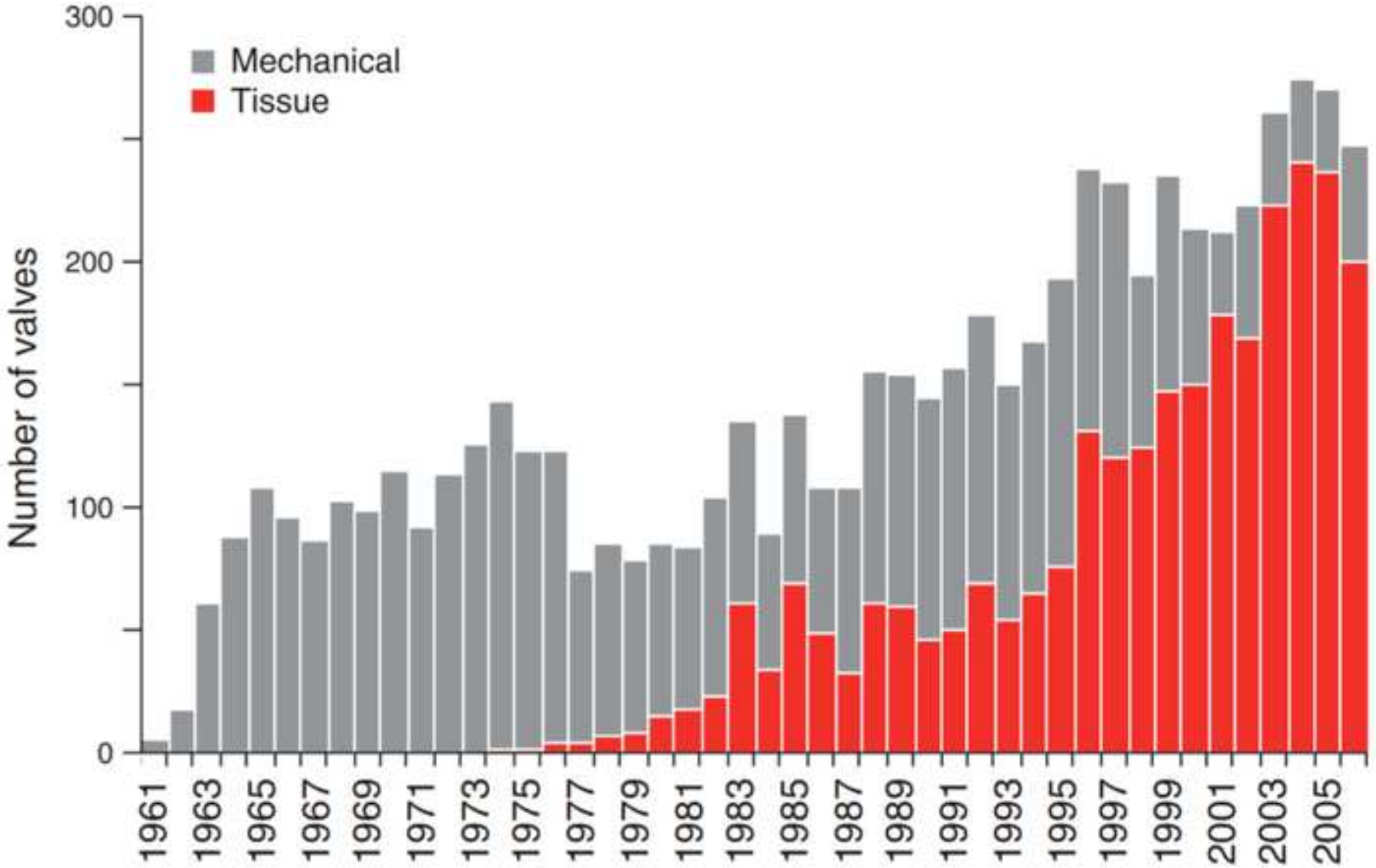

Figure 2

Click here to download Figure Figure 2.png

Figure 3

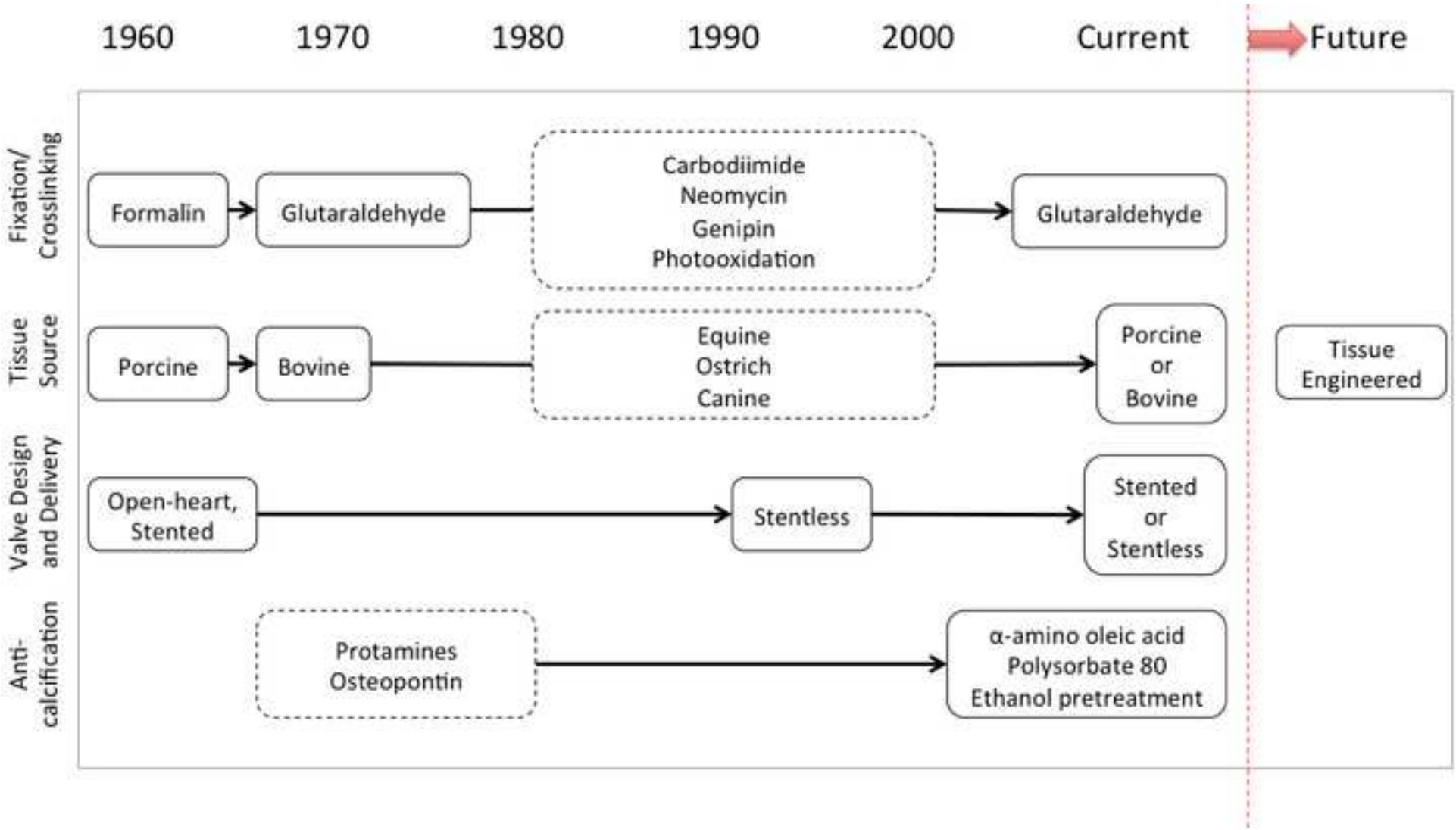

Figure 4

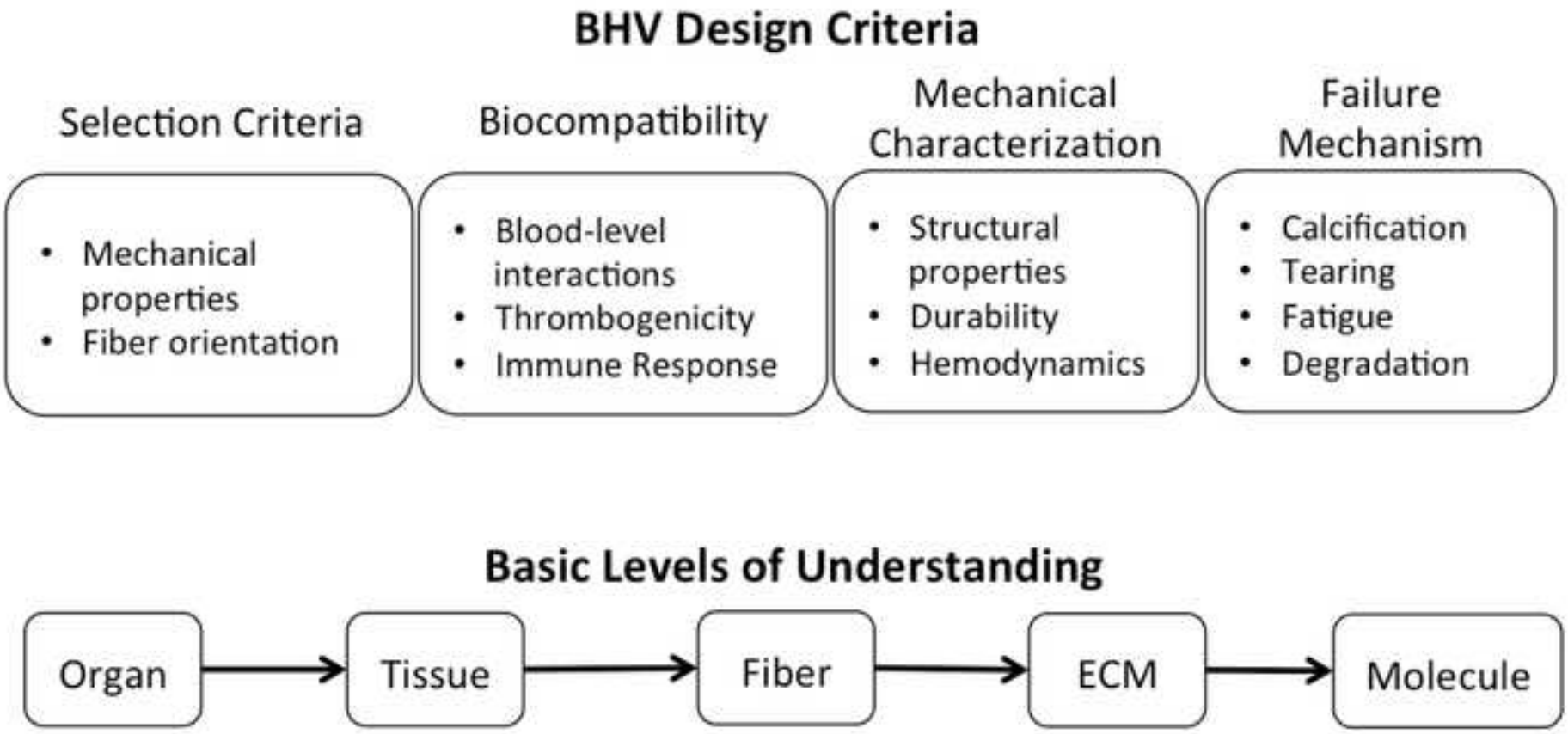

Figure 5

Click here to download Figure Figure 5.png

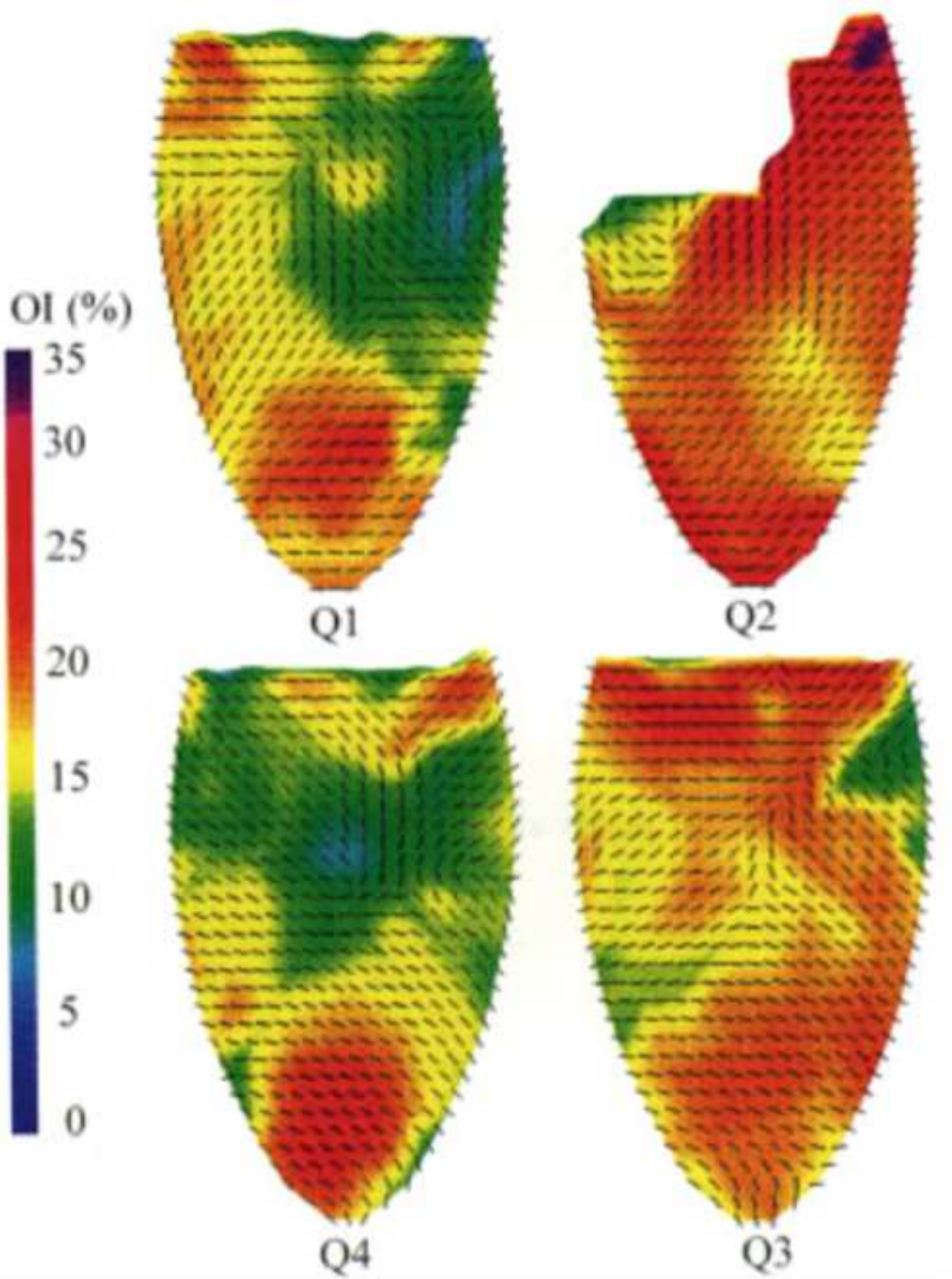

Figure 6

Click here to download Figure Figure 6.png

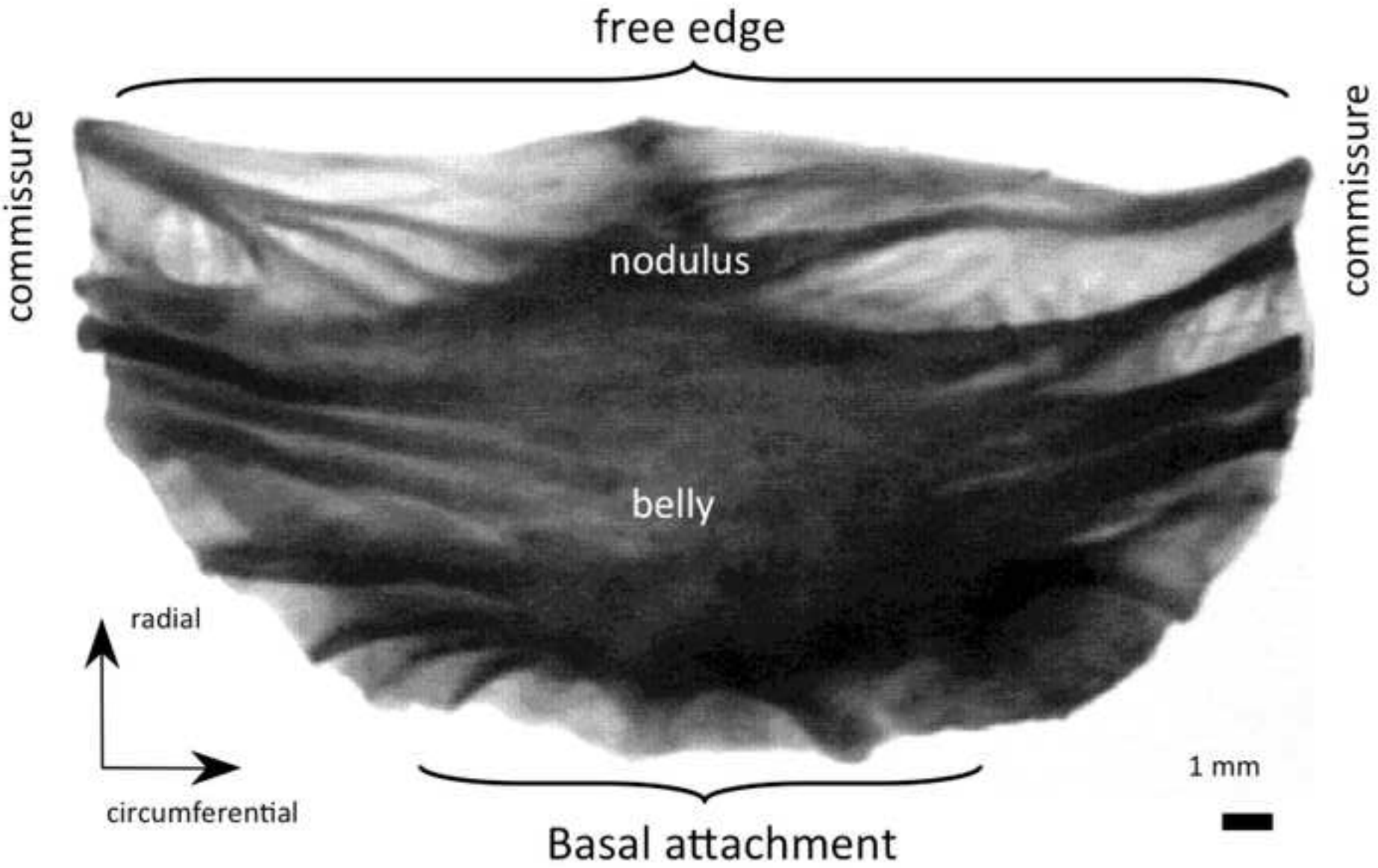

Figure 7

Click here to download Figure Figure 7.png

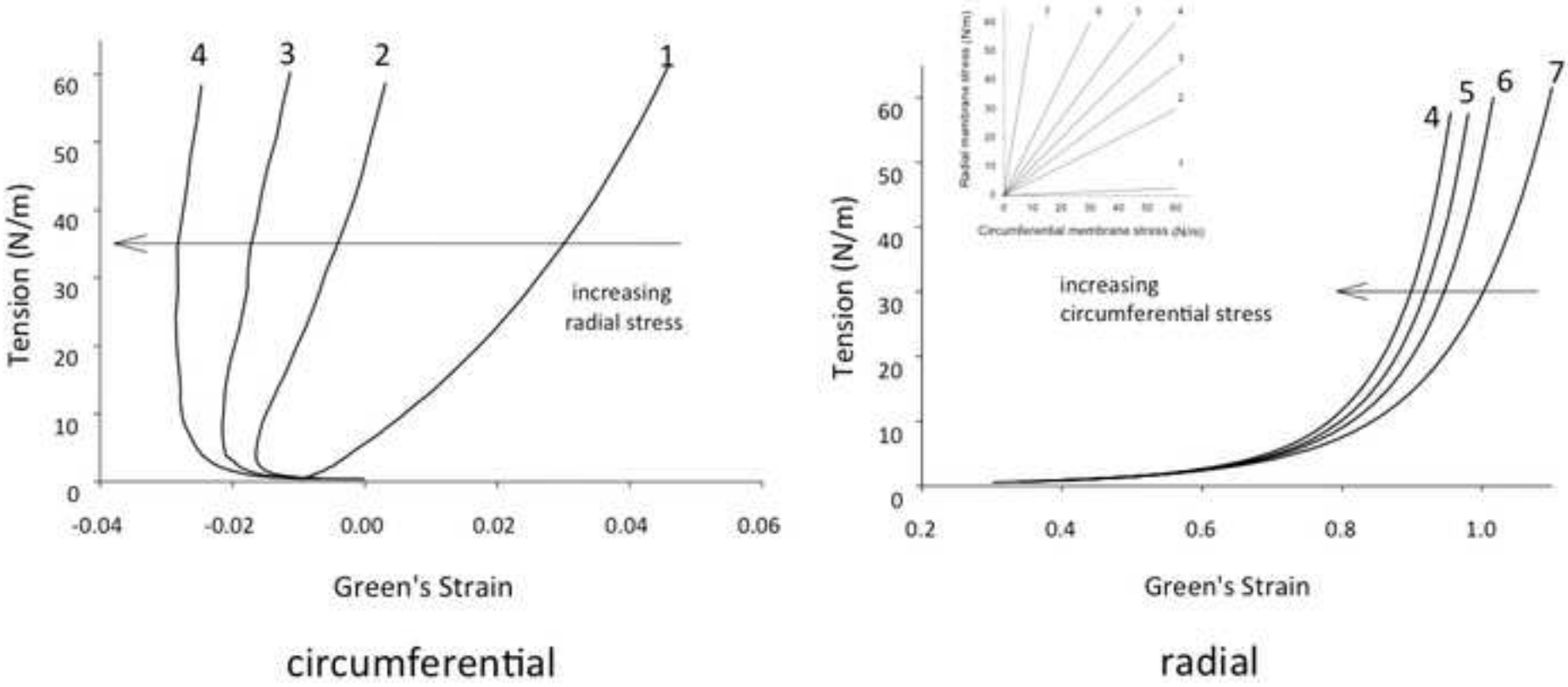

Figure 8

Click here to download Figure Figure 8.png

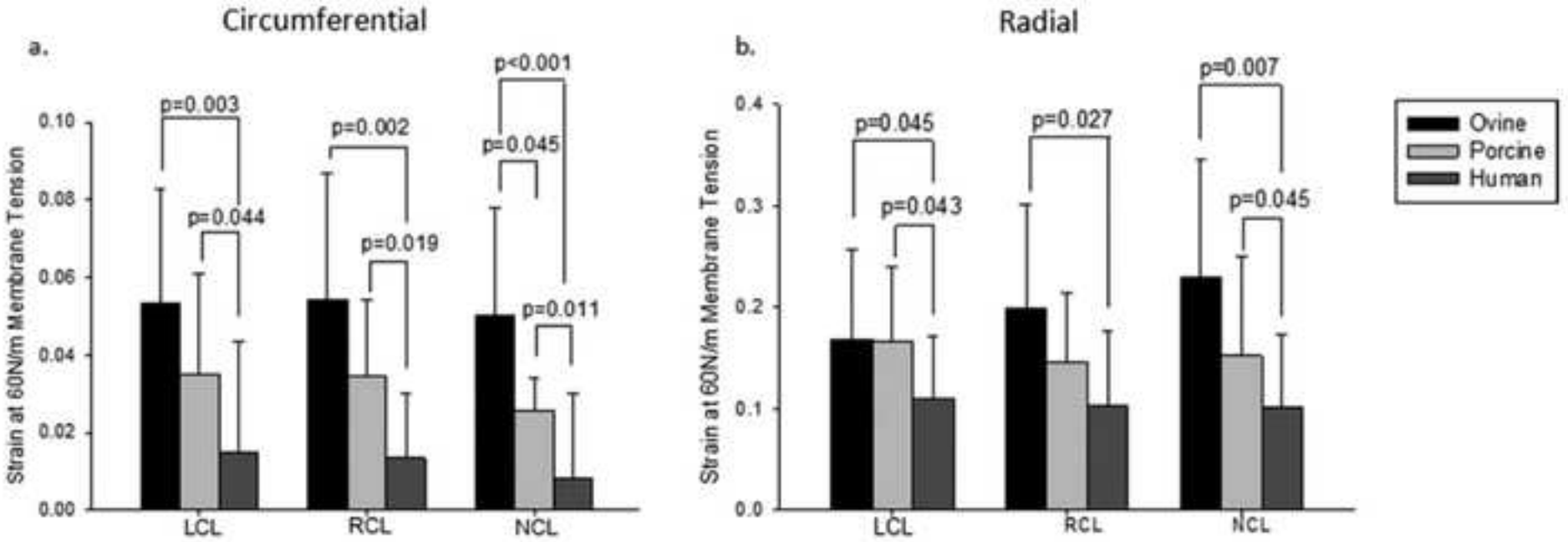

Figure 9

Click here to download Figure Figure 9.png

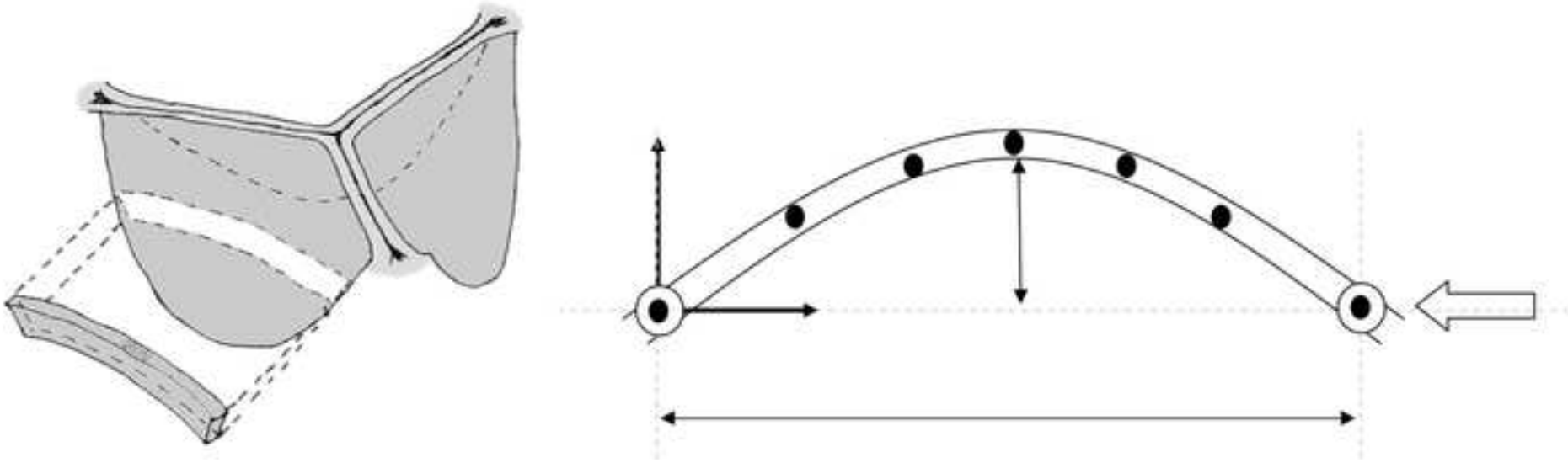

Figure 10

Click here to download Figure Figure 10.png

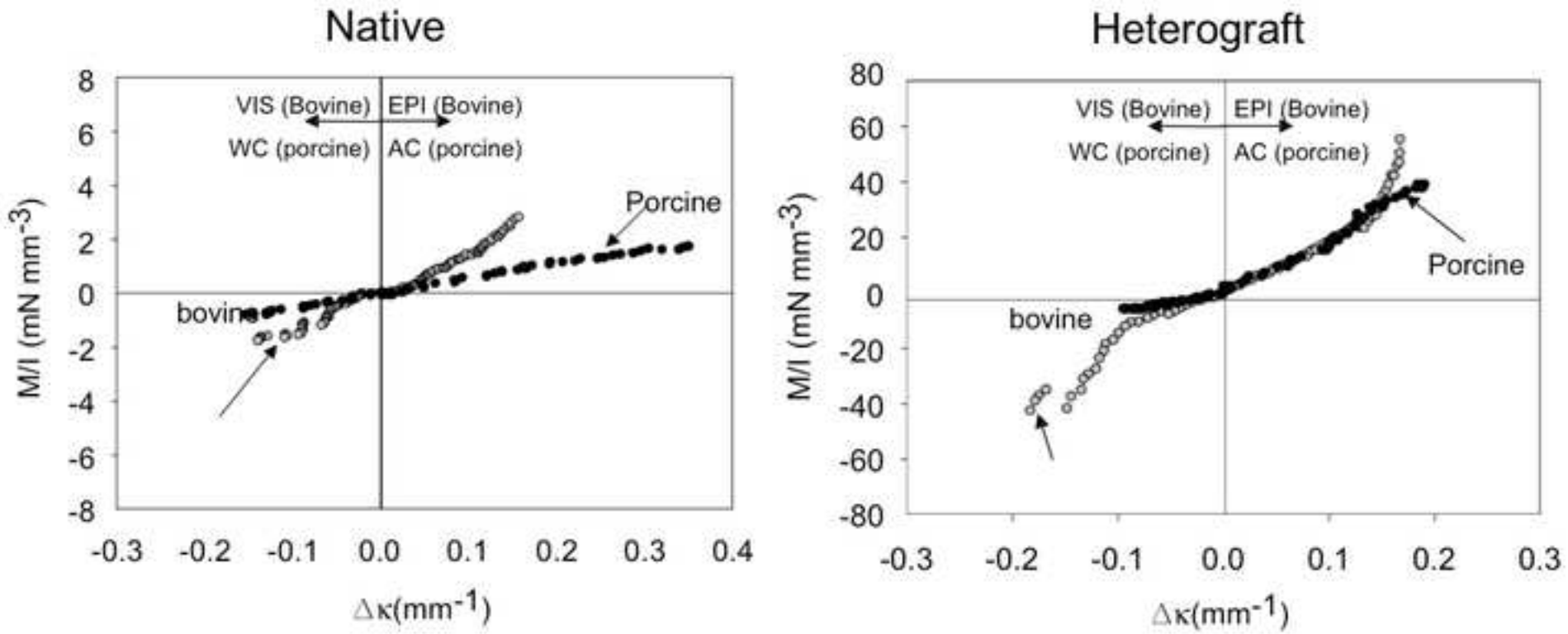

Figure 11

Click here to download Figure Figure 11.png

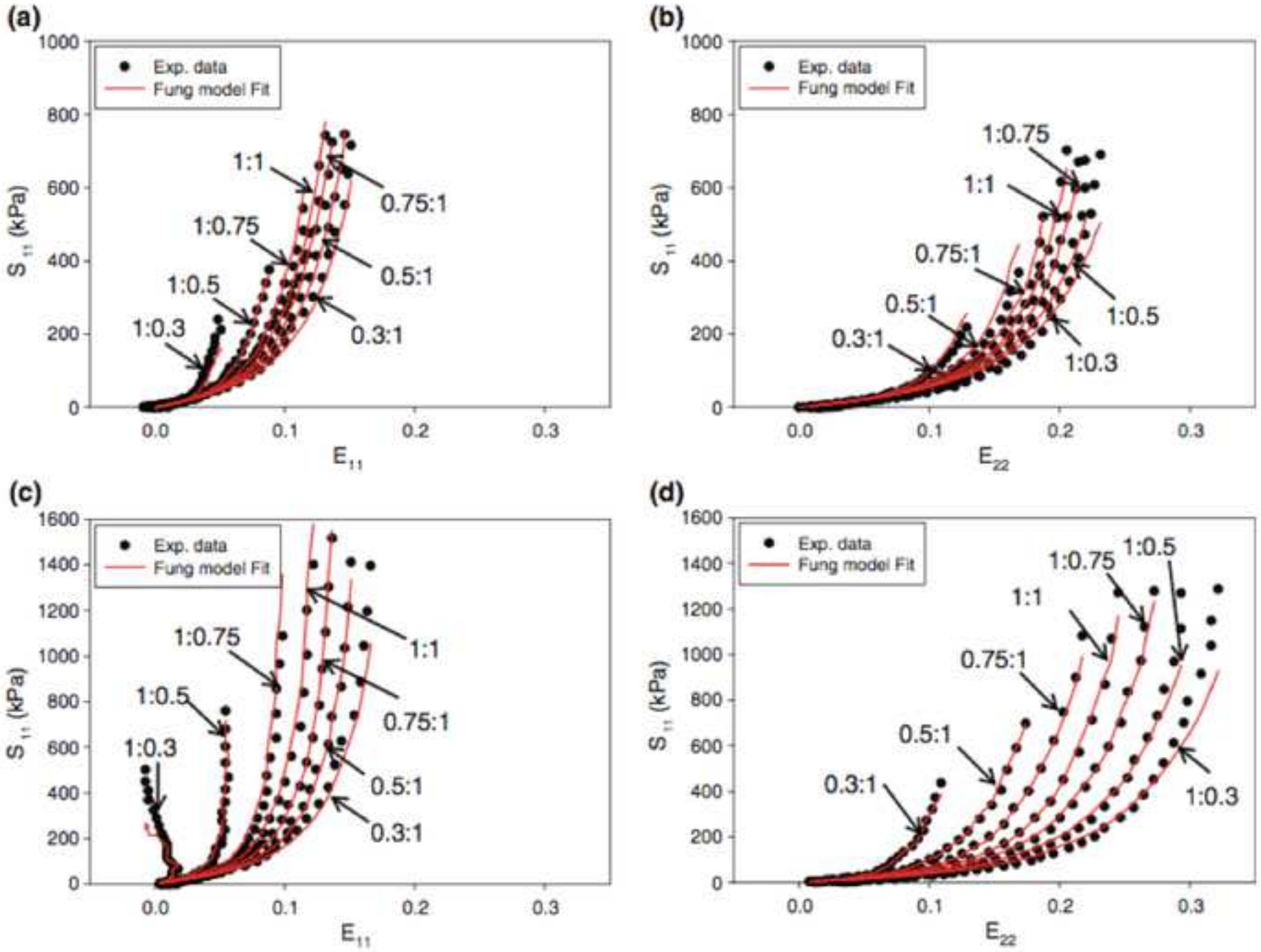

Figure 12

Click here to download Figure Figure 12.png

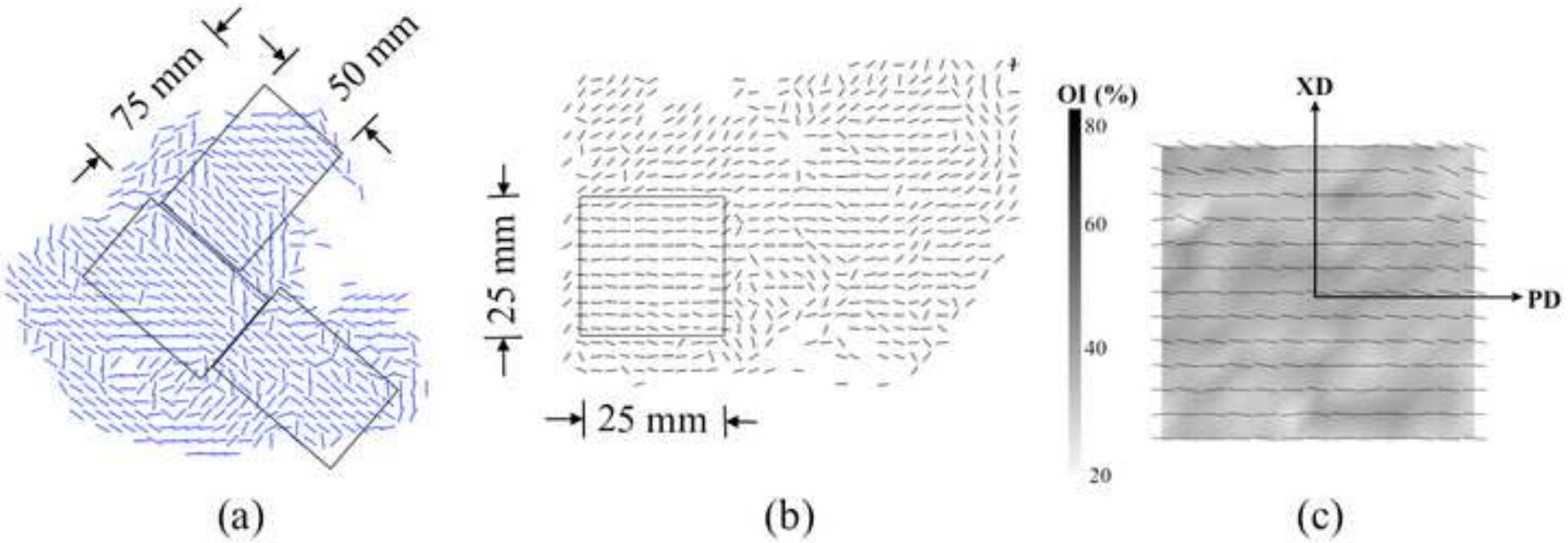

Figure 13

Click here to download Figure Figure 13.png

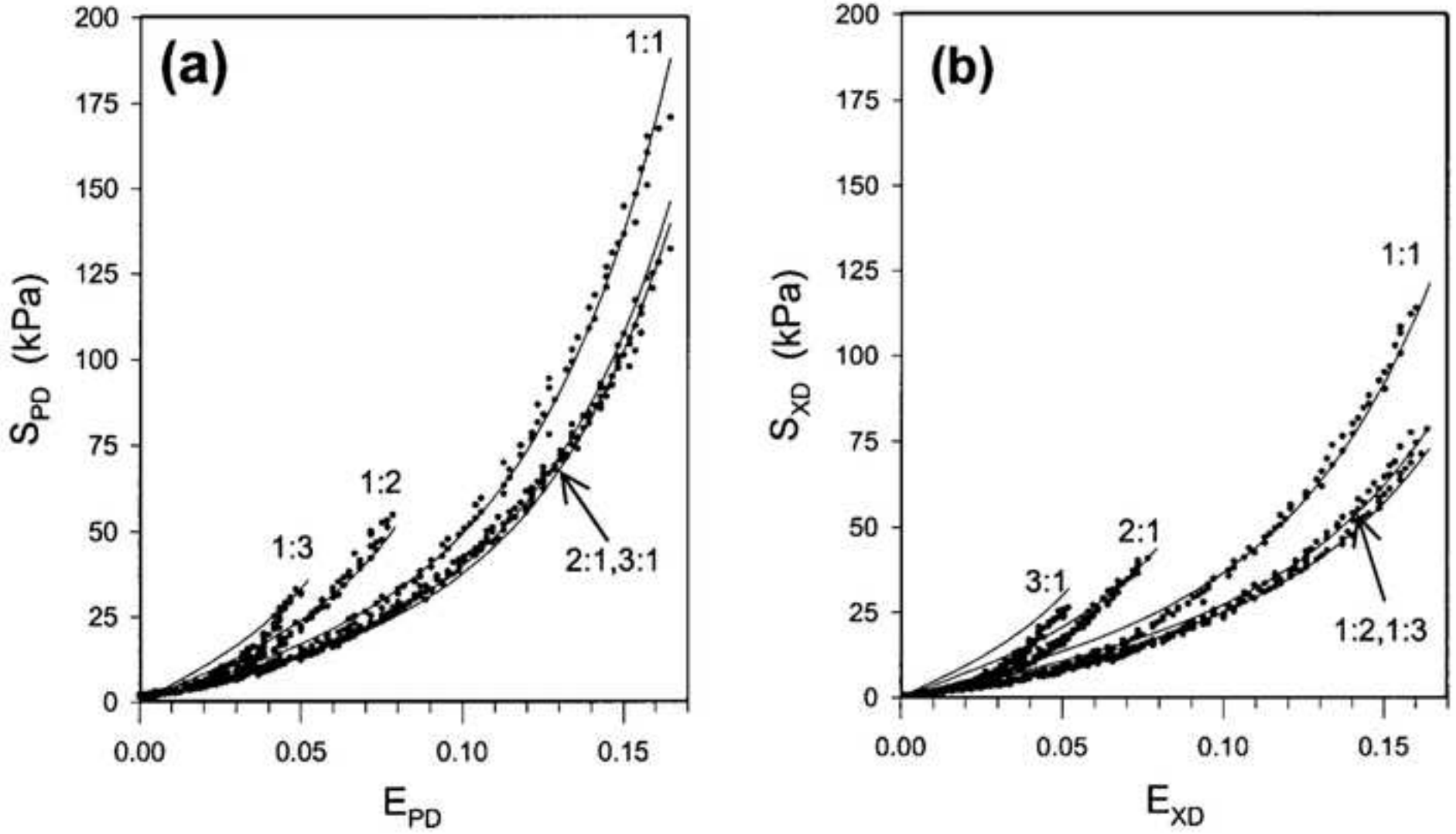

Figure 14

Click here to download Figure Figure 14.png

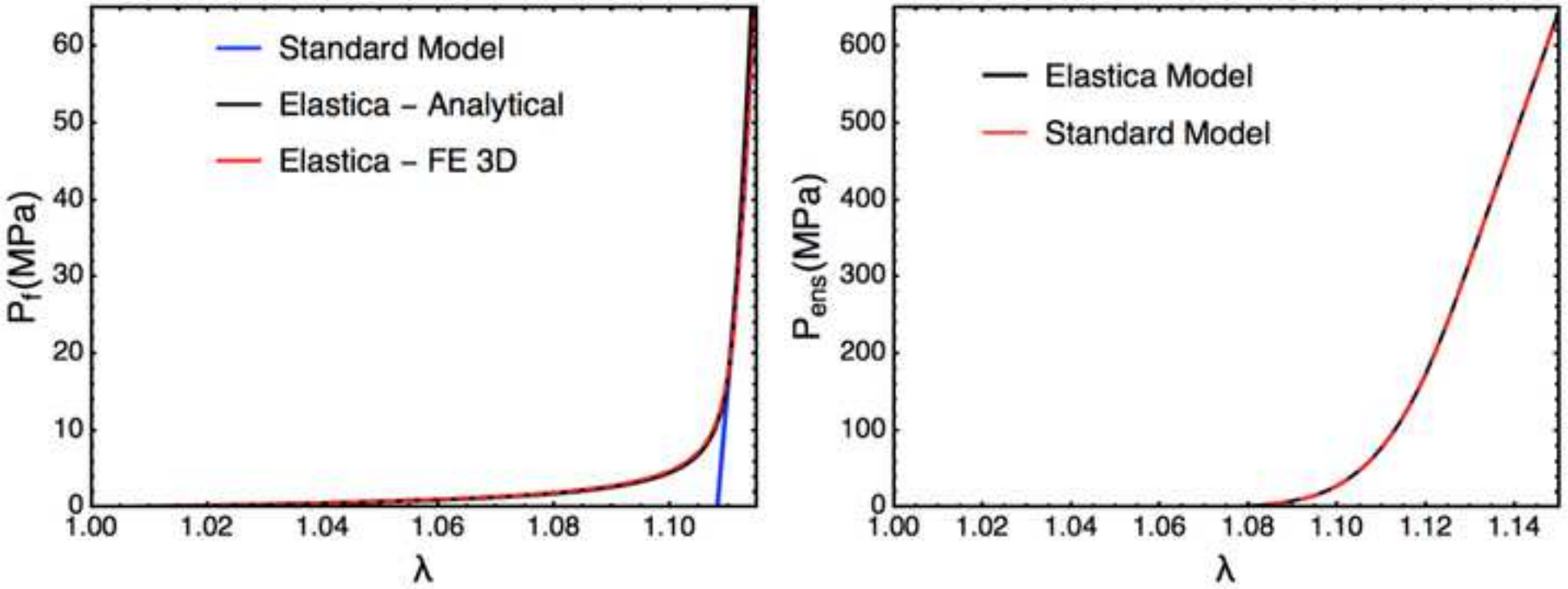

Figure 15

Click here to download Figure Figure 15.png

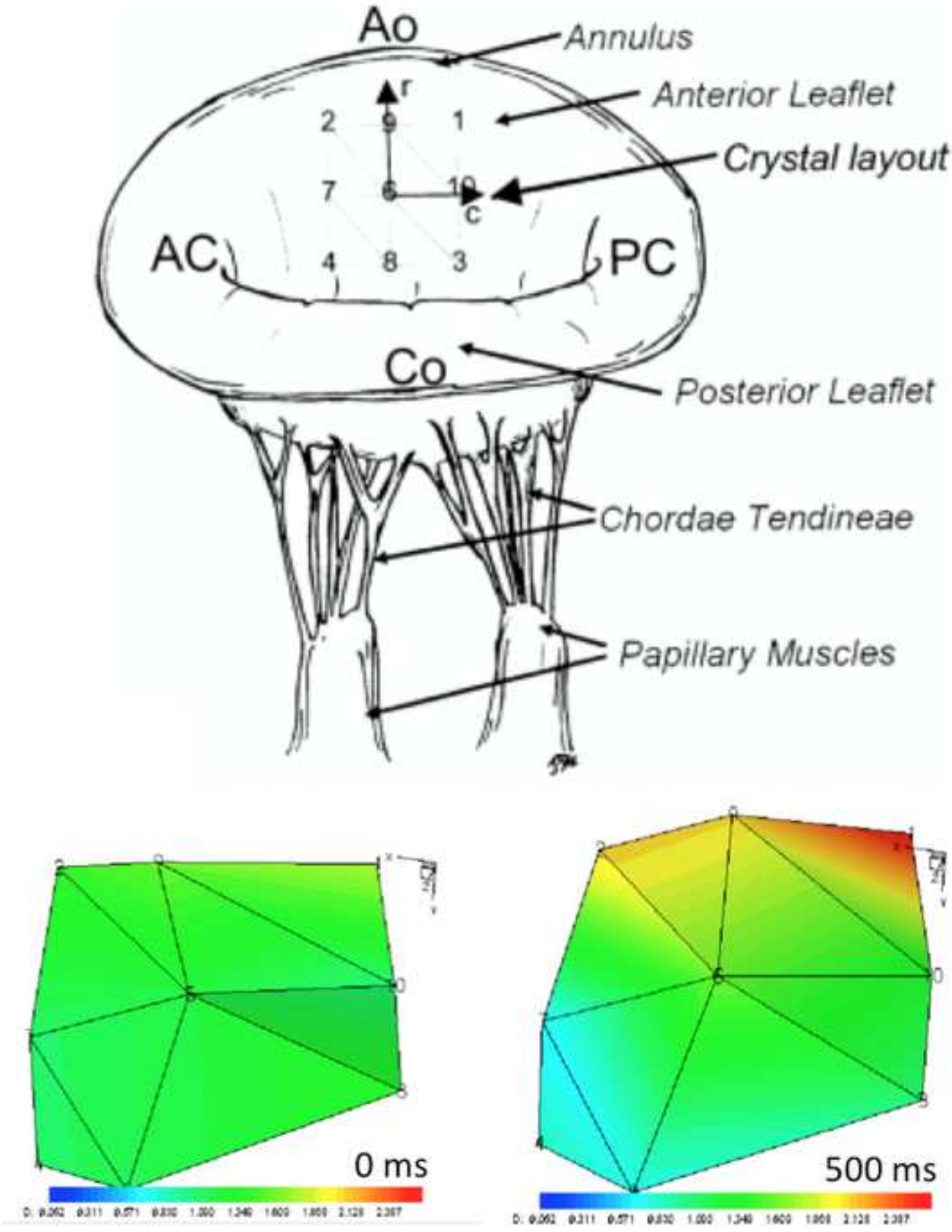

Figure 16

Click here to download Figure Figure 16.png

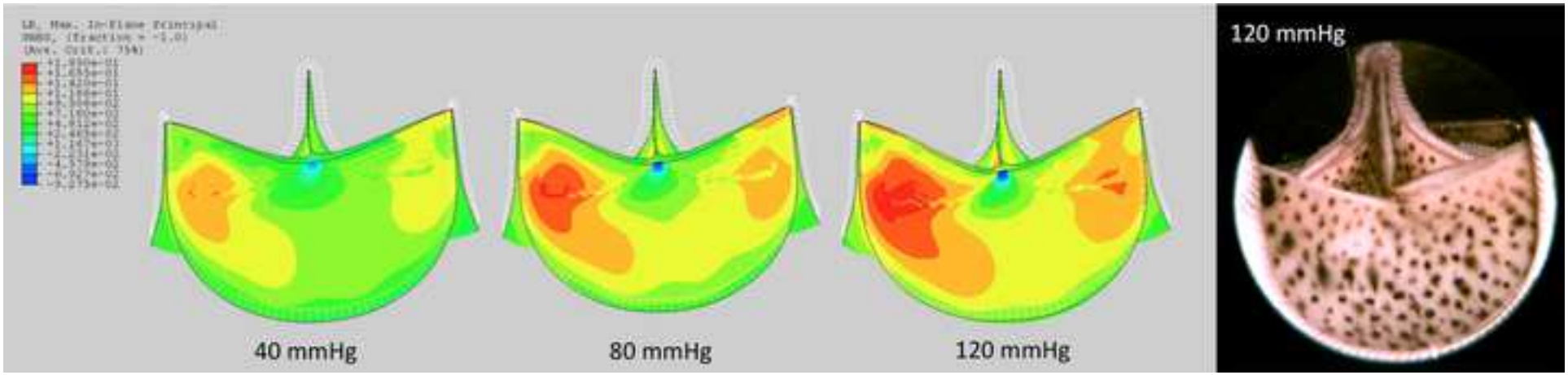

Figure 17

Click here to download Figure Figure 17.png

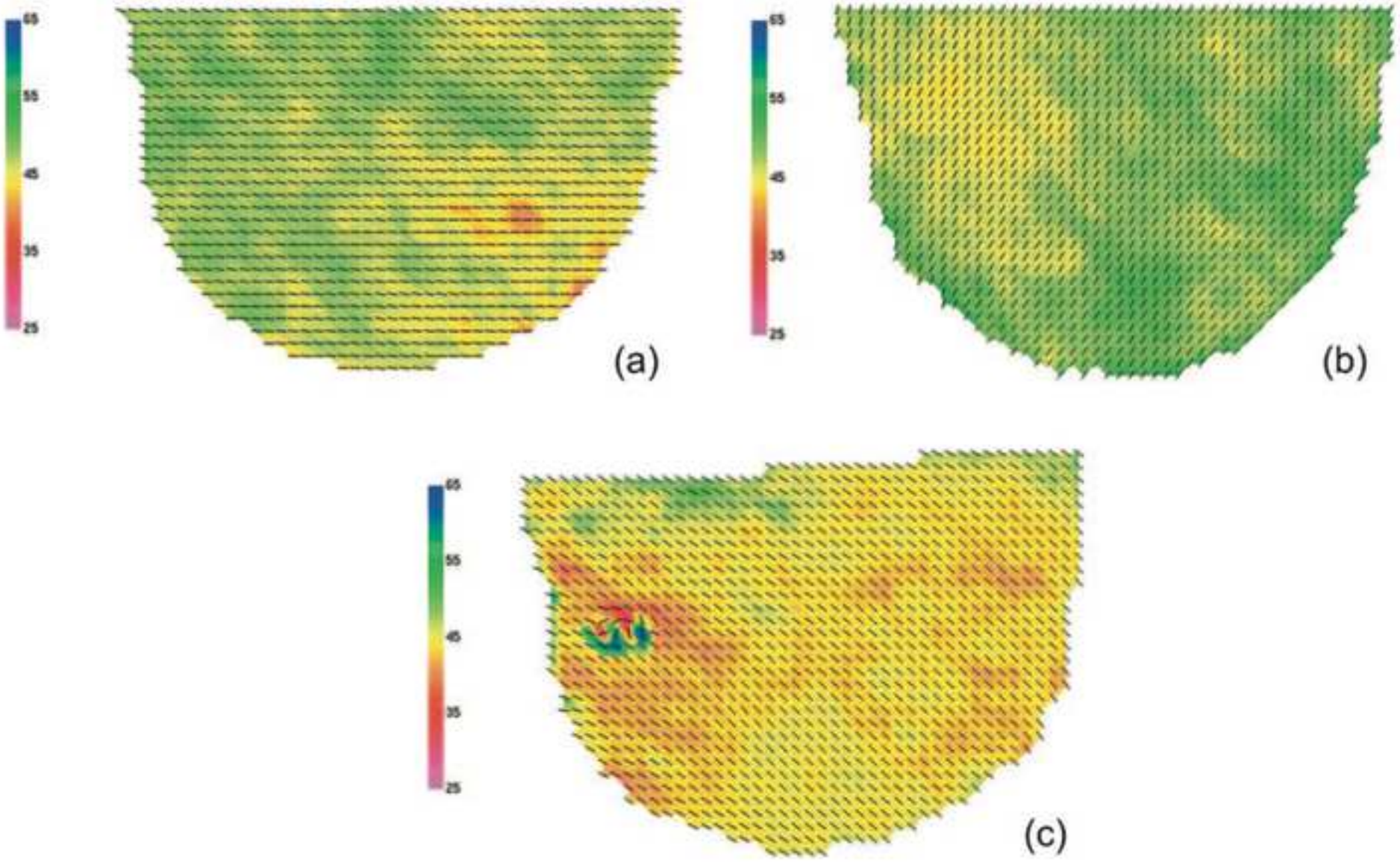

Figure 18

Click here to download Figure Figure 18.png

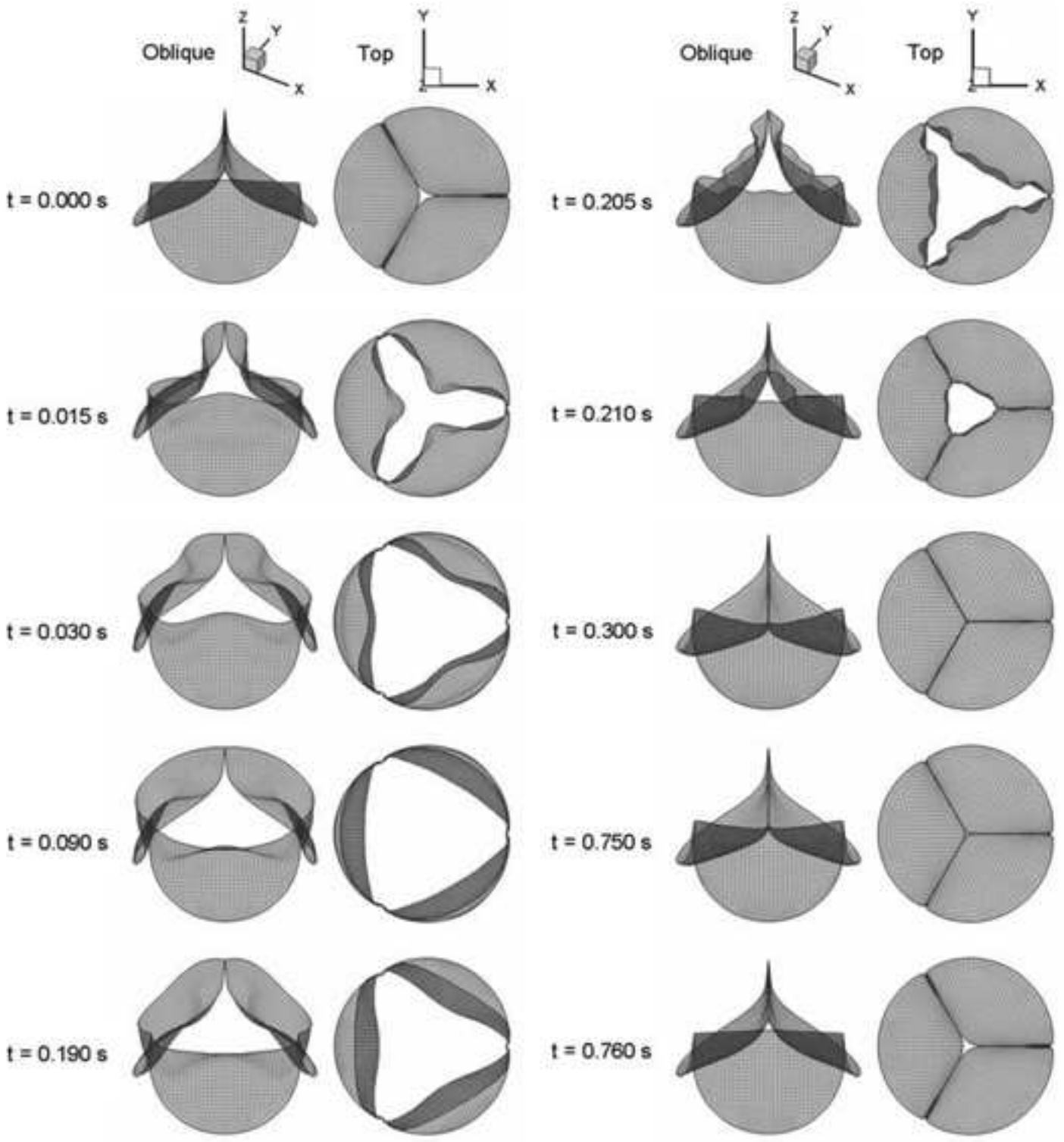

Figure 19

Click here to download Figure Figure 19.png

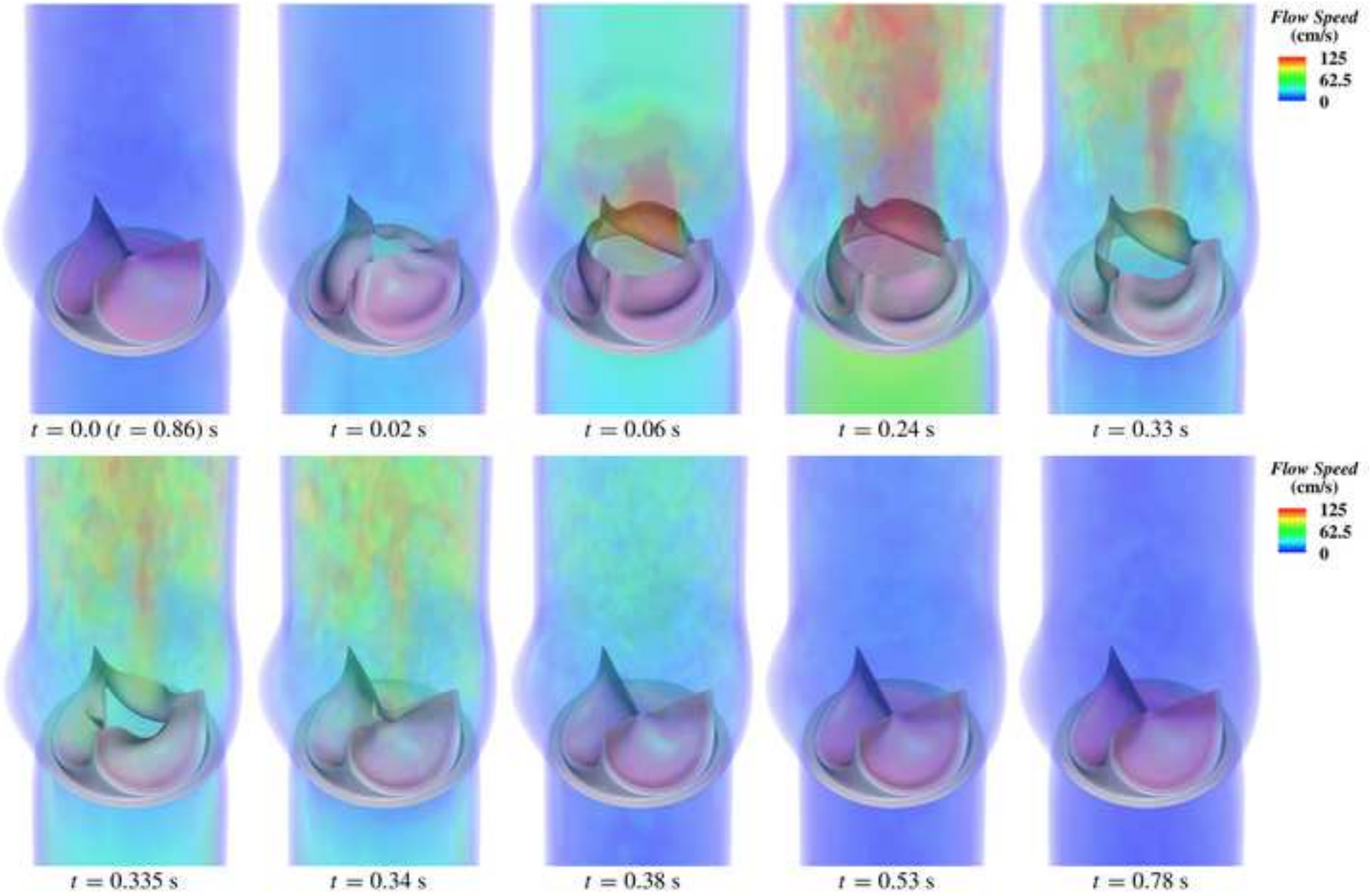

Figure 20

Click here to download Figure new figure 20.jpg